VILNIUS UNIVERSITY
CENTER FOR PHYSICAL SCIENCES AND TECHNOLOGY

VYTENIS BARKAUSKAS

IMPACT OF NUCLIDE COMPOSITION EVOLUTION TO RBMK SPENT FUEL NUCLEAR SAFETY AND IRRADIATED GRAPHITE RADIATION SAFETY CHARACTERISTICS

Doctoral dissertation

Physical sciences, physics (02P)

Vilnius, 2016

Doctoral dissertation was prepared at Center for Physical Sciences and Technology in 2010 – 2015, Vilnius, Lithuania

Scientific supervisor:

dr. Artūras Plukis (Center for Physical Sciences and Technology, Physical Sciences, Physics — 02P)

VILNIAUS UNIVERSITETAS
FIZINIŲ IR TECHNOLOGIJOS MOKSLŲ CENTRAS

VYTENIS BARKAUSKAS

NUKLIDINĖS SUDĖTIES EVOLIUCIJOS ĮTAKA RBMK REAKTORIAUS PANAUDOTO KURO BRANDUOLINĖS SAUGOS IR APŠVITINTO GRAFITO RADIACINĖS SAUGOS CHARAKTERISTIKOMS

Daktaro disertacija

Fiziniai mokslai, fizika (02P)

Vilnius, 2016

Daktaro disertacija rengta 2010 – 2015 metais Fizinių ir technologijos mokslų centre

Mokslinis vadovas:

dr. Artūras Plukis (Fizinių ir technologijos mokslų centras, fiziniai mokslai, fizika — 02P)

Acknowledgements

I would like to thank all the people who had great impact on my research both professionally and personally over the last several years.

Firstly I would like to express my gratitude to my supervisor dr. Artūras Plukis for his guidance and patience during the past six years. I am grateful to dr. Rita Plukienė for her helpful advices and practical comments on drafts of the papers. I would also like to thank dr. Jonas Reklaitis for his assistance, valuable comments during writing process and for his wit and humor during nanoseconds of procrastination. I am also thankful to my former boss and current friend, head of the division of Safety Analysis in VATESI, dr. Evaldas Kimtys, who brought me in this field and taught me a lot. Many thanks to my former and current colleagues, Vladas, Nerijus, Elena and Lina, for all the cheerful time we spent together.

Finally I have to acknowledge with gratitude, the immeasurable support and love of my family. I would like to thank my mother for being the source of unconditional love, care and a perfect example of dedication and constant persistence in her work. I am especially grateful to Veronika, my miraculous wife, a role model of inner calmness and strength, for her love, support and patience during all these years. I also thank our three wonderful children Elžbieta, Adelė and Antanas for being my inspiration and source of endless smiles.

Vytenis Barkauskas

Contents

Introduction

The decommissioning of RBMK-1500 type reactors is an absolutely unique project worldwide that is performed in Lithuania. The specific issues of nuclear safety are part of this project. Nuclear safety is defined as the achievement of the proper conditions, the prevention of the accidents or the mitigation of the consequences, resulting in protection of people and the environment from the radiological hazards [1]. Those hazards are avoided or mitigated using technical and organizational measures of protection. In a very general approach the main objectives of the technical measures are to ensure control of a nuclear chain reaction, a proper heat removal and a sufficient shielding of the radiation exposure [1, 2].

The most hazardous material remaining after an operation of a nuclear reactor is the nuclear fuel, therefore the most important objective during the decommissioning stage of the nuclear power plant is to store or reprocess it safely. As the decision regarding future of the spent nuclear fuel is currenty not taken, dry storage is chosen as a temporary solution [3, 4]. The spent nuclear fuel characterization regarding the composition and the related activity is vital for the proper evaluation if the spent nuclear fuel could be stored safely, i.e. the main safety objectives could be achieved. The main parameter defining the nuclear chain reaction is the effective neutrons multiplication factor (k_{eff}) defined as a measure of the increase or decrease of the number of the free neutrons which could cause fissions [5–7].

One of the possible ways to evaluate k_{eff} is to assume the fresh nuclear fuel composition. However this approach gives a very conservative evaluation and k_{eff} is significantly over-predicted. Therefore burn-up credit approach might be applied taking into account reduction of the fissile material and production of the neutron absorbing nuclides [8–12]. The burn-up credit approach has been an attractive research area for scientific comunity for at least two decades already [13–17]. This approach requires the precise and validated evaluation

of the spent nuclear fuel composition.

The burn-up credit approach for the criticality analysis of a spent nuclear fuel cask should start with the proper evaluation of the spent nuclear fuel composition, choosing the relevant nuclides with specific properties, performing k_{eff} calculations and finally — the uncertainty and sensitivity analysis [18–22]. The validated calculation models intended for the spent nuclear fuel composition evaluation are necessary for this purpose. These models are attractive due to their ability to predict the spent nuclear fuel inventory and related characteristics of interest precisely enough, whereas the experiments in this field are costly and complicated. On the other hand, the modeling calculations could be employed as a tool to evaluate planned experiments or to predict the certain quantities, e.g. activities or doses, which are necessary. Not only the measured experimental concentrations but also additional data related to the irradiation history and the reactor design are needed to perform a precise modeling of the spent nuclear fuel composition, to ensure the validity of the model and to understand its limitations [11, 19, 20]. The increasing computational capabilities as well as more precise data of cross-section libraries allow us to analyze more and more sophisticated models of the nuclear fuel composition evolution. One can find a number of recent studies performed in the field of spent nuclear fuel composition modeling of various reactors that are publicly available [23–27].

There are two main options for the burn-up credit calculations regarding the spent nuclear fuel composition — use of the actinide-only burn-up credit, or the full burn-up credit taking into account additional stable neutron-absorbing fission products and burnable absorbers. The burn-up credit approach was applied for safety justification of the spent fuel storage systems of various reactors, including spent nuclear fuel casks of the RBMK-1500 reactor fuel [8–10, 28]. However there are no results regarding the burn-up credit application for higher than 2.0% enrichment nuclear fuel with the burnable absorbers [29–31]. This problem is relevant to the RBMK-1500 decommissioning, as the

spent nuclear fuel of the higher initial enrichment is planned to be stored in a more capacious spent nuclear fuel cask CONSTOR®RBMK-1500/M2 [4,32,33]. These new dry storage and transportation casks were not studied in the light of the burn-up credit, while the safety analysis showed that only particular loading schemes of these casks might be used due to the sufficient heat removal and criticality safety issues [4]. Erbium burnable absorber, used in higher than 2.0% enrichment fuel, affects the reactor performance, but it was not studied how k_{eff} of the storage cask was affected. Moreover, the very important effect of the heterogeneous axial burn-up of the spent nuclear fuel assembly on k_{eff} in the storage cask of RBMK-1500 reactor fuel has not been studied yet.

Besides the nuclear fuel another hazardous material used inside the RBMK type reactor is graphite, which was under a constant neutron irradiation during all the reactor operation. The main hazard of graphite is radiation of the activation products such as ^{14}C, ^{3}H or ^{36}Cl, etc. Recent publications in this field are devoted to radionuclide behaviour in the graphite as well as deposition and activities of impurities are studied [34–38]. One of the class of the radioactive nuclides are actinides which are created by activation of the uranium impurities inside graphite through a number of (n, γ), (n, p) or (n, α) reactions. The long-term power operation of the reactor results in quite a significant build-up of long-lived isotopes of radioactive actinides, such as Pu, Am, Cm, etc. Thinking about graphite reprocessing, which is attractive from the sustainability point of view, an essential topic is characterization of the most significant radionuclides inside graphite. Characterization of the radionuclides is very important not only for solving the problem of the efficient reprocessing, but also for prediction of the contamination in further applications and also evaluating the radiological consequences of the temporary storage or disposal in the repository.

The composition evolution of the nuclear fuel and material activation problems are difficult to solve due to the large number of the differential equations

defining transport of free neutrons as well as need for the large amount of parameter information such as the cross-sections defining interactions of neutrons with matter and data collection after calculations. Therefore, there are specific neutron transport and depletion computer codes that are used to solve these complex problems. These codes may have very different capabilities, but in general their versatility, flexibility, and possibility of coupling with other codes determine their popularity in the scientific and industrial use [7, 39, 40].

The increasing computational capabilities allow us to numerically simulate more sophisticated experiments in reactor structures, while the state-of-art codes give more precise solutions of the neutron transport and material activation problems and these conditions are vital in approaching the problems studied here. The fission and activation of uranium during the irradiation inside the nuclear reactor determine changes in the material composition inside two main materials of the reactor — nuclear fuel and graphite — and new hazardous radionuclides are formed. The precise characterization of these nuclides is the first step towards better understanding of behaviour of the hazardous material. This understanding is extremely important to avoid possible accidents and minimize hazards caused by the peaceful use of nuclear energy.

Main goal and tasks of the research work

The main goal of this study is to evaluate the nuclear fuel and reactor graphite composition changes during operation of the RBMK type reactor using appropriate computational methods and to investigate the influence of actinides and other strongly neutron-absorbing nuclides on the nuclear safety taking into account a concept of the burn-up credit as well as to investigate radiation safety characteristics of the actinides in the RBMK reactor moderator graphite.

In order to achieve this goal the following tasks have to be performed:

- Creation of the representative numerical models of the RBMK reactor lattice and the spent nuclear fuel cask and numerical simulations burning the nuclear fuel in the RBMK reactor in order to generate one-group cross-section libraries for nuclear fuel. Evaluation of the spent nuclear fuel composition against available experimental data to ensure the validity of the model.

- Evaluation of the effective neutron multiplication factor k_{eff} inside the RBMK spent nuclear fuel cask introducing the changes of the spent nuclear fuel composition due to burn-up.

- Investigation of the influence of the average axial nuclear fuel assembly burn-up profile inside the spent nuclear fuel cask on k_{eff} and identification of the differences in comparison with the uniform axial burn-up profile and their physical reasons.

- Precise evaluation of the reactor neutron spectrum and flux distribution using the average burn-up composition of nuclear fuel and investigation of the build-up of the long-lived actinides in the graphite from very small fraction of uranium impurities in the virgin nuclear graphite during operation of the RBMK type reactor.

Novelty and relevance of the results

The nuclear fuel depletion was numerically modeled by using a simple but representative model of the RBMK lattice. Calculations were performed using SCALE 6.1 code. The model of the RBMK lattice addresses resonance and self-shielding effects more adequately and adds precision to the numerical experiment of nuclear fuel burn. New one neutron energy group cross-section libraries for the spent nuclear fuel composition and activity calculations were created for the 2.4–2.8% enrichment nuclear fuel with the erbium burnable

absorber. The use of one-group cross-section libraries allow a fast prediction of the RBMK reactor spent nuclear fuel inventory and related characteristics. Results give essential information for planned experiments or decommissioning activities. For the first time, these libraries were used to optimize criticality analysis of the spent nuclear fuel cask CONSTOR®RBMK-1500/M2 introducing different approaches — actinide-only and full burn-up credit — for the RBMK reactor spent nuclear fuel. Besides, the average axial burn-up profile was introduced and studied to evaluate the end-effect due to inhomogeneous burn-up of the nuclear fuel assembly. Furthermore, the model was extended to 3D geometry with additional structural components and used to calculate specific activities of uranium activation products in the RBMK reactor graphite and to compare SCALE 6.1 modeling results with those of the experiment and the other modeling results.

The results obtained are important for the nuclear safety at the decommissioning stage of the nuclear power plants with RBMK type reactors as this research provides novel results of main nuclear safety characteristics such as k_{eff} of systems with a significant fissile material content taking into account new effects and the activities of the main long-lived actinides in the graphite moderator.

Statements for the defence

1. A simplified numerical model of the infinite RBMK reactor lattice consisting of 14 fuel channels and 2 control and protection system channels is suitable for the generation of one-group cross-section libraries, used for the nuclear fuel composition evaluation.

2. The evaluation of RBMK spent nuclear fuel cask effective neutron multiplication factor, taking into account actinides, fission products and burnable absorbers, show a decrease of k_{eff} in comparison with actinide-only

case in high burn-up spent nuclear fuel due to the increasing concentration of the fission products, but not due to the erbium burnable absorber.

3. A significant positive end-effect on k_{eff} is found to exist in the RBMK reactor fuel storage cask due to non-uniform fissile ^{235}U depletion in the nuclear fuel assembly whereas build-up of plutonium isotopes has no significant effect.

4. The developed 3D model of the RBMK reactor lattice is suitable for radiological characterization of graphite in the reactor plateau region.

Author's contribution and results published

The author has performed the numerical modeling, analyzed the obtained data, and together with co-authors prepared the publications.

The results are presented in 4 peer-reviewed scientific papers:

1. R. Plukienė, A. Plukis, V. Barkauskas, A. Gudelis, R. Gvozdaitė, G. Duškesas, V. Remeikis, Actinides in irradiated graphite of RBMK-1500 reactor, Nuclear Engineering and Design, **277**, 95–105 (2014).

2. R. Plukienė, A. Plukis, A. Puzas, R. Gvozdaitė, V. Barkauskas, G. Duškesas, J. V. Cizdziel, D. Bussan, V. Remeikis, Actinides input to the dose in the irradiated graphite of RBMK-1500 reactor, Nuclear Engineering and Design, **300**, 530–535 (2016).

3. V. Barkauskas, R. Plukienė, A. Plukis, Actinide-only and full burn-up credit in criticality assessment of RBMK-1500 spent nuclear fuel storage cask using axial burn-up profile, Nuclear Engineering and Design, **307**, 197–204 (2016).

4. V. Barkauskas, R. Plukienė, A. Plukis, V. Remeikis, Generation of RBMK-1500 spent nuclear fuel one-group cross-section libraries and their

evaluation against experimental data, Lithuanian Journal of Physics *(accepted for publication)*.

The results have been presented at the conferences:

1. V. Barkauskas, A. Plukis, Modeling of RBMK-1500 spent nuclear fuel axial burn-up, 9th annual conference of young scientists on energy issues CYSENI 2012: international conference, Kaunas, Lithuania, 24–25 May, 2012, Kaunas.

2. V. Barkauskas, A. Plukis, Preparation of effective cross-section libraries for calculation of spent nuclear fuel inventory of RBMK type reactors, 10th annual conference of young scientists on energy issues CYSENI 2013: international conference, Kaunas, Lithuania, 29–31 May, 2013, Kaunas.

3. V. Barkauskas, A. Plukis, Dalijimosi produktų, svarbių branduolinei saugai, skaitinis vertinimas RBMK reaktoriaus PBK, 40-oji Lietuvos nacionalinė fizikos konferencija, 10–12 birželio, 2013, Vilnius.

4. V. Barkauskas, A. Plukis Burn-up credit approach for criticality assessment of new RBMK-1500 spent nuclear fuel storage cask, 12th annual conference of young scientists on energy issues CYSENI 2015: international conference, Kaunas, Lithuania, 27–28 May, 2015, Kaunas.

5. V. Barkauskas, A. Plukis, RBMK-1500 panaudoto branduolinio kuro konteinerio kritiškumo vertinimas atsižvelgiant į vertikalaus išdegimo profilį, 41-oji Lietuvos nacionalinė fizikos konferencija, 17–19 birželio, 2015, Vilnius.

6. R. Plukienė, A. Plukis, A. Puzas, V. Barkauskas, D. Germanas, V. Remeikis, Cm apšvitintame RBMK-1500 reaktoriaus grafite, 41-oji Lietuvos nacionalinė fizikos konferencija, 17–19 birželio, 2015, Vilnius.

7. R. Plukienė, A. Plukis, E. Lagzdina, A. Garbaras, A. Puzas, R. Gvozdaitė, V. Barkauskas, D. Germanas, V. Remeikis, Nuclides determining the dose in the irradiated graphite of RBMK-1500 reactor, International Scientific Conference "Radiobiology: Minimizing Radiation Risks", 29–30 September, 2016, Gomel, Belarus.

1. Research field review

1.1. Modeling

A numerical modeling of the spent nuclear fuel composition is inseparable from an experimental evaluation, because the experiment provides actual data, which allow to evaluate if the numerical predictions are sufficiently precise. The iterative process of the comparison between the experimental and model results employing the statistical tools is called validation. Only when an acceptable agreement between the experimental assay and modeling results is achieved, model calculations are assumed to be validated. The validation gives justified confidence for further use of the numerical modeling. More general definition of validation is given in [41]: validation is the process of determining the degree to which the considered model is an accurate representation of the real world from the perspective of the intended uses of the model.

The validated calculation models for the spent nuclear fuel composition modeling are attractive due to their ability to predict the spent nuclear fuel inventory and related characteristics of interest without the need of performing costly and complicated experiments. On the other hand model calculations could be employed as a tool to evaluate planned experiments or to predict certain quantities, e.g. the activities or doses, which are necessary in preparation stage. The validation of the fuel burn-up modeling has to be based on the reference data. Not only the measured concentrations but also additional data related to the irradiation history and reactor design are necessary to perform a precise modeling of the spent nuclear fuel composition. The short review of the available spent nuclear fuel composition modeling calculations, as well as the problems identified in this field is presented in this chapter.

Physical assumptions regarding the spent nuclear fuel modeling are presented in chapter 2. The time evolution of the nuclide concentrations during

and after the irradiation in the reactor is described by Bateman equations (Eq. 2.17). The main irradiation parameter is neutron flux, which is obtained solving the neutron transport problems defined in section 2.1. Usually when the experimental results are presented, some relevant modeling results are given in the same paper or report. The results of more detail modeling are often presented in the separate papers referring to the generalized experimental results as well as discussing specific issues of the numerical calculations.

One of the aim of these thesis is to extend the knowledge about the material composition changes in the RBMK reactor caused by neutron irradiation. I would like to make a short review regarding modeling that was performed in this field previously. Main calculations were performed using MCNP, ORIGEN and SCALE codes for the depletion evaluation of RBMK fuel [22, 27, 28, 42]. SCALE, HELIOS codes were used to calculate concentrations of some isotopes [43]. Furthermore there were some studies related with Ignalina NPP decommissioning project [3].

In [27] the Monteburns code system was used —- an automatic-cyclic coupling of the MCNP and ORIGEN2 codes. In this paper the fuel evolution of the 2.0 % enrichment RBMK fuel assembly without erbium burnable absorber was simulated and the concentration for the actinides (Pu, Am, Cm) and some fission products (Cs and Nd) were calculated and compared with the experimental results. The modeling results were found to be in good agreement with the experimental data for the main actinides characterizing nuclear waste: ^{239}Pu, ^{241}Pu, ^{244}Cm. The analysis of the plutonium isotopic ratios also was performed. It was also found that the fuel burn-up in the inner ring of the fuel pellets is lower up to 22% compared to the outer fuel ring.

In [22] the sensitivity study of RBMK-1500 spent nuclear fuel nuclide composition modeling was performed by investigating the reactor parameters (coolant density, fuel and graphite temperatures, fuel irradiation history, axial fuel assembly power profile) and the specific model parameters (model geo-

metry description, resonance self-shielding parameters, etc.). It was found that the inventory of some trans-uranium elements significantly depends on the neutron spectrum in the fuel, which mainly depends on the water density and the graphite temperature.

In [28] the concentrations of ^{238}Pu, ^{240}Pu, ^{242}Pu, ^{242}Cm and ^{244}Cm nuclides were modeled in the RBMK-1000 spent nuclear fuel and compared to the available experimental data, in later publication [42] modeled burn-up range was extended as well as γ and neutron activities for the spent nuclear fuel were calculated. Moreover, [28] gives publications review about the modeling and experiments performed for RBMK reactor fuel up to 2001.

Kovbasenko et al. [43] performed the numerical modeling of RBMK-1000 spent nuclear fuel using SCALE and HELIOS packages. Concentrations of ^{234}U, ^{235}U, ^{236}U, ^{238}U, ^{238}Pu, ^{239}Pu, ^{240}Pu, ^{241}Pu, ^{242}Pu, ^{237}Np and ^{243}Am obtained were compared with experimental data. The results obtained show quite good agreement with experimental data for uranium isotopes, concentrations of ^{239}Pu, ^{240}Pu and ^{241}Pu isotopes are also quite well modeled, however concentrations of other nuclides differ more than 30%. In this paper infinite neutron multiplication factor for wet storage facility was calculated using burn-up credit approach, taking into account concentrations of 5 selected actinides as well as sensitivity of k_∞ to main reactor parameters — water density and temperature — was reviewed.

The report on Reactor Fuel Isotopics and Code Validation for Nuclear Applications [23] presents the available composition modeling data of the various commercial reactors and summarizes the accuracy of the depletion modeling using ORIGEN code. In general, when using the current ENDF/B-VII.0 nuclear data libraries in SCALE, the major actinides are predicted within 5% of the measured values. There is a larger uncertainty for modeling of radioactive fission products when compared to either the actinides or the stable fission products in the spent nuclear fuel. Specifically, more data of actinides impor-

tant to criticality analysis are needed for well characterized VVER, RBMK, CANDU, MAGNOX, and AGR reactor types. Measured fission product data are, in general, very limited for reactors other than PWRs and BWRs.

Most of the calculations performed in order to evaluate the nuclear fuel burn-up are related with the international benchmark programmes related with either simulation of experiments (see Section 1.3) or burn-up credit evaluations, also modeling on specific cases of research reactors is often reported [44, 45].

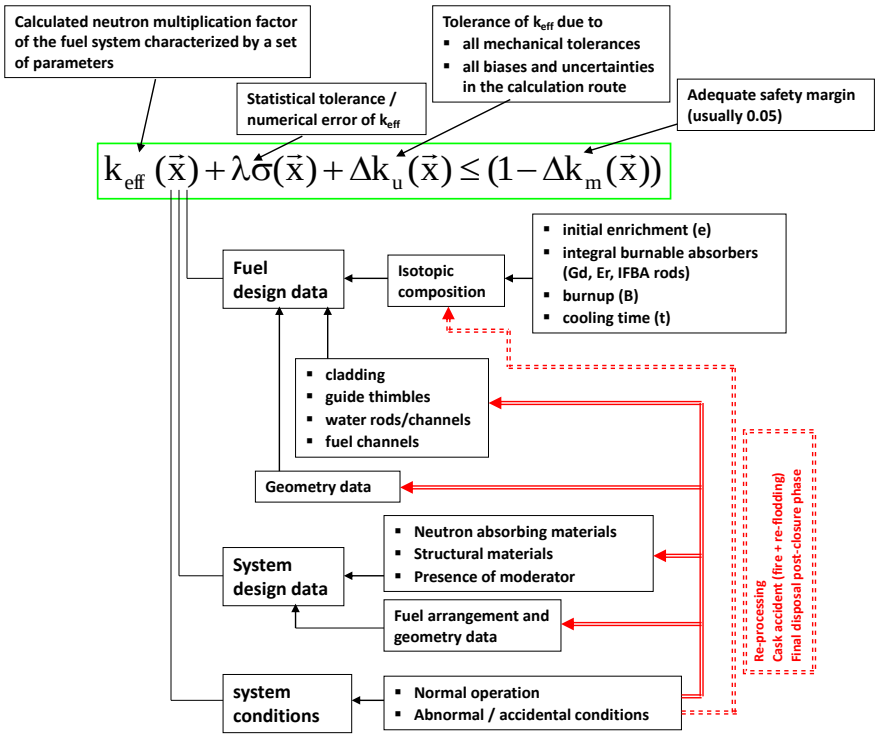

Figure 1.1: k_{eff} evaluation aspects taking into account burn-up credit [46].

There is a number of reports on the application of burn-up credit publicly available, OECD Nuclear energy agency has even made a comprehensive bibliography regarding Burn-up credit studies [47]. Burn-up credit evaluations started in 1980s, when the problem arose where to store the increasing amount of the spent nuclear fuel. Also the efforts to increase the utilization of the nuclear fuel inside the reactor has lead to increasing fuel enrichment. Storage of this fuel of higher enrichment was not foreseen in the licenses of the nuclear

power plants, therefore safety of storage had to be additionally justified. The evaluation of the decrease of fissile nuclides content in the spent nuclear fuel during irradiation was introduced to justify criticality safety of the nuclear fuel storage systems. Further studies showed that sufficiently precise nuclear fuel composition evaluation was not a trivial problem.

There is a large number of the evaluation aspects which have to be considered to properly evaluate k_{eff} taking into account fuel burn-up. First, spent nuclear fuel should be properly characterized. This characterization consists of evaluation of fuel isotopic composition, structural components and geometry. Second, spent nuclear fuel storage system should be defined precisely as possible taking into account geometry, composition of structural components and operating conditions. Then different sources of uncertainties should be considered and evaluated. k_{eff} evaluation scheme is given in Fig. 1.1.

International Atomic Energy Agency has published four technical documents summarizing technical meetings on burn-up credit topic from 1997 to 2005 [8–10, 48]. These documents provides information about the use of burn-up credit approach in different countries. Also summaries of the on-going research projects were provided and main issues from the nuclear safety regulators were discussed. Furthermore a number of the topical studies were performed by Oak Ridge National laboratory and SCALE code developers [18, 19, 49–51]. Some specific documents regarding regulatory guidance of burn-up credit applications were issued by US Nuclear Regulatory Commission [52–55]. While the research papers are published constantly in the relevant journals presenting results of evaluation of k_{eff} of the casks or benchmark calculations [13–17, 56].

US Nuclear Regulatory Commission (US NRC) provides useful information about k_{eff} behavior during storage of the cask [55]. Fig. 1.2 shows the expected reactivity behavior for spent nuclear fuel in a hypothetical GBC-32 cask. The results show that after 100 years after fuel discharge from the reactor, the re-

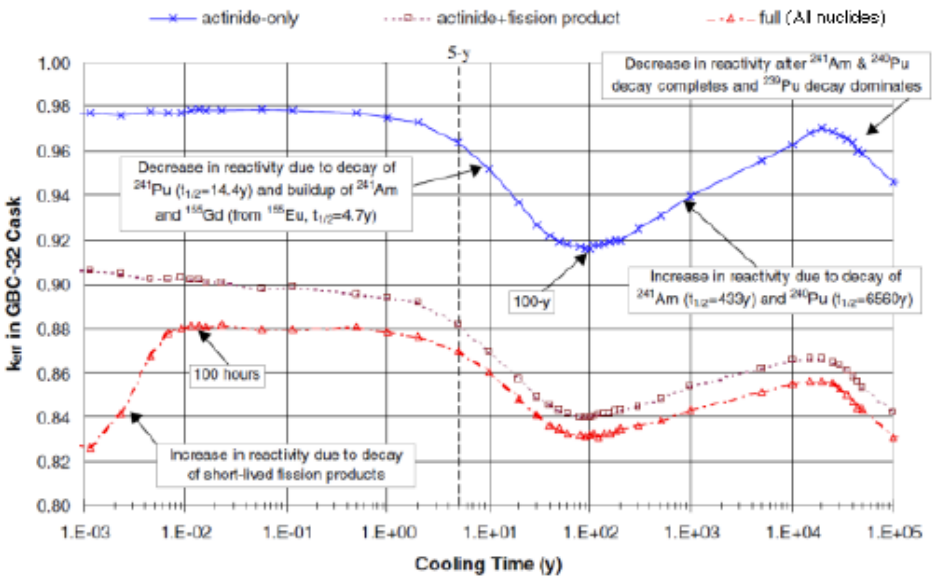

Figure 1.2: Reactivity behavior in the GBC-32 cask as a function of cooling time for fuel with 4.0% ^{235}U initial enrichment and 40 GWd/MTU burnup [55].

activity of the cask starts to increase due to decay of ^{241}Am. Therefore quality and integrity of storage systems should be maintained for a time which surpass a lifetime of several generations of people. I.e. the assurance of safe spent nuclear fuel storage is and will remain relevant for at least several centuries.

Wagner et. al. [19] discusses the non-uniform axial burn-up distribution caused by axial variations in flux, which is mainly attributed to leakage at the fuel ends. It is summarized that the uniform axial distribution is conservative for low burn-ups, but becomes increasingly non-conservative as burn-up increases in case of PWR spent nuclear fuel and the reactivity effect of the axial burn-up distribution must be addressed in a comprehensive and conservative manner in safety analyses.

Publication [18] discusses peculiarities of BWR burn-up, the sensitivity to parameters such as specific power, fuel and moderator density, operating his-

tory and axial-profile. Parks et al. [49] identified the most important technical issues regarding burn-up credit evaluation at that time perspecive which were operating history, axial and horizontal profile distributions, fission products influence on k_{eff}, as well as the need of sensitivity and uncertainty studies. The burn-up credit application in criticality analysis in CASTOR®RBMK-1500 and CONSTOR®RBMK-1500 was presented in 2002 [9] and 2004 [28]. Some normal operation and accident cases were calculated in these studies, as well as the different composition of fuel for criticality analysis was used, but no impact of axial burn-up profile on k_{eff} was evaluated. Also the fuel of 2.8% enrichment was not studied and CONSTOR®RBMK-1500/M2 type casks were not designed at that time.

One important branch of research performed in this field is the study of sensitivity and uncertainty analysis. Sensitivity and uncertainty analysis is very complicated subject, it would require not less time and effort as the preparation of this dissertation. Therefore, it is outside of our current scope of research, but is considered for the future.

The microscopic cross-section data may be the major contributor to the overall k_{eff} uncertainty. Information presented in the papers show that ^{235}U(n,f), ^{238}U(n, γ), ^{239}Pu(n,f) reactions and the average number of neutrons released per fission from ^{235}U and ^{239}Pu are the main contributors to the total uncertainty during evaluation of k_{eff}. The engineering parameters (pellet diameter, fuel enrichment and density, and moderator density) might have more important effect on the calculated quantities, often higher than the effect of nuclear cross-section data [20, 21, 24, 57, 58]. To sum up, the uncertainty in the burn-up credit calculations is mainly dominated by contributions from reactions of major actinides, while contributions from minor actinides and fission products are comparable to the statistical uncertainties in the k_{eff} results [51]. The precise geometry description and the algorithms used in Monte Carlo codes help to reduce errors due to modeling and the computation algorithm,

but problems due to the material cross-section processing and multi-group approximations should be considered as a possibly significant source of k_{eff} estimation errors [59].

1.2. Experimental methods

The experimental methods used for the nuclide composition measurements in the spent nuclear fuel covers the destructive and non-destructive techniques. The direct experimental burn-up credit evaluation in reactor type facilities is also possible, as well as the other more sophisticated methods. The main ex-perimental techniques are discussed in OECD/NEA report and in the references within [11], therefore only short presentation of the methods used worldwide will be given here.

The destructive experiment starts with the proper sample selection from the nuclear fuel rod taking into account axial and radial burn-up profiles, and the accumulation of the nuclides in the cladding and in the gap between the fuel pellet and the fuel cladding. The most common solvents for the spent nuclear fuel are the nitric acid and the mixtures of the nitric acid and the hydrofluoric acid. The spent fuel fragment is dissolved in the acidic solutions. The solid metalic residuals are dissolved again in different molarity and composition acids. The solutions are analyzed separately and the results are combined in the end. The chromatographic separation is used to separate high concentration elements like uranium and other low concentration elements

These mass spectrometric techniques are commonly used for analysis [60]:

- Thermal ionisation mass spectrometry (TIMS)
- Inductively coupled plasma mass spectrometry (ICPMS)
- Sector field inductively coupled plasma mass spectrometry (SF-ICPMS)
- Quadrupole mass spectrometry

- Secondary ion mass spectrometry (SIMS) [61, 62]

Radiometric methods used for characterization of nuclides include classic radiometric spectroscopy methods [11, 63], the particular method applied depends on nuclides of interest:

- Gamma spectrometry. Gamma-emitting radionuclides without the need of extensive or complex sample preparation. For the analysis of spent fuel solutions it is used to measure gamma-emitting fission products (e.g. ^{106}Ru, ^{125}Sb, ^{137}Cs, ^{144}Ce, ^{154}Eu, ^{155}Eu) and minor actinides (^{241}Am and ^{243}Cm).

- Alpha spectrometry is used for the measurement of the alpha-emitting isotopes of uranium, plutonium, americium and curium.

- Liquid scintillation counting (for the alpha and beta emitters). In this technique the sample and the scintillator material are incorporated in a homogeneous liquid medium by adding an aliquot of separated radionuclide to the scintillation cocktail. Beta-emitting radionuclides like ^{147}Pm, ^{99}Tc and ^{90}Sr are measured using this technique.

The non-destructive methods are in particular interest of the scientific and safeguards community, as these methods allows to evaluate the composition and the amount of the nuclear materials and it is useful for the safeguards accountancy. The main non-destructive methods are defined in several reports and papers [64–68]. Basically these methods are orientated towards the determination of the concentrations of actinides or fissile isotopes, however gamma spectrometry methods may also be applied for the quantitative evaluation of the fission product concentration [69, 70]. These techniques are used:

- Passive neutron emission

- Induced neutron emission

- Passive Neutron Albedo Reactivity
- Photofission
- Neutron Differential Dieaway
- Delayed Neutron
- Delayed Gamma
- Passive prompt Gamma spectroscopy
- Differential Dieaway Self-Interrogation
- Gross (or Total) Neutron
- Neutron Multiplicity
- ^{252}Cf Interrogation with Prompt Neutron Detection
- Self-Interrogation Neutron Resonance Densitometry
- X-Ray Fluorescence
- Lead Slowing Down-time Spectrometry
- Nuclear Resonance Transmission Analysis
- Nuclear Resonance Fluorescence

Also, especially sophisticated methods exists, e.g. the nuclear waste imaging and spent fuel verification by muon tomography [71].

The direct burn-up credit experimental evaluation is performed in the reactor facility. For example in LWR-PROTEUS experiment case [72] desired neutron spectrum was created in the research reactor and after the insertion of the investigated spent nuclear fuel sample, reactivity effects with a moved calibrated fine control rod maintaining reactor exactly critical were studied. In case of REBUS experiments in Venus facility [10] measuring of the spent

nuclear fuel reactivity effect was performed measuring a critical water level in the reactor.

1.3. Experimental research review

The experimental research related with the determination of commercial reactors nuclear fuel isotopic composition as well as the direct measurements of k_{eff} are crucial for proper validation of the nuclear fuel related calculations such as the evaluation of burn-up credit, activity in case of accidents or thermal characteristics. Regarding burn-up credit, direct measurements of k_{eff} are also being performed. However all these experiments require much effort and resources due to the hazards related with the high radiation levels therefore there are only limited amount of publicly available data on the nuclear fuel composition.

The experimental research on the commercial nuclear power reactors fuel was started in 1970s by Japan atomic energy research institute (JAERI) [73], PWR and BWR fuel samples were investigated using various experimental techniques (see Section 1.2) to identify burn-up and nuclide composition. The composition evaluation experiments with the spent nuclear fuel discharged from the research reactors started even earlier — in the 60s [74]. The nuclides investigated were the isotopes of uranium, caesium, neodymium and several uranium activation products. Later in the 1990s the isotopic composition database system on the spent fuels in the light water reactors (SFCOMPO) was created by JAERI to collect the assay data on the isotopic composition of 10 (6 PWRs and 4 BWRs) light water reactors from Japan and the USA spent nuclear fuels at the beggining [75]. In 2001 the system SFCOMPO with data from 14 reactors was transferred from JAERI to the NEA Data Bank [76]. Data from 246 samples are available, including 30 samples from fuels that included burnable absorbers(Gd_2O_3).

Several other experimental programmes related with the isotopic composition measurements are:

- CERES programme of experiments was carried out from 1991—1997 through measurements in the Minerve reactor at Cadarache in France and the Dimple critical facility in the UK. The reactivity measurements have been made in Dimple on irradiated PWR and BWR fuel samples from the US and on two irradiated MOX samples from the French PWR [77, 78].

- French experimental programme based on the spent nuclear fuel chemical analysis has been carried out in France since 1993. The uranium, plutonium, neptunium, americium and curium isotopes have been analysed in PWR UO_2 and MOX fuel samples. Furthermore the 15 fission products selected by the OECD for burn-up credit criticality calculations have been measured [79].

- ARIANE was an international program designed to improve the database of PWR isotopic measurements for the spent nuclear fuel source term and isotopic inventory validation. It was coordinated by Belgonucleaire and completed in March 2001 [80].

- The LWR-PROTEUS Phase II experimental program was conducted at the Proteus research reactor at the Paul Scherrer Institute (PSI) in Switzerland in the early 2000s. One of its purposes was to gain more insight into the reactivity changes caused by the fuel burn-up [72, 81].

- REBUS international program was dedicated to the validation of the computer codes for the criticality calculations that take into account the reduction of the reactivity of the spent fuel as a result of burn-up credit. The program was completed in December 2005. The program included the core physics experiments at a critical test facility Venus, the non-destructive burn-up measurements of irradiated fuel rods with

gamma-ray spectroscopy, and the radiochemical isotopic analysis of pellet samples which were implemented in Belgium. The radiochemical analysis techniques included alpha- and gamma-spectrometry, ICP-MS, and TIMS [10, 82].

The results of several other experiments have also been published: the destructive examination of the nuclear fuel samples of Vandellós commercial reactors in Spain using various experimental techniques [83, 84], PWR and BWR fuel composition investigation in Japan [85, 86] and Korea [87].

The RBMK-1000 reactor fuel non-destructive examination using neutron scanning, alpha-spectrometry and mass spectrometry was performed in Russia [88]. The isotopic composition and the mass fraction of the actinides and certain fission products in the spent RBMK fuel from the Leningrad nuclear power plant were determined. The samples which were cut from the fuel elements with a known irradiation history and mass ranging from one to several grams were used for the destructive analysis. The destructive post irradiation examination of the spent nuclear fuel from VVER-440, VVER-1000 and RBMK-1000 was performed in Russian Khlopin Radium Institute by means of alpha-spectrometry and mass spectrometry [89]. During analysis of these two publications it was found out, that they report the same experiments, but [89] reports more detail information on initial enrichment, as well as some more nuclides were added.

1.4. Conclusions

In conclusion, the studies performed in the field of isotopic composition determination give quite good agreement between experimental and modeling results. However, regarding RBMK reactor fuel lack of both systematic experimental and modeling data is observable [23]. There are no nuclide composition data for RBMK nuclear fuel with erbium burnable absorber. One of

the possible way to present systematic nuclide composition data is one neutron energy group libraries, which are essential tool for fast and precise nuclear fuel composition evaluation. As no composition data are available for different enrichment fuel with erbium burnable absorber, differences during burn-up and their reasons are also not discussed in the literature.

The one-group cross-section libraries are suitable for k_{eff} evaluation of spent nuclear fuel storage systems applying concept of burn-up credit. Assumptions of different composition and application of axial burn-up profile are necessary to study burn-up credit. This problem was partly addressed in previous studies of RBMK spent nuclear fuel casks, however detailed analysis with highest enrichment fuel was not performed. The results of such study would give deeper understanding about impact of nuclides on k_{eff}. A study of the axial burn-up profile might give valid information whether inhomogeneous burn-up has positive or negative contribution on k_{eff} and what are the reasons of this effect.

It is also assumed, that application of RBMK lattice model allows to solve wider spectrum of depletion and activation problems. Therefore it was used for evaluation of the uranium impurities activation in order to evaluate activities of the actinides created by uranium neutron activation. In previous studies only activation of light elements was investigated [90]. This issue is discussed in Chapter 5.

2. Methodology

2.1. Methods of neutron transport calculations

History of a nuclear energy is inseparable from the discovery of the neutrons which cause fission and activation of the materials used in the field of nuclear energy. Neutron motion and interactions with the material are subjects of a neutron transport theory. The key starting element of this theory is the neutron transport equation (eq. 2.1) also known as Boltzmann equation. It defines the neutron flux evolution in time at a certain point in space, considering neutron source and removal terms.

Equation 2.1 is derived using these basic assumptions: neutron is a neutral point particle, which might with a certain probability (defined by time-independent cross-sections) be deflected or captured by a point nucleus. The interactions between neutrons are not considered. There might exist the neutron sources (external or from the fissions inside the system analyzed). Also a term regarding incoming and outgoing neutrons in the volume of interest is included.

$$\begin{aligned} \frac{1}{v}\frac{\partial\Phi(\vec{r},\vec{\Omega},E,t)}{\partial t} &= -\vec{\Omega}\vec{\nabla}\Phi(\vec{r},\vec{\Omega},E,t) - \Sigma_t(\vec{r},\vec{\Omega},E,t)\Phi(\vec{r},\vec{\Omega},E,t)+ \\ +Q(\vec{r},\vec{\Omega},E,t) &+ \int_{E'}\int_{\Omega'}\Sigma_s(\vec{r},\vec{\Omega'}\rightarrow\vec{\Omega},E'\rightarrow E,t)\Phi(\vec{r},\vec{\Omega'},E',t)d\vec{\Omega'}dE' \end{aligned} \tag{2.1}$$

where:

$\Phi(\vec{r},\vec{\Omega},E,t)$ — angular neutron flux at position $\vec{r}$, in direction $\vec{\Omega}$, at energy E, at time t;

$\Sigma_t(\vec{r},\vec{\Omega},E,t)$ — total macroscopic cross-section at position $\vec{r}$, in direction $\vec{\Omega}$, at energy E, at time t;

$Q(\vec{r},\vec{\Omega},E,t)$ — neutron source at position $\vec{r}$, in direction $\vec{\Omega}$, at energy E, at time t;

$\Sigma_s(\vec{r}, \vec{\Omega}' \to \vec{\Omega}, E' \to E, t)$ — scattering macroscopic cross-section at position $\vec{r}$, in direction $\vec{\Omega}$, at energy E, at time t;

v — neutron velocity;

$\vec{\nabla}$ — nabla operator.

If we assume $\partial\Phi(\vec{r}, \vec{\Omega}, E, t)/\partial t = 0$, we would have a stationary equation and the solution of this equation would be the time-independent flux. In this study we are basically having this situation — we use solutions of the time-independent equation to calculate flux for set of the parameters. Dynamics of the flux was not a subject of our work, therefore further we proceed with the discussion about the solutions of the time-independent neutron transport equation only.

There are two basic classes of methods for solving the neutron transport equation: deterministic method and Monte Carlo method. They will be presented here in a short manner. It is presumed, that all necessary cross-section parameters are known, but in Section 2.3 these issues are addressed. Methods presented here are discussed in detail in several classic books and review publications [5–7, 91].

A basic deterministic method has two approaches regarding neutron energy and cross-section treatment — continuous-energy approach and multi-group approach. Continuous-energy approach is not practical in large systems calculation, as it processes very fine (up to tens of thousands energy points) spectra giving more precise, but also more time consuming result. In our case much more practical is the multi-group approach.

The equation simplification starts with neutron energy range discretization into g groups and formation of energy intervals between values of E_g and E_{g+1}.

Further we integrate $\Phi(\vec{r}, \vec{\Omega}, E)$ with respect to E, and we obtain $\Phi_g(\vec{r}, \vec{\Omega})$ from time-independent neutron transport equation 2.1. This function defines flux of energy group g as function of spacial variables $\vec{r}$ and $\vec{\Omega}$.

$$\Phi_g(\vec{r}, \vec{\Omega}) = \int_{E_g}^{E_{g+1}} \Phi(\vec{r}, \vec{\Omega}, E) dE \tag{2.2}$$

$\Phi(\vec{r}, \vec{\Omega}, E)$ is simplified and replaced by product of energy part and spacial part of flux:

$$\Phi_g(\vec{r}, \vec{\Omega}, E) = f(E)\Phi_g(\vec{r}, \vec{\Omega}),\ E_g < E < E_{g-1}; \tag{2.3}$$

Energy-dependent spectral function $f(E)$ satisfies normalization condition:

$$\int_0^\infty f(E)dE = 1 \tag{2.4}$$

If we choose multi-group method, we also should know (or reasonably assume the form of this function) spectral function $f(E)$ in order to have sufficiently accurate group-averaged cross-sections $\sigma_g(E_g)$ for calculations. Evaluation of $f(E)$ is not a trivial problem. The most simple assumption is that $f(E)$ is a constant and inversely proportional to width of the energy group:

$$f(E) = \frac{1}{\Delta E_g} \tag{2.5}$$

However this approximation is sufficiently precise only in energy regions where $\sigma(E)$ has no resonances. The flux intensity change due to self-shielding effect should be taken into account in the vicinity of resonances as well as for the highly neutron thermalizing materials. The main assumption regarding self-shielding treatment is that in a resonance, the flux decreases approximately inversely proportionally to the total cross-section. As the cross-section parameters of bulk materials are known, resonance self-shielding problem could be defined as a proper evaluation of the group flux at the resonance. One of possible assumptions is known as Bondarenko method [92, 93] when group flux is simply expressed as function inversely proportional to total macroscopic cross-section:

$$f(E) \sim \frac{1}{N\sigma_t(E)} \tag{2.6}$$

More complicated, but also more precise is Nordheim integral method to address the self-shielding of materials within resonance region taking into account the impact of the moderator. Nordheim integral is complicated integral expression which allows evaluate $f(E)$, taking into account material cross-sections, Dancoff factor, energy variations of the neutron flux in the moderator, etc.

If we go back to 2.3 assumption, we should continue to analyze the angular flux part responsible for the spacial propagation of neutrons $\Phi(\vec{r}, \vec{\Omega})$. Methods of spherical harmonics and discrete ordinates are usually employed to solve this part of the neutron transport equation. These methods illustrates the concept of an angular discretisation of the angular neutron flux. The main idea of the spherical harmonics method, is the angular flux expansion into the spherical harmonics using Legendre polynomials [94].

If for simplicity sake we take case of plane geometry, neutron flux could be defined as a function of coordinate x. Angular distribution depends on coordinate x and μ where μ is directional component of x, $\mu = cos\theta$ and θ is the direction of particle movement with respect to the x axis. So in case of plane geometry $\Phi(\vec{r}, \vec{\Omega})$ is simplified:

$$\Phi(\vec{r}, \vec{\Omega}) = \Phi(x, \mu) \tag{2.7}$$

If we put 2.7 in the time-independent neutron transport equation for one-group flux, it could be written as:

$$\mu \frac{\partial \Phi(x,\mu)}{\partial x} + \Sigma(x)\Phi(x,\mu) = Q(x,\mu) + \int_{-1}^{1} \Sigma_s(x, \mu' \to \mu)\Phi(x,\mu)d\mu' \tag{2.8}$$

Solution is obtained expanding $\Phi(x, \mu)$ using Legendre polynomials:

$$\Phi(x,\mu) = \sum_{n=0}^{\infty} \frac{(2n+1)}{2} P_n(\mu)\Phi_n(x) \tag{2.9}$$

where

$$\Phi(x) = \int \Phi(x,\mu)P_n(\mu)d\mu \tag{2.10}$$

After we replace $\Phi(x, \mu)$ in 2.8 with expression of 2.9, and use Legendre polynomials recurrence formula, we obtain set of N+1 differential equations:

$$-\frac{n}{2n-1}\Phi'_{n-1}(x) - \frac{n+1}{2n+3}\Phi'_{n+1}(x) - \Sigma(x)\Phi_n(x) + \Sigma_s(x)\Phi_n(x) + Q_n = 0 \tag{2.11}$$

The precision and subsequently calculation time of the solution is determined by N value, which is chosen, as when we assume that $\Phi'_{N+1}(x) = 0$.

Discrete ordinates method [95] is more generalized case of the spherical harmonics when instead of 2.9 we use other discretization. These discretization schemes are quite complicated, but the principle is the same — expansion of Φ and computation of weight coefficients w_n.

$$\Phi(x,\mu) = \sum_{n=0}^{\infty} w_n(\mu)\Phi_n(x) \tag{2.12}$$

Cases for two and three dimensions are even more complicated. In three dimensional case the discrete ordinates are the directions associated with the points placed at the centers of the mesh elements, the corresponding weights are the mesh element areas normalized to 4π [7]. The equation for angular flux might be simplified using discrete ordinates on a case by case basis, taking into account problem dependent geometries and sources. Discrete ordinates method is problematic subject which is widely discussed in publications nowadays. E.g. discrete-ordinates solution for the problem of particle transport in duct [96] or neutron transport solution of single uranium fuel pin using an S_{16} level symmetric angular quadrature set [97]. Other form of neutral transport equation is integral neutron transport equation which is useful in cell and subassembly calculations [91], however detail analysis of this topic is outside the scope of this dissertation.

The non-deterministic method of solving neutron transport problem is a stochastic method called Monte Carlo method [98,99]. Historically this method was developed in Manhattan project to solve neutron and γ-particles transport problem. The general idea of Monte Carlo computational method is simulation of a finite number of particle histories defined by the set of numbers which are randomly chosen from the appropriate probability distributions defining the particle parameters. One of the main advantages of this approach is that it eliminates the need to write out the Boltzmann equation explicitly [7].

In the neutron transport calculations parameters defining the particle are for example energy and scattering angles. Particle history begins at initial coordinates with set of variables, sampling particle distance of travel to the

collision. Then, taking into account to given cross-sections and particle parameters, collision is treated either as an absorption either as a scattering event.

If it is (n, γ) reaction, particle history ends. The capture also might cause a fission, in this case new particles with new parameters are generated. Scattering might be elastic, or inelastic. In both cases new set of parameters are generated for scattering angle and energy (in case of inelastic scattering). The particle history is followed until it is absorbed or leaves the system. For correct Monte Carlo evaluation of the neutron transport problem we need a representative distribution of the neutrons in terms of energy, coordinates and direction of movement.

One advantage of Monte Carlo method is possible continuous treatment of the energy and other parameters therefore errors caused by discretization could be avoided. However computation of the detailed local quantities, such as the flux within a spatial cell, can be difficult to estimate due to the need of sufficient number of particles, as well as the case with low neutron flux, when specific techniques of variance reduction are needed [7, 100].

During Monte Carlo calculation N samples of variable x are generated and $\bar{x}$ mean of the desired variable is calculated:

$$\bar{x} = \frac{1}{N} \sum_{n=1}^{N} x_n \tag{2.13}$$

while statistical uncertainty is calculated as:

$$\sigma_N^2 = \frac{1}{N} \sum_{n=1}^{N} (x_n - \bar{x}) \tag{2.14}$$

The errors in this type of calculations are related with the stochastic origin of the calculations. Regarding statistical uncertainty of Monte Carlo solutions — it depends on number of particles generated: $\sigma_{st} \sim N^{-1/2}$, therefore the time and available computational speed determines the accuracy of the calculations.

Regarding other methods of the neutron transport calulations, a number of

hybrid deterministic-probabilistic methods are also developed and discussed in the scientific literature [100–102] .

The time-dependent behavior of the neutrons in a system with fissionable material depends on the ratio between the production terms (terms with plus sign in eq. 2.1) and the absorption and leakage terms (terms with minus sign in eq. 2.1). We assume that neutron source term are only neutrons from fissions:

$$Q(\vec{r}) = \nu\Sigma_f\Phi(\vec{r}) \tag{2.15}$$

where ν is average number of neutrons from one fission.

If the production term exceeds the absorption and leakage terms, the neutron population increases, and in the reversed case it decreases. It would be convenient to obtain a measure for the neutron population dynamics, without having to solve a complicated time-dependent equation 2.1. One can obtain a measure of the neutron population dynamics introducing a coefficient k The source term is divided by k in a steady-state equation. Physically this means that one adjusts the system to be critical by changing neutron production per fission. Mathematically this gives an eigenvalue equation with eigenvalue k. If we ignore scattering term, apply diffusion approximation [5, 7] and integrate over the volume of the system we would obtain this equation for k:

$$k = \frac{\int \nu\Sigma_f\Phi(\vec{r})dV}{\int \Sigma_t\Phi(\vec{r})dV - \int \vec{\nabla}D(\vec{r})\vec{\nabla}\Phi(\vec{r})dV} \tag{2.16}$$

where $D(\vec{r})$ is diffusion coefficient. This coefficient k, which defines neutron population dynamics in critical or sub-critical systems is called the effective neutron multiplication factor (k_{eff}).

Generally k_{eff} calculations are not trivial. To calculate it, one should know information about material composition and geometry of the system, precise microscopic cross-sections of the materials. Also physical effects (e.g. Dopler effect, self-shielding etc.) should be properly addressed. k_{eff} value might be affected even by neutron energy interval discretization used in calculations

— different number of energy groups used, usually give slightly different k_{eff} value. To sum up, k_{eff} calculation spent nuclear fuel storage cask and identification of main contributors to k_{eff} provides deeper knowledge about physics of spent nuclear fuel storage systems.

2.2. Bateman equations

Changes of the nuclide concentrations in time during and after the irradiation are evaluated using well-known set of extended Bateman equations 2.17, which are the first order differential equations. "Extended" means that new terms representing nuclear fission and activation are added to the original set of Bateman equations [103].

$$\frac{dN_i(t)}{dt} = \sum_j f_{j\to i}\sigma_{f,j}N_j(t)\Phi + \sigma_{c,i-1}N_{i-1}(t)\Phi + \sum_j l_{j\to i}\lambda_j N_j(t) - \\ -\sigma_{f,i}N_i(t)\Phi - \sigma_{c,i}N_i(t)\Phi - \lambda_j N_j(t) \tag{2.17}$$

where

$N_i(t)$ — concentration of nuclide i at time t;

$f_{j\to i}$ — branching fraction of j nuclide fission to nuclide i;

$\sigma_{f,j}$ — microscopic energy-averaged neutron induced fission cross-section of nuclide j;

Φ — energy-averaged neutron flux;

$l_{j\to i}$ — branching fraction of j nuclide decay to nuclide i;

λ_j — decay constant of nuclide j ;

$\sigma_{c,i}$ — microscopic energy-averaged neutron capture cross-section of nuclide i.

The positive terms in the right side of the equation represents an increase while negative terms represents a decrease of the nuclide concentration due to fissions, neutron capture and decay.

The main difficulties of solving Bateman equations comes from the fact that simulating nuclear fuel we have a large number of nuclides in the fuel or

other material, and consequently a large set of the equations and parameters is necessary. In practice it is assumed that we can remove short-lived nuclides with a very low decay constants and terms with a very low cross-sections and/or branching factors. The other problem is already discussed above — proper evaluation of the neutron flux, which depends on material composition. Therefore if we are calculating evolution of the nuclear fuel or activation of the other materials in the reactor, these two problems are interrelated and should be solved together. Due to very large number of variables and equations, numerical computational methods and codes are more practical to use. They are discussed below.

2.3. Computer codes and cross-section libraries

The solution procedure of the neutron transport or depletion (or activation) problems are complicated due to large number of differential equations as well as need of preparation of the parameter information e.g. regarding problem-dependent cross-sections processing and data collection after calculations. Monte Carlo methods are especially demanding of the computational power. Therefore specific computer codes for the neutron transport and depletion calculations are used to solve these problems of various complexity. Basically they take input data of problem geometry, material composition, cross-section data and computes values of desired quantities. These codes may have very different capabilities, but in general their versatility and flexibility, and coupling possibility with other codes determines their popularity in scientific and industrial use. Several codes are presented here which are usually used for reactor or nuclear fuel calculations, but they could have much broader spectrum of possible applications (e.g. characterization of the experiments with pulsed neutron sources etc.). A large database with detailed descriptions

of codes is available at OECD/NEA Data Bank website [76].

Regarding deterministic neutron transport calculations in which steady-state neutron transport equation (See eq. 2.1) is solved, NEWT [95, 104] from SCALE code system, PARCS [105] and French APOLLO3 [106] codes are widely used. CASMO-5 is a coupled state-of-the-art reactor physics code for modeling PWR and BWR fuel [107].

Monte Carlo neutron transport codes are these: French code TRIPOLI-4 [108]. MCNP6 [109] is general-purpose code developed in Los Alamos National laboratory that can be used for neutron, photon, electron, or coupled neutron/photon/electron transport. Oak Ridge National laboratory developes KENO [110] code. Serpent [111] is Finnish three-dimensional continuous-energy Monte Carlo coupled reactor physics burn-up calculations code. PHITS (Particle and Heavy Ion Transport code System) is a general purpose Monte Carlo particle transport simulation code developed in Japan [112].

Depletion and activation codes solve 2.17 equations. The most popular depletion and activation codes are Origen-S [113], Origen-ARP [114] which performs calculations with the ORIGEN-S code using pre-generated problem-dependent cross-sections, Monteburns [115] is a burn-up code coupling MCNP with Origen. The depletion capability was added to the PARCS code by developing an external depletion code — DEPLETOR [116]. CINDER90 code, usually used together with MCNPX, predicts the evolution of nuclide densities of radioactive material, or a material exposed to neutron irradiation [117]. A code developed in the United Kingdom, Fispact-II is an inventory code capable of performing modeling of the activation, transmutations and burn-up induced by neutron, proton, alpha, deuteron or gamma particles incident on matter [118].

The main requirement for these codes is acceptable agreement with experimental data, e.g. with data from Criticality Safety Benchmark Evaluation Project [119]. In order to compare them in a consistent manner, neutron

transport benchmark calculations are performed [39,120,121] to validate codes against the experimental data.

Neutron reactions with nucleus are defined using cross-section concept. Cross-section express the likelihood of particular interaction between an incident neutron and a target nucleus. For a given nucleus and reaction type, the cross-section strongly depends on the neutron energy. Some typical nuclear reaction databases exist which contain the evaluated cross-sections, spectra, angular distributions, fission product yields and thermal scattering law data of neutron induced reactions. Most notable of them are US evaluated nuclear data library ENDF/B-VII.1 [122], Japanese JENDL-4.0 [123] library and OECD/NEA developed JEFF-3.2 library [124].

2.4. SCALE package

SCALE code package is a state-of-the-art comprehensive modeling and simulation tool for nuclear safety analysis and design that is developed by Oak Ridge National Laboratory (ORNL) in the USA. It is suitable for calculations of various criticality safety and radiation shielding problems. Using SCALE, spent nuclear fuel and radioactive source term characterization, as well as sensitivity and uncertainty analysis could be performed. At the start of this research, SCALE version 6.0 [40] and a bit later version 6.1 were released. The motivation for choosing this tool for calculations was its long history of validation against experimental data [125, 126], constant development, flexibility regarding specific problems and user-friendly interface. SCALE 6.1 has tens of different modules, however here are presented those that are mostly used in calculations presented in this dissertation.

The TRITON computer code is SCALE control module for transport, depletion, sensitivity and uncertainty analysis. Transport calculations to solve neutron transport problems (see Section 2.1 for theoretical background) could

be performed using deterministic NEWT and probabilistic KENO-VI codes.

NEWT is a deterministic multi-group discrete-ordinates neutron transport computer code within two-dimensional geometry. NEWT uses cross-sections processed by other SCALE modules, using geometry and parameters of materials inputs. NEWT calculates fluxes, multi-group cross-sections and subsequently power distributions. These parameters could be used later in all necessary material depletion and activation calculations needed for a lattice physics analysis. NEWT allows the lattice-physics calculations in which, for example, material homogenization (using averaged cross-sections) could be performed.

KENO-VI is Monte Carlo transport code used to calculate energy- dependent and region-dependent flux and fission parameters as well as to evaluate k_{eff} in a multi-group and a continuous energy mode.

ORIGEN-S solves 2.17 equation system and calculates time-dependent concentrations, activities, and radiation source terms for a large number of isotopes simultaneously using a multi-group and a continuous energy distributions.

ORIGEN-ARP is the depletion analysis sequence used to perform point-depletion calculations with the ORIGEN-S code using problem-dependent cross-sections. Problem-dependent cross-section libraries are generated using the ARP (Automatic Rapid Processing) module using an interpolation algorithm that operates with the pre-generated libraries.

STARBUCS is calculation sequence for automating criticality safety calculations of the spent nuclear fuel systems employing burn-up credit. It automatically performs all necessary calculations with ORIGEN-ARP to determine spent fuel compositions, self-shielded cross sections using BONAMI or NITAWL, and the k_{eff} of the spent nuclear fuel configuration.

Problem dependent cross-section data are prepared by the following procedure: CRAWDAD module reads cross-sections from the material cross-section libraries (e.g. ENDF/B-VII.0) for each material appearing in a problem and combines all data into a single problem-dependent CENTRM library file. Then

BONAMI or NITAWL performs the resonance self-shielding calculations, WORKER creates a working format library from a master format library, CENTRM calculates a point-wise continuous flux spectrum using the point-wise continuous cross-section library and PMC collapses the point-wise continuous cross sections to a set of multi-group cross sections which are used for the transport calculations by NEWT or KENO-VI. Regarding the depletion and activation calculations, COUPLE computes problem-dependent ORIGEN-S neutron cross-sections from a multi-group working format library that are used by ORIGEN-S to calculate the isotopic concentrations.

In addition to these capabilities SCALE6.1 may also be used for the radiation shielding calculations as well as the sensitivity and uncertainty analysis. ENDF/B-VII.0 cross-section data library available with SCALE package was used in all calculations.

3. Cross-section libraries

3.1. RBMK nuclear fuel and its nuclide composition

There are two graphite moderated, boiling water RBMK-1500 reactors at the Ignalina site in the north-east of Lithuania. Unit 1 operated in 1984–2004, Unit 2 — in 1987–2009. One of the most important remaining issues regarding nuclear safety is the spent nuclear fuel (SNF) storage. There are about 22000 assemblies of SNF which have to be safely stored until the final decision regarding SNF management — reprocessing or disposal — is made. Part of SNF assemblies is stored in the existing interim dry type SNF storage facility containing 20 CASTOR®RBMK-1500 and 98 CONSTOR®RBMK-1500 storage casks containing 2.0% ^{235}U initial enrichment uranium SNF bundles. Up to 200 of new CONSTOR®RBMK-1500/M2 type casks for storage and transportation are designed to be used for SNF storage in the dry type storage facility in the vicinity of the Ignalina NPP. One of the key elements of the safety analysis of these facilities is SNF characterization regarding the composition and related activity as well as the neutron emission.

Information about the quantity of fissile isotopes in nuclear fuel also might be used for safeguards purposes [127]. The SNF composition determination using direct or indirect experimental techniques is rather expensive and technically complicated. Therefore, computer modeling is often used to evaluate SNF characteristics [22, 27, 42]. However, validation of these results is also essential: results of calculations of varying complexity should correspond to the available experimental knowledge [23, 88, 89].

New computational codes, the improved computational speed and improved capabilities (e.g. 3D modeling geometry) for burn-up analysis allow evaluating the fuel depletion more precisely. Use of pre-generated reactor and burn-up

specific cross-section libraries allows rapid simulating of the fuel composition and related parameters with acceptable accuracy [128]. This information might be used for various applications, e.g. as a reference point, designing experiments regarding determination of the fuel composition, properly evaluating the effective neutron multiplication factor in systems with spent nuclear fuel, estimating doses in case of probable accidents, etc. The availability of accurate and validated calculation results is essential for the possible use of burn-up credit in SNF storage facility analysis. Information of the exact operating conditions might be used for evaluation of a fast and sufficiently precise axial and horizontal composition profile.

The main aim of this part is to create the representative numerical model of the RBMK reactor lattice and numerically simulate the nuclear fuel burn in the reactor in order to generate one neutron energy group cross-section libraries for nuclear fuel. And subsequently to perform comparison of the predicted spent nuclear fuel composition with available experimental data to ensure the validity of the model. Validated one group cross-section libraries for 2.4–2.8% enrichment fuel with erbium burnable absorber were not created up to this time. These libraries allow not only simple evaluation of SNF composition and activity but also provide background for further novel studies of burn-up credit effect in SNF storage systems with this type of fuel.

Pre-generated burn-up specific cross-section libraries for various type reactors and fuels are validated and available [129]. Library for RBMK-1000 fuel depletion modeling also exists, however there are no libraries for erbium fuel used in RBMK-1500 type reactors [128, 130]. Calculations of the fuel depletion in RBMK-1500 type reactor and generation of one group cross-section libraries for SNF composition calculations for erbium fuel are presented here. In order to introduce one-group cross section libraries for burn-up credit calculations of RBMK-1500 spent nuclear fuel we are focusing on the precise evaluation (taking into account comparison of calculations against the experimental data) of

fissile and non-fissile actinides which are important for burn-up credit calculations. Available experimental data of fission products (Nd and Cs isotopes) were also compared to modeling results.

Concentrations of these actinides (^{234}U, ^{235}U ^{236}U, ^{238}Pu, ^{239}Pu, ^{240}Pu, ^{241}Pu, ^{242}Pu, ^{237}Np, ^{241}Am, ^{243}Am) were calculated for RBMK-1500 erbium fuel and for non-erbium fuel taking into account different reactor operation conditions. Obtained data were compared to existing experimental data and results of other calculations. Actinides used for "actinide-only" calculations were taken from NEA study [11]. Besides, ^{242}Cm and ^{244}Cm concentrations were evaluated. Cm isotopes are important for the thermal and radiation shielding evaluation during dry storage, but not so vital regarding burn-up credit calculations. ^{142}Nd, ^{143}Nd, ^{144}Nd, ^{145}Nd, ^{146}Nd, ^{148}Nd, ^{150}Nd and ^{137}Cs concentrations were also calculated, as limited experimental data exist for them too. Concentration ratios of these nuclides are often used to precisely evaluate burn-up of nuclear fuel [131].

Only limited experimental data are available for the composition of RBMK type reactor fuel [88,89], especially regarding fuel with erbium burnable absorber used in Ignalina NPP RBMK-1500 type reactors. Most of RBMK-1000 physical characteristics are very similar to those of RBMK-1500, therefore the use of experimental data from RBMK-1000 is properly justified. Also modeling was performed in this area: MCNP and ORIGEN codes were used for depletion calculations for RBMK-1000 fuel and comparison with experimental data was performed by [27, 28, 42]. SCALE, HELIOS codes were used by [43] to calculate concentrations of some isotopes. RBMK-1500 type reactor SNF depletion calculations and SNF storage cask criticality calculations were performed by Smaizys and Poskas [9]. Furthermore there were some studies related with Ignalina NPP decommissioning projects [3].

3.2. Generation of one-group cross-section libraries

SCALE 6.1 code package, which is widely used for criticality and burn-up calculations to justify safety of various activities in nuclear field, was used for calculations here [40]. TRITON control module employing NEWT (2D geometry and deterministic calculation method to solve neutron transport equations and calculate neutron flux) and ORIGEN-S (used for depletion calculations) codes was used to generate cross-section libraries. Cross-sections of nuclides were obtained from ENDF/B-VII.0 cross-section data library. NEWT code is used to solve the Boltzmann's transport equation for neutrons (See eq.2.1). In general, the transport equation can be difficult to apply and solve analytically. Hence, simplifications and numerical approximations are used in the code sequence to solve the equation.

ORIGEN-S solves the Bateman equation for systems with neutron flux and calculates the atom density of a set of chosen nuclides (See eq. 2.17). ORIGEN-ARP was used to perform point-depletion calculations with the ORIGEN-S code using problem-dependent cross-section libraries which were generated using the ARP (Automatic Rapid Processing) module. There are number of prepared cross-section libraries available within SCALE for different reactors and fuels [128, 130].

The cross-sections for uranium-based fuels mainly depend on the fuel enrichment, burn-up and water density during burn-up as described in [132]. A set of libraries was generated changing above mentioned parameters. These libraries are used for interpolation of the cross-sections of desired fuel parameters.

The interpolation of cross-section libraries which are used by ORIGEN-S is performed as a function of burn-up first, and then other parameters (enrichment, moderator density) are additionally used for the interpolation as it will

be explained in more detail in the next section.

Model and calculations

A simplified model of the RBMK-1500 reactor core fragment with 14 fuel assemblies and 2 control rods distributed according to the real RBMK-1500 reactor core geometry was used for modeling (see Fig. 3.1). The Control and Protection System (CPS) rod with neutron absorber B_4C as used in the original design of RBMK was inserted and the other CPS rod was extracted, while channels were filled with water of the chosen density.

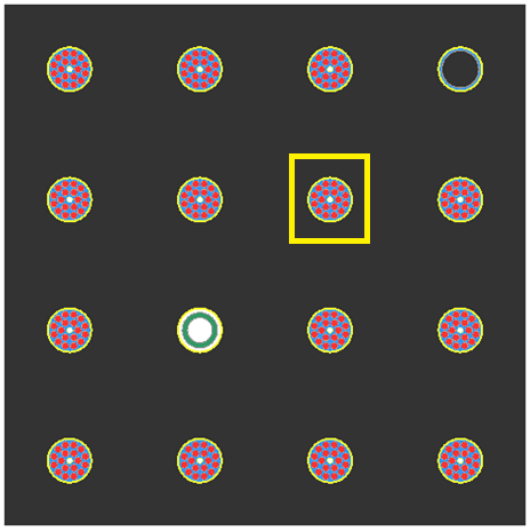

Figure 3.1: RBMK-1500 reactor lattice with fuel(14) and CPS(2) channels. Fuel assembly in marked channel was used for depletion calculations to obtain cross-section libraries

RBMK-1500 fuel assembly consists of 2 fuel bundles each of them has 18 fuel rods arranged in two concentric rings with the central carrier rod at the centre. The fuel rod was treated as a zirconium alloy tube homogeneously filled with uranium dioxide with or without burnable erbium absorber. The pellet density was reduced to ensure that the amount of fuel material inside the tube corresponds to actual data [29]. The gap between the pellet and cladding as well as the hole in the middle of the pellet were excluded to simplify geometry

and reduce computational time. The central carrier rod was defined as a hollow tube made from zirconium alloy. Water as a moderator and lattice cell with triangular pitch with half-pitch of 0.802 cm were chosen for self-shielding calculations in CENTRM module [22, 133]. Periodical boundary conditions were applied for reactor segment walls, which correspond to an infinite lattice comprised of such segments and are suitable for efficient modeling of neutron fluxes in the RBMK-1500 reactor core.

Temperatures of graphite and cooling water were kept equal to 873 K and 567 K, respectively, which correspond to the real operating conditions of the RBMK-1500 reactor [29]. The density of the cooling water in the model varied from 0.2 g/cm^3 to 0.8 g/cm^3 and the density of graphite was 1.675 g/cm^3. The average k_{eff} value of such a system for 12 GWd/tU burn-up fuel varied from 0.934 (for 2% enrichment, 0.2 g/cm^3 water density) and 1.012 (for 2.8% enrichment, 0.4 g/cm^3 water density. k_{eff} uncertainty (convergence criterion of calculations) did not exceed 0.001.

Depletion calculations for the preparation of cross-section libraries consisted of two steps. The first step was a depletion of the fresh fuel in all fuel channels to the average burn-up (12 GWd/tU). The second step was depletion of fuel in one fuel channel (marked channel in Fig. 3.1), while the composition (set of 100 nuclides consisting of initial fuel material, activation and fission products) taken from the first step calculations and corresponding to the average fuel burn-up was kept constant in remaining fuel channels. The neutron fluxes were calculated by NEWT module using three 160 day time steps (power was kept constant: 25 MW/tU, corresponding reactor thermal power — 4700 MW) for the first step calculations, the average burn-up was achieved at all fuel channels after this step. The second step calculations for libraries were performed using a more detailed 100 day time step, keeping the 25 MW/tU power constant up to 30 GWd/tU burn-up. The same procedure was applied for non-erbium fuel with 2.0% enrichment and 2.4% (with 0.41% mass of Er_2O_3 burnable

absorber), 2.6% (0.5% Er_2O_3) and 2.8% (0.6% Er_2O_3) enrichment fuel with erbium burnable absorber. The natural erbium isotopic composition was used for calculations (isotopic mass fractions are: 1.7% ^{164}Er, 33.4% ^{166}Er, 22.9% ^{167}Er, 26.9% ^{168}Er, 15.1% ^{170}Er).

After these steps, files containing cross-section libraries were collected and grouped taking into account the enrichment and water density used in the calculations. Two separate libraries were created: the first one for 2.0% enrichment fuel without erbium and the second one — for 2.4–2.8% enrichment erbium fuel depending on the different initial fuel composition. Cross-sections were stored as average one-group values that were obtained by weighting multi-group neutron cross-sections. The cross-section libraries are sets of the cross-section data, representing certain reaction probabilities for a given parameters. For example, in Fig. 3.2 the neutron absorption cross-section as a function of fuel burn-up for ^{240}Pu is given. The cross-section decrease is explained by increasing effect of resonance self-shielding in the fuel with increasing burn-up and subsequent reduction of the thermal neutrons capture rate.

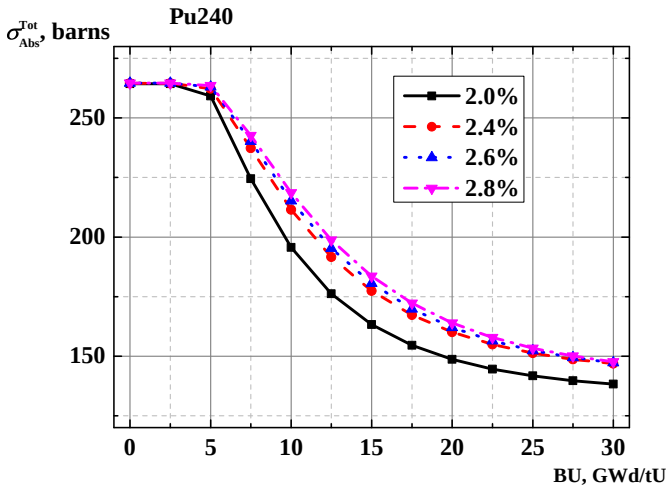

Figure 3.2: ^{240}Pu neutron absorption cross-section normalized to the energy-averaged flux as a function of fuel burn-up for different enrichment fuel.

3.3. Evaluation of the libraries

In order to validate our results we have taken available RBMK-1000 reactor fuel experimental data [88, 89] and also independent TRITON point-depletion calculations presented in [42] to assure that concentrations predicted by cross-section libraries are in satisfactory agreement with independent point depletion calculations and experimental data. More detailed TRITON calculations are available only for ^{238}Pu, ^{240}Pu and ^{242}Pu. For all nuclides only data from two different burn-up fuel assemblies for 2% enrichment fuel are available. Due to different positions of fuel samples taken for destructive examination, their burn-up was re-evaluated taking into account concentrations of Nd isotopes [131]. Data for 2.02% and 2.09% initial enrichment fuel are also available. Measured concentrations of different enrichment fuel are marked differently in all figures. Attention should be drawn that experimental data given in [88, 89] are the same, although in [88] initial enrichment was reported to be 2.0% in all fuel samples.

The nuclide concentration dependence on burn-up and coolant density for the validation of cross-section library results was evaluated using the ORIGEN-ARP code. Two cases were analyzed: the constant power and the constant neutron fluence. The average power of 22.5 MW/tU was used for constant power calculations and the initial power of 22.5 MW/tU for fresh fuel was used in the constant neutron fluence case. Two coolant density values were chosen for composition calculations: 0.4 g/cm^3 and 0.8 g/cm^3.

Concentrations of actinides important to burn-up credit (^{234}U, ^{235}U ^{236}U, ^{238}Pu, ^{239}Pu, ^{240}Pu, ^{241}Pu, ^{242}Pu, ^{237}Np, ^{241}Am, ^{243}Am), ^{242}Cm, ^{244}Cm as well as of some fission products (^{142}Nd, ^{143}Nd, ^{144}Nd, ^{145}Nd, ^{146}Nd, ^{148}Nd, ^{150}Nd and ^{137}Cs) were calculated for RBMK-1500 erbium fuel and for non-erbium fuel. Comparison was performed between calculated and experimentally measured concentrations expressed in grams of certain isotope per metric ton of ^{238}U.

Uranium isotopes

Differences between different uranium isotopes are mainly determined by the initial composition, therefore largest differences for different enrichment fuel are observable for ^{234}U (Fig. 3.3) and ^{235}U (Fig. 3.4) isotopes. The difference is proportional to the initial enrichment. Experimental values for 2% enrichment fuel shows satisfactory agreement (difference between experimental and calculated values is 9–14% for ^{234}U, 13–16% for ^{235}U, 5–14% for ^{236}U (Fig. 3.5)) with values generated from cross-section libraries.

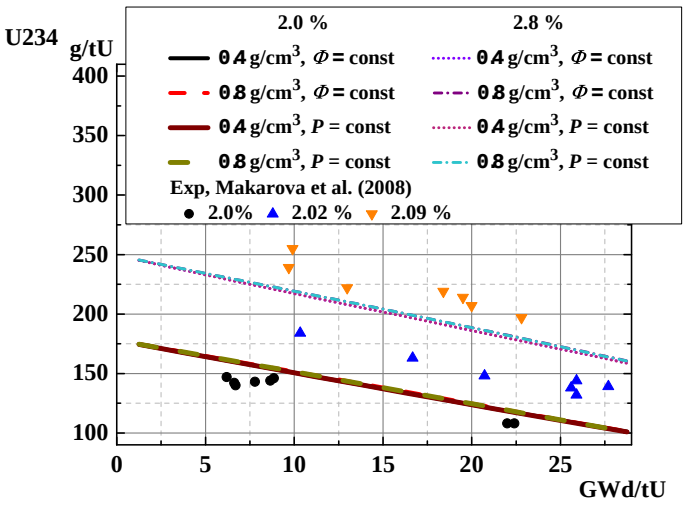

Figure 3.3: ^{234}U concentrations for different enrichment RBMK-1500 fuel calculated using generated neutron cross-section libraries in constant flux and constant power cases and experimental points from [89].

Difference between experimental and calculated values in case of ^{234}U isotope is caused by a slightly different initial composition in 2.02% and 2.09% initial enrichment fuel, but the computational evaluation follows the experimental tendency of a linear decrease of ^{234}U concentration as burn-up increases. ^{236}U differences in experimental data for 2.02% and 2.09% initial enrichment fuel are assumed to be caused by a different initial composition due to the fact that 2.02% and 2.09% initial enrichment fuel is manufactured using regener-

ated uranium obtained through reprocessing of SNF. Modeled concentrations of ^{235}U show good agreement with experimental results.

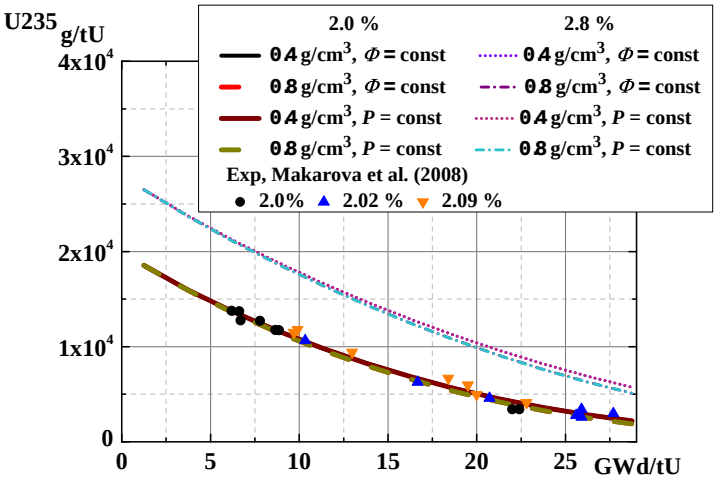

Figure 3.4: ^{235}U concentrations for different enrichment RBMK-1500 fuel calculated using generated neutron cross-section libraries in constant flux and constant power cases and experimental points from [89].

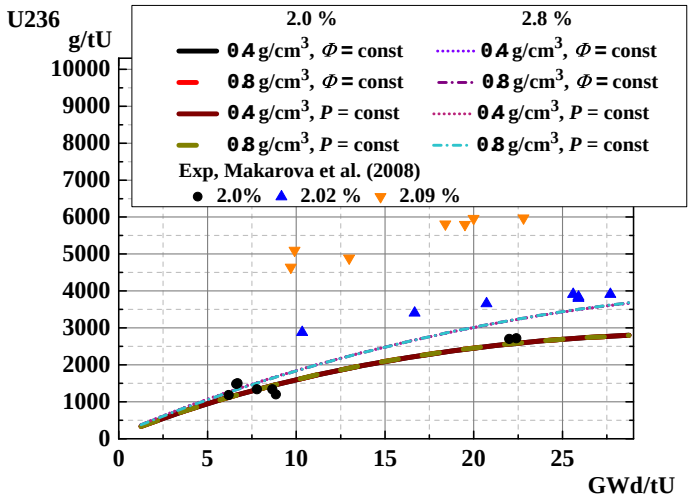

Figure 3.5: ^{236}U concentrations for different enrichment RBMK-1500 fuel calculated using generated neutron cross-section libraries in constant flux and constant power cases and experimental points from [89].

Plutonium isotopes

Plutonium isotopes are analyzed considering a different enrichment of RBMK-1500 fuel and compared with existing experimental data for ^{238}Pu (Fig. 3.6), ^{239}Pu (Fig. 3.7), ^{240}Pu (Fig. 3.8), ^{241}Pu (Fig. 3.9), ^{242}Pu (Fig. 3.10). Concentrations of plutonium ^{238}Pu ^{240}Pu, ^{241}Pu, ^{242}Pu isotopes in nuclear fuel are highest in 2.0% enrichment fuel, with the exception of ^{239}Pu the predicted concentration of which is highest in 2.8% enrichment fuel.

In case of ^{238}Pu, experimental values exceed our prediction up to 2 times for 2.02% and 2.09% initial enrichment fuel, and this is caused by a different initial concentration of parent nuclide ^{237}Np which is obtained through activation of ^{236}U discussed above. The comparison of our results with other values obtained by [89] shows better agreement with our prediction. Agreement with experimental and calculated values is satisfactory for other plutonium isotopes — the difference between experimental and calculated values is 5–6% for ^{239}Pu, 5–25% (highest difference for low burn-up) for ^{240}Pu, 5–15% for ^{241}Pu, 5–19% for ^{242}Pu. Our calculations show good agreement with TRITON point-depletion calculations.

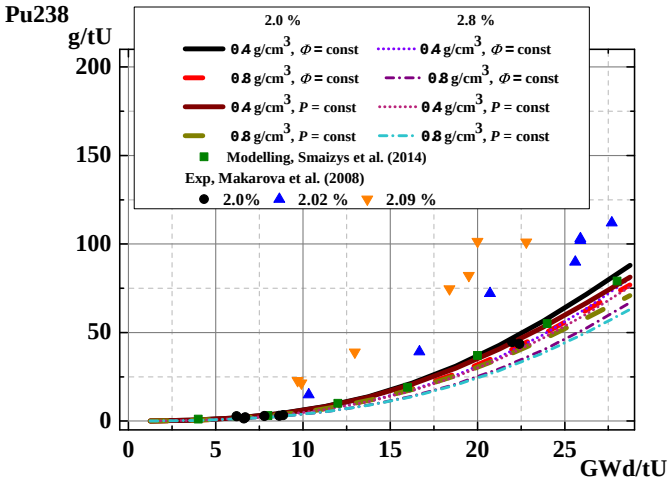

Figure 3.6: ^{238}Pu concentrations for different enrichment RBMK-1500 fuel calculated using generated neutron cross-section libraries in constant flux and constant power cases and experimental points from [89] as well as point depletion modeling results from [42].

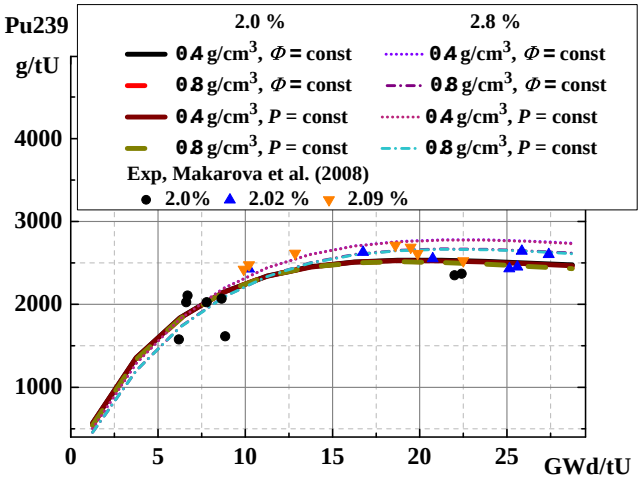

Figure 3.7: ^{239}Pu concentrations of generated libraries for different enrichment RBMK-1500 fuel calculated using generated neutron cross-section libraries in constant flux and constant power cases and experimental points from [89].

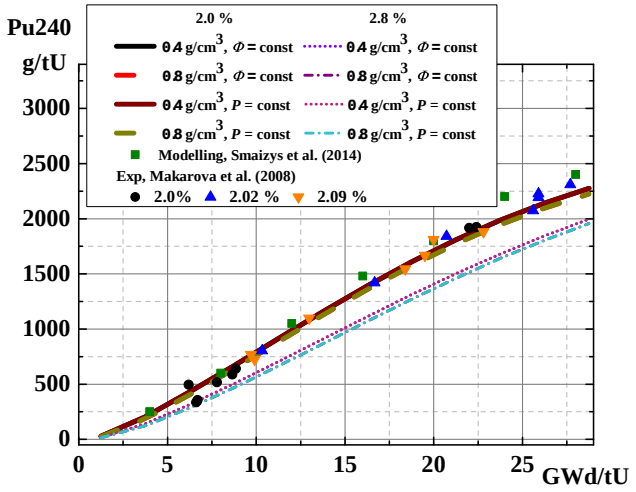

Figure 3.8: ^{240}Pu concentrations for different enrichment RBMK-1500 fuel calculated using generated neutron cross-section libraries in constant flux and constant power cases and experimental points from [89] as well as point depletion modeling results from [42].

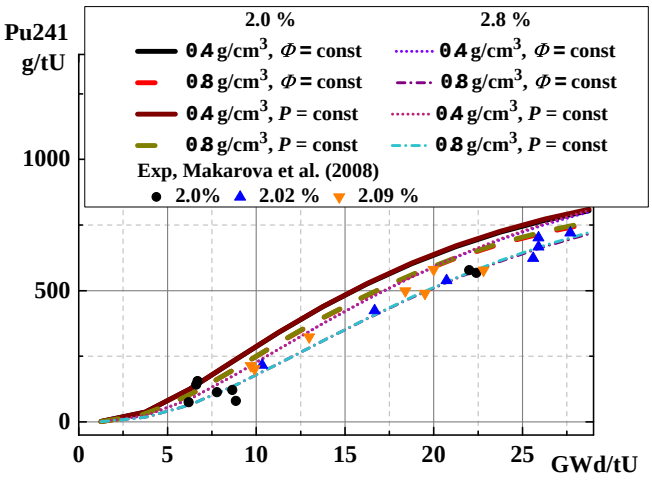

Figure 3.9: ^{241}Pu concentrations of generated libraries for different enrichment RBMK-1500 fuel calculated using generated neutron cross-section libraries in constant flux and constant power cases and experimental points from [89].

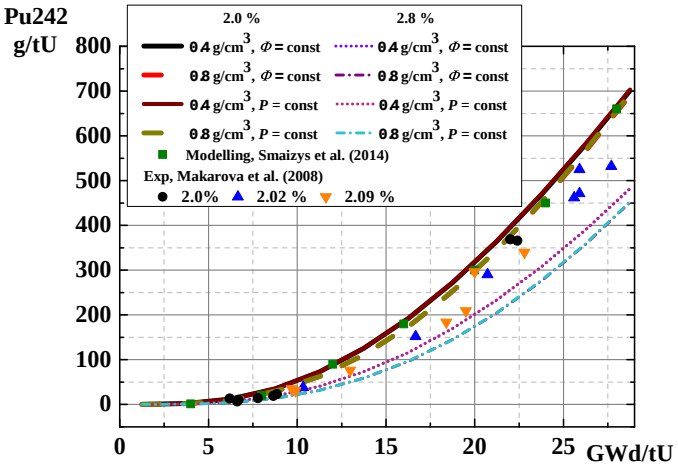

Figure 3.10: ^{242}Pu concentrations for different enrichment RBMK-1500 fuel calculated using generated neutron cross-section libraries in constant flux and constant power cases and experimental points from [89] as well as point depletion modeling results from [42].

Americium and neptunium

Prediction of the concentration of ^{241}Am (Fig. 3.11) completely does not correspond to experimental values of [89]. As we analyzed other studies performed in this field [23], we found that possible concentrations (modeled and experimental) of ^{241}Am in other reactor types showed similar results to our calculations, therefore we believe that experimental values either are not correct or are not presented correctly. We assumed that concentrations given in [89] were 1000 times lower than actual, therefore we give updated experimental values in Fig. 3.11. These results show better agreement, especially at low burn-up.

^{243}Am (Fig. 3.12) difference shows good agreement with experimental values with the difference up to 23%, while ^{237}Np (Fig. 3.13) shows a difference of 22-29% for 2% initial enrichment fuel, while concentrations of experimental values of ^{237}Np for 2.02% and 2.09% initial enrichment fuel follow the trend of

parent nuclide ^{236}U.

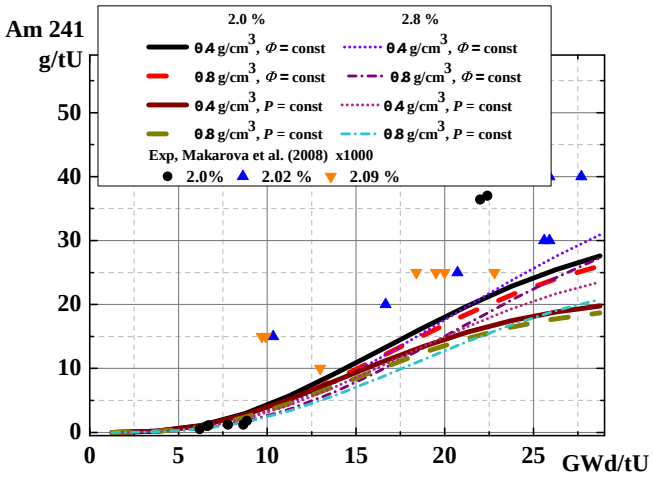

Figure 3.11: ^{241}Am concentrations for different enrichment RBMK-1500 fuel calculated using generated neutron cross-section libraries in constant flux and constant power cases and experimental points from [89].

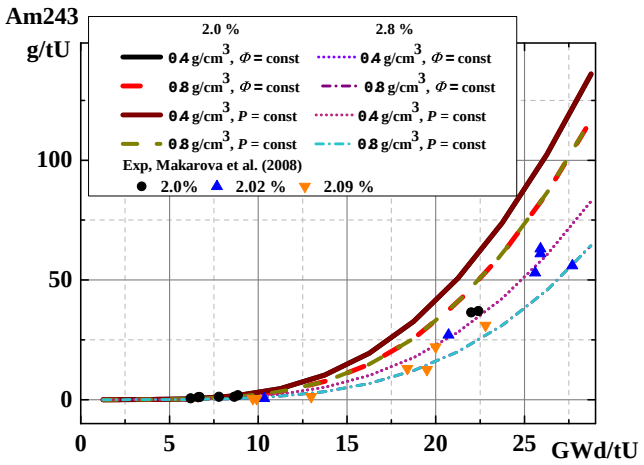

Figure 3.12: ^{243}Am concentrations for different enrichment RBMK-1500 fuel calculated using generated neutron cross-section libraries in constant flux and constant power cases and experimental points from [89].

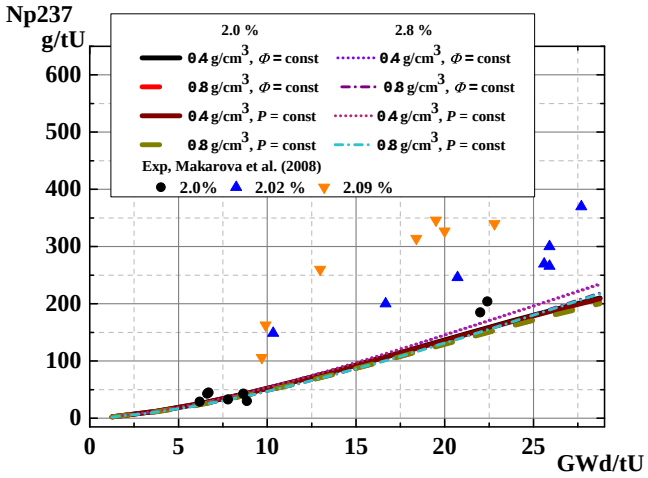

Figure 3.13: ^{237}Np concentrations for different enrichment RBMK-1500 fuel calculated using generated neutron cross-section libraries in constant flux and constant power cases and experimental points from [89].

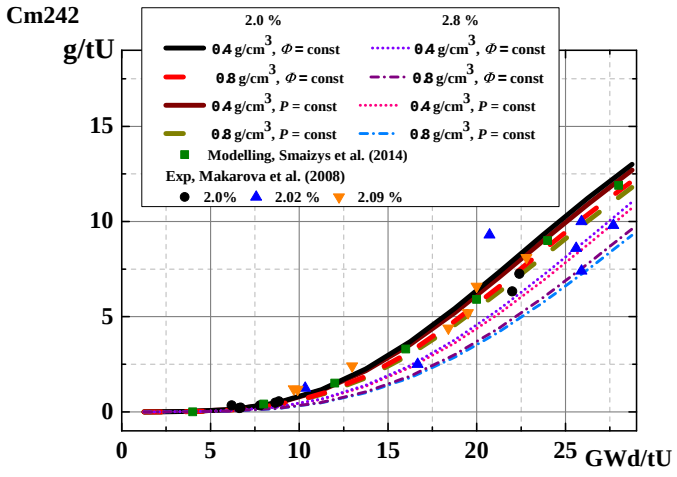

Figure 3.14: ^{242}Cm concentrations for different enrichment RBMK-1500 fuel calculated using generated neutron cross-section libraries in constant flux and constant power cases and experimental points from [89] as well as point depletion modeling results from [42].

Curium

Comparison of ^{242}Cm and ^{244}Cm modeling and experimental values by [89] in Fig. 3.14 and 3.15 shows good agreement with our prediction, except for ^{244}Cm in case of high enrichment where differences reach 40%.

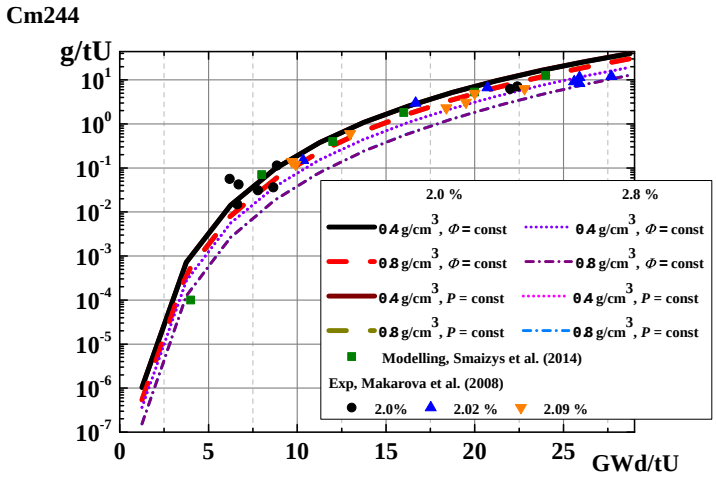

Figure 3.15: ^{244}Cm concentrations for different enrichment RBMK-1500 fuel calculated using generated neutron cross-section libraries in constant flux and constant power cases and experimental points from [89] as well as point depletion modeling results from [42].

Fission products

The comparison between available experimental data given in [130] regarding fission products was also performed. Only ^{142,143,144,145,146,148,150}Nd and ^{137}Cs concentration measurements data are available. Good agreement was found between modeling and experimental results of available fission product measurements (See Figs. 3.16-3.23), except for ^{142}Nd and ^{144}Nd (Fig. 3.17 and 3.19), where differences between prediction and experimental values reach 50% for ^{142}Nd.

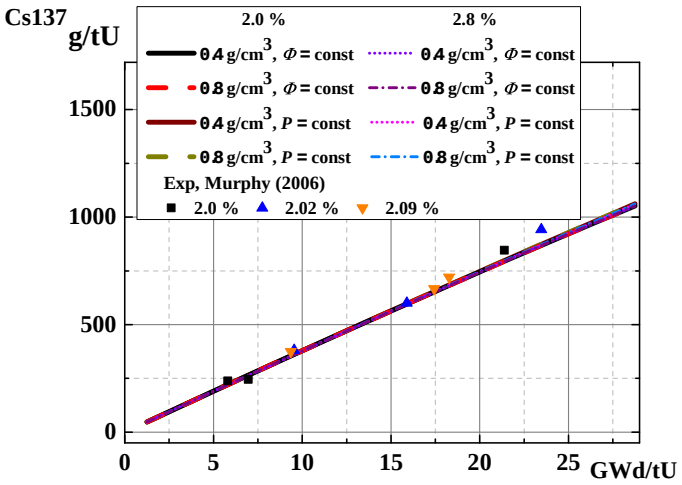

Figure 3.16: ^{137}Cs concentrations for different enrichment RBMK-1500 fuel calculated using generated neutron cross-section libraries in constant flux and constant power cases and experimental points from [130].

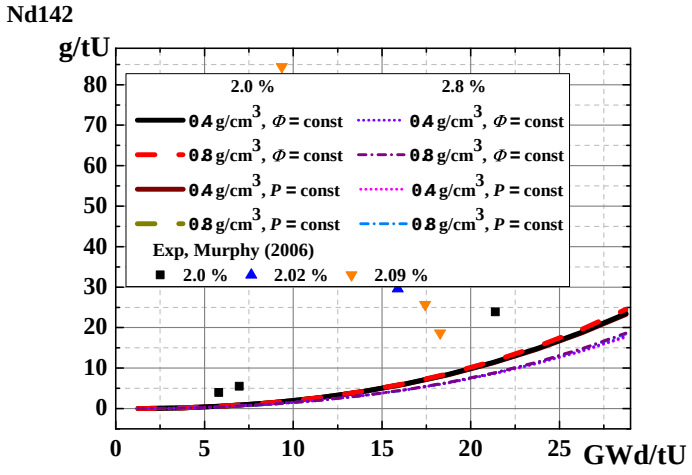

Figure 3.17: ^{142}Nd concentrations for different enrichment RBMK-1500 fuel calculated using generated neutron cross-section libraries in constant flux and constant power cases and experimental points from [130].

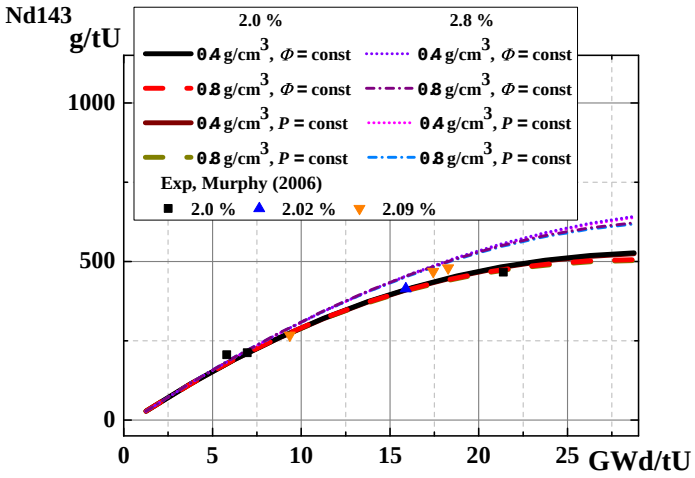

Figure 3.18: ^{143}Nd concentrations for different enrichment RBMK-1500 fuel calculated using generated neutron cross-section libraries in constant flux and constant power cases and experimental points from [130].

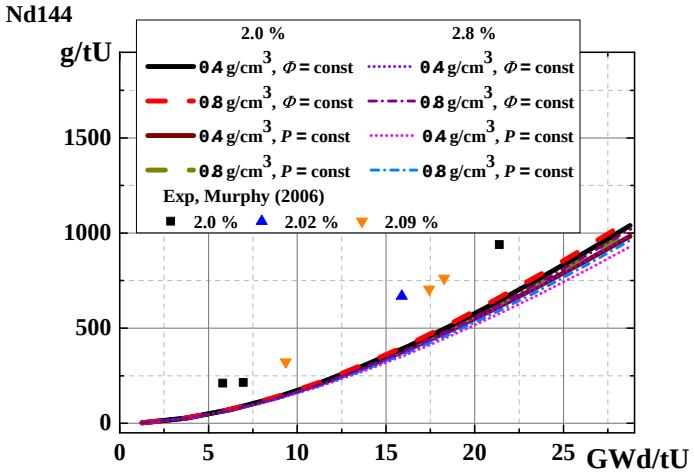

Figure 3.19: ^{144}Nd concentrations for different enrichment RBMK-1500 fuel calculated using generated neutron cross-section libraries in constant flux and constant power cases and experimental points from [130].

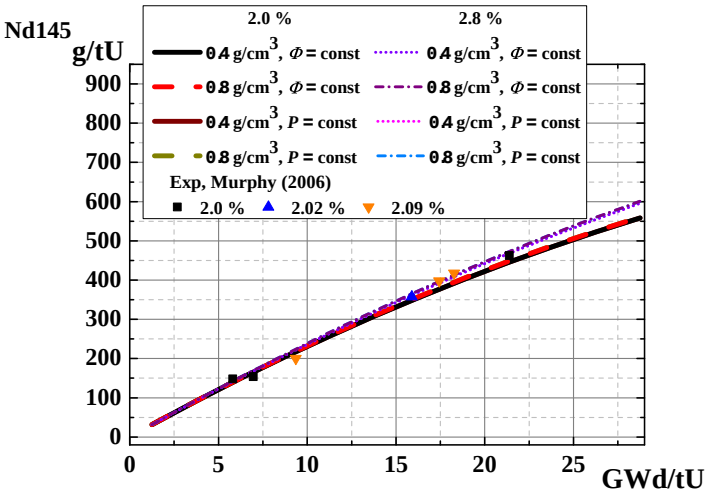

Figure 3.20: ^{145}Nd concentrations for different enrichment RBMK-1500 fuel calculated using generated neutron cross-section libraries in constant flux and constant power cases and experimental points from [130].

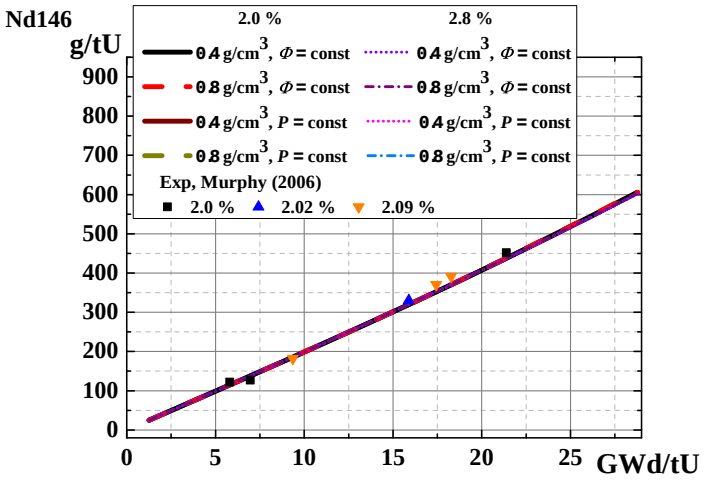

Figure 3.21: ^{146}Nd concentrations for different enrichment RBMK-1500 fuel calculated using generated neutron cross-section libraries in constant flux and constant power cases and experimental points from [130].

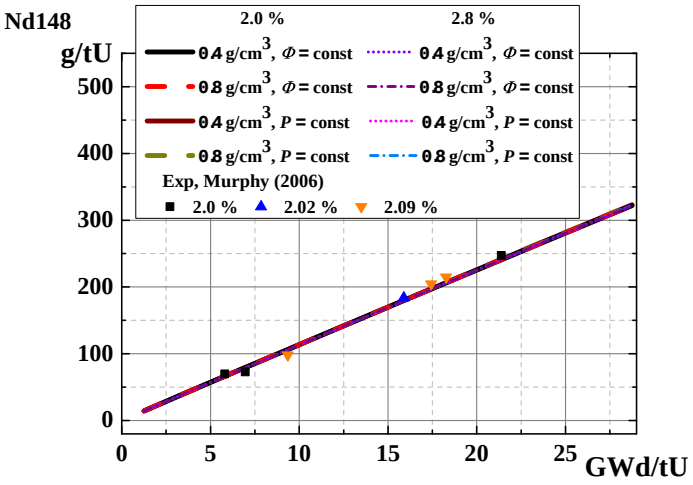

Figure 3.22: ^{148}Nd concentrations for different enrichment RBMK-1500 fuel calculated using generated neutron cross-section libraries in constant flux and constant power cases and experimental points from [130].

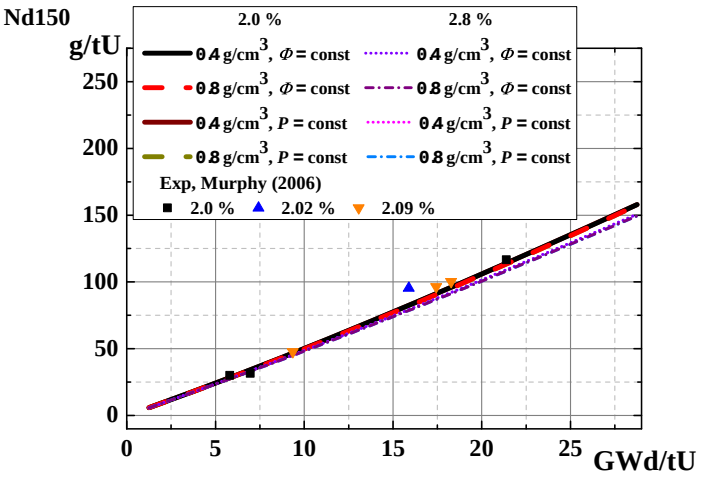

Figure 3.23: ^{150}Nd concentrations for different enrichment RBMK-1500 fuel calculated using generated neutron cross-section libraries in constant flux and constant power cases and experimental points from [130].

Role of enrichment and burnable absorber in the fuel

Enrichment and burnable absorber plays an important role in the SNF composition. Isotopic composition differences for actinides between 2% and 2.8% enrichment fuel at highest burn-up are given in Table 3.1.

Table 3.1: Isotopic composition differences for actinides between 2% and 2.8% enrichment fuel at 29 GWd/tU burn-up

Nuclide	$(\boldsymbol{N}_{2.8}\text{-}\boldsymbol{N}_{2.0})/\boldsymbol{N}_{2.8}$
^{234}U	32%
^{236}U	23%
^{238}Pu	-28%
^{239}Pu	11%
^{240}Pu	-15%
^{241}Pu	11%
^{242}Pu	-36%
^{237}Np	15%
^{241}Am	-40%
^{243}Am	-52%
^{242}Cm	-27%
^{244}Cm	-60%

According to [42] the initial enrichment of RBMK-1000 fuel has no significant effect on the results of nuclide concentrations. Our results show a different trend, especially for ^{234}U, ^{236}U, ^{237}Np and ^{238}Pu. Fuel analyzed in the above mentioned publication was of 1.8-2.2% enrichment without erbium burnable absorber. Therefore, conclusions regarding fuel enrichment in our case should be made not disconnecting different enrichment and the presence of burnable absorber in the fuel.

Higher concentrations of ^{241}Am, ^{243}Am (at low burn-up only), ^{242}Cm, ^{244}Cm, ^{238}Pu, ^{240}Pu, ^{242}Pu are calculated in lower enrichment fuel of the same burn-up. Other nuclides analyzed show a higher concentration in higher enrichment fuel. Regarding Nd and Cs isotopes, a trend of a very low dependence on the fuel enrichment and the presence of burnable absorber is noticed, but ^{142}Nd and ^{143}Nd show different behavior.

Change during burn-up

^{238}Pu, ^{239}Pu, ^{240}Pu, ^{241}Pu, ^{242}Pu, ^{237}Np, ^{241}Am, ^{243}Am, ^{242}Cm and ^{244}Cm nuclides in our model are born as activation nuclides as the initial fuel composition is assumed to consist of uranium isotopes. The concentration of these isotopes increases with increasing burn-up, thus the build-up rate of up to 30 GWd/tU of these nuclides exceeds the burn-up and decay rate. The only exception is ^{239}Pu, the concentration of which of around 23 GWd/tU reaches the maximum value and starts to decrease.

The initial concentration ^{234}U and ^{235}U decreases, while concentration of ^{236}U increases with burn-up. A decrease of ^{234}U is linear with increasing burn-up, while build-up of ^{236}U and burn-out of ^{235}U are slightly decreasing with higher burn-up.

Constant power vs. constant flux

There are no significant differences between the constant flux and constant power cases, the only nuclides, concentrations of which are affected by a different approach, are ^{241}Am and ^{238}Pu. Differences for ^{241}Am isotope was obtained due to its sensitivity to the neutron energy spectrum and the operational power (slightly variable in the constant flux case). Difference for ^{238}Pu is caused by alpha decay of ^{242}Cm to ^{238}Pu, as in constant flux case fuel is approximately 200 days longer in the reactor in comparison with constant power case at burn-up 29 GWd/tU.

Axial nuclear fuel burn-up distribution modeling

The axial burn-up calculations of RBMK-1500 reactor fuel were performed and ^{235}U depletion and build-up of ^{239}Pu, ^{240}Pu and ^{241}Pu were studied in the upper half of one fuel channel for 2.8% enrichment nuclear fuel with erbium burnable absorber. The work was performed in order to assess coolant (water) axial profile influence on the fuel burn-up as well as concentration differences in inner and outer fuel pins. Periodic boundary conditions were used for the side boundaries and mirror boundary conditions for top and bottom of one fuel channel. The inner and outer fuel pins were divided into ten regions of equal length along the reactor core and numbered starting from the center of the core. All concentration values were normalized to the maximum concentration value obtained for the region for a given burn-up.

Evolution of distribution of ^{235}U in 2.8% enrichment fuel is given Fig. 3.24. In Fig. 3.24a ^{235}U distribution changes at the beginning of irradiation of fuel in the reactor (up to 3 GWd/tU) are given. The difference between concentrations increases between the fuel bundle ends at the start of the fuel irradiation. However this difference does not grow after certain burn-up (6 GWd/tU) is achieved (Fig. 3.24b and 3.24d). After the long term operation in the reactor core, depletion caused axial distribution becomes more flat and when burn-up of 15 GWd/tU is achieved, the axial distribution of ^{235}U does not vary essentially along channel axis. Outer and inner rings have the same tendency, but inner ring is depleted more homogeneously — lowest values achieved are 95.2% and 94.0% respectively.

Formation of the analyzed isotopes of plutonium (^{239}Pu, ^{240}Pu and ^{241}Pu) shows the same trend —- very fast formation of plutonium isotopes at the center of the reactor core (differences between concentrations at fuel bundle ends reach 25% for ^{239}Pu, 40% for ^{240}Pu and 50% for ^{241}Pu), and then flattening of the axial distribution curve when burn-up gets higher (Figs. 3.25-3.27).

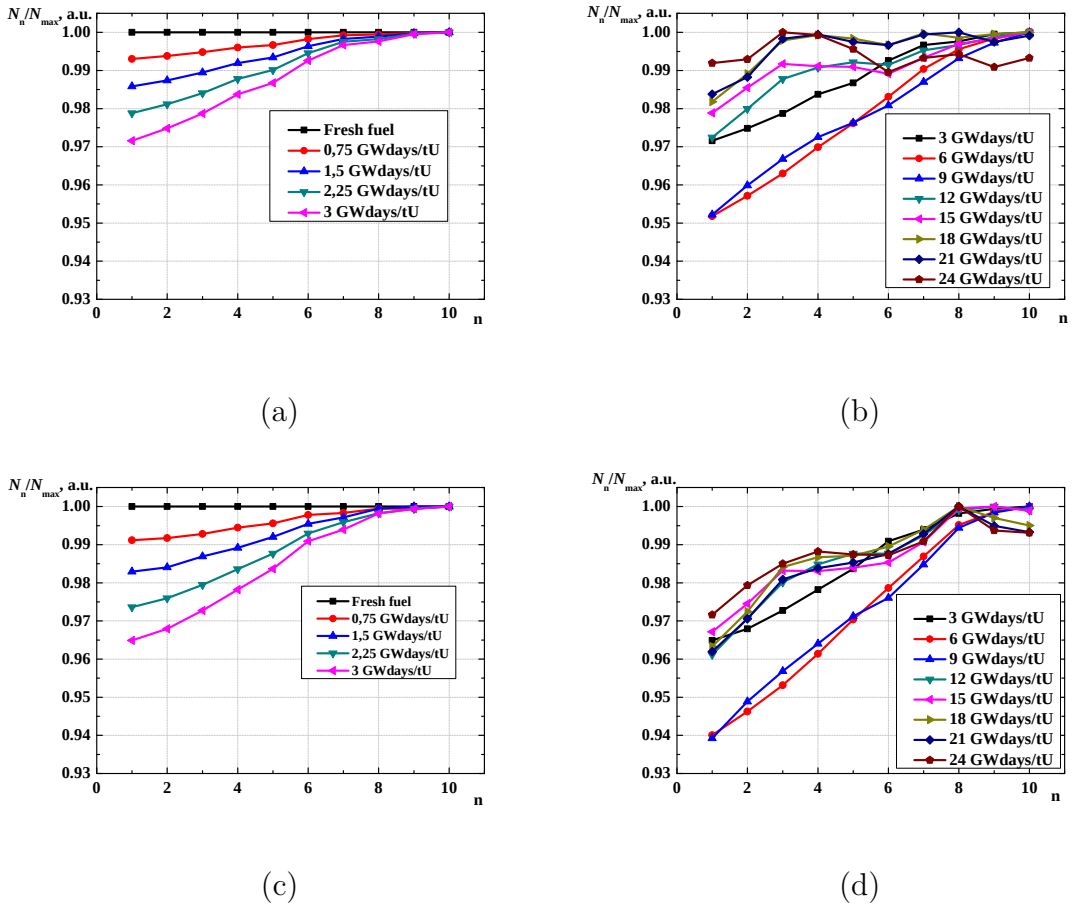

(a) (b)

(c) (d)

Figure 3.24: Relative ^{235}U concentration distribution in case of 2.8% enrichment fuel for different burn-up (Inner ring: a) 0—3 GWd/tU, b) 3-–24 GWd/tU; for outer ring: c) 0—3 GWd/tU, d) 3—24 GWd/tU.)

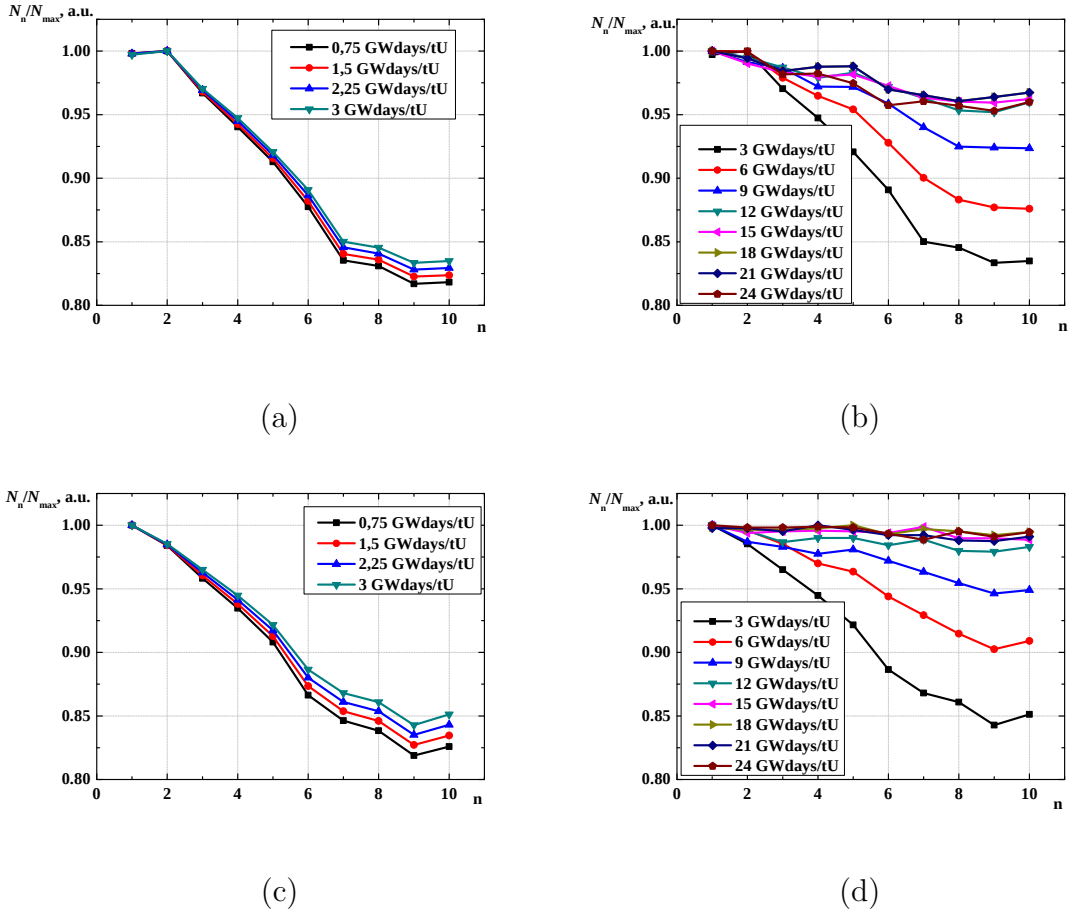

Figure 3.25: Relative ^{239}Pu concentration distribution in case of 2.8% enrichment fuel for different burn-up (Inner ring: a) 0—3 GWd/tU, b) 3-–24 GWd/tU; for outer ring: c) 0—3 GWd/tU, d) 3—24 GWd/tU.)

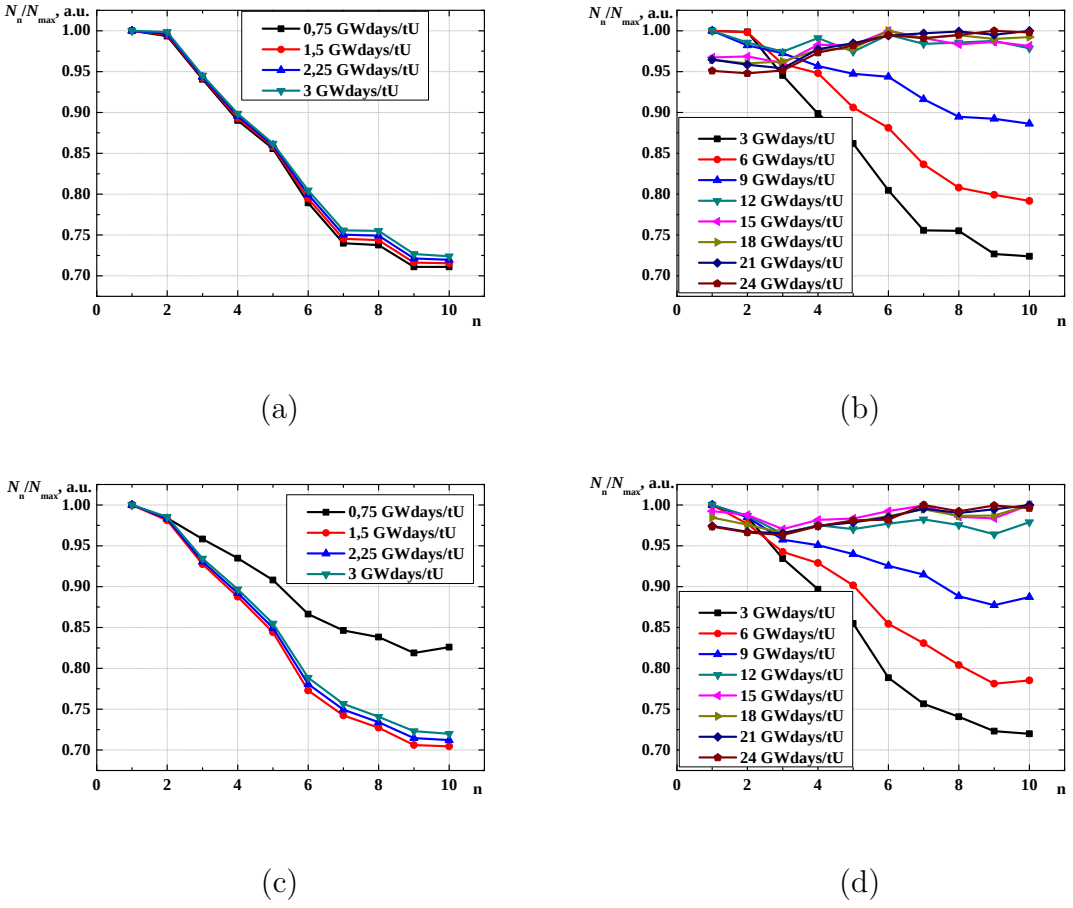

Figure 3.26: Relative ^{240}Pu concentration distribution in case of 2.8% enrichment fuel for different burn-up (Inner ring: a) 0—3 GWd/tU, b) 3-–24 GWd/tU; for outer ring: c) 0—3 GWd/tU, d) 3—24 GWd/tU.)

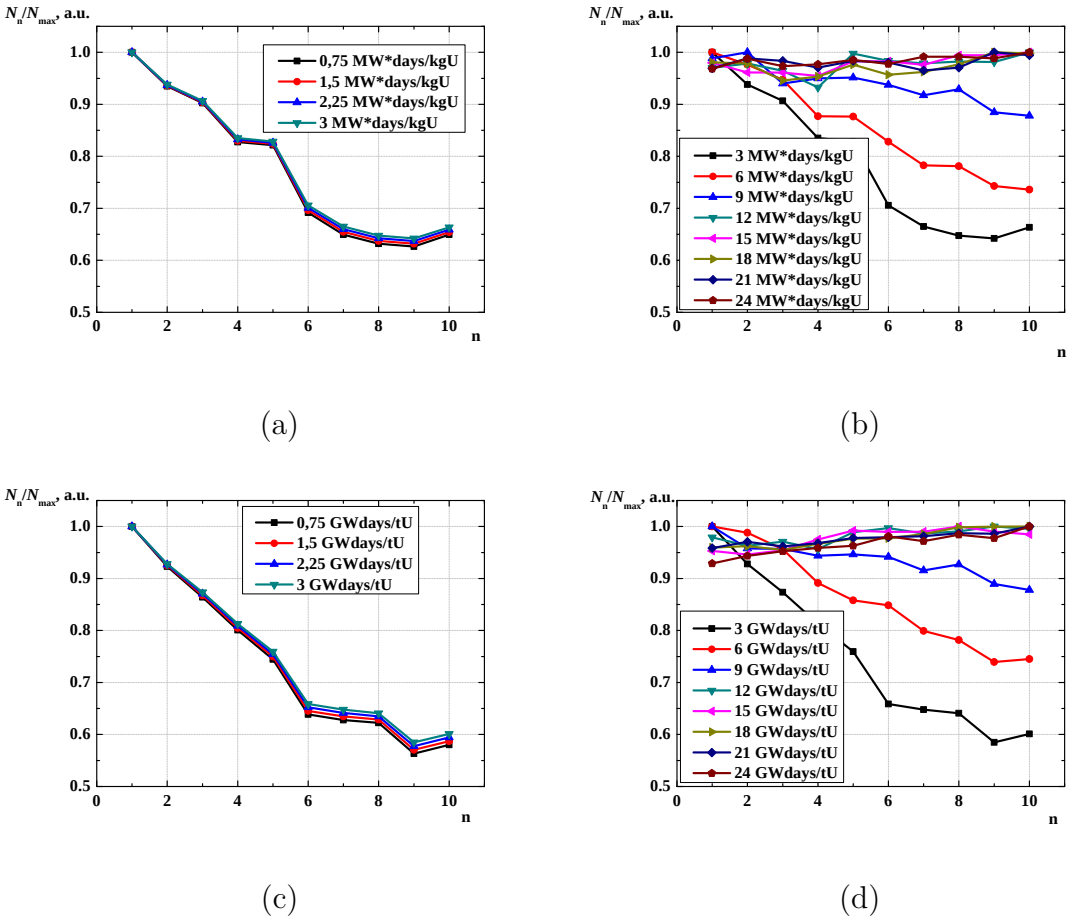

Figure 3.27: Relative ^{241}Pu concentration distribution in case of 2.8% enrichment fuel for different burn-up (Inner ring: a) 0—3 GWd/tU, b) 3-–24 GWd/tU; for outer ring: c) 0—3 GWd/tU, d) 3—24 GWd/tU.)

It was found, that axial distribution of uranium and plutonium isotopes is different at different burn-up. However the trend was observed, that distribution flattens when burn-up value of around 15 GWd/tU is achieved. One should pay attention that neutron leakage was not evaluated, therefore in order to assess axial burn-up properly, neutron leakage must be taken into account. This short analysis shows that water density has very important contribution in axial burn-up profile in RBMK-1500 type reactor.

Role of water density

The coolant (water) density during fuel irradiation plays a crucial role in the precise evaluation of nuclide concentrations. The coolant density and the axial power profile have the largest influence on the considered physical reactor core parameters and fuel assembly conditions, therefore they should be modeled as close to real conditions as possible [22]. These differences are mainly determined by differences in the neutron spectrum caused by the water density and the fuel composition (Fig. 3.28).

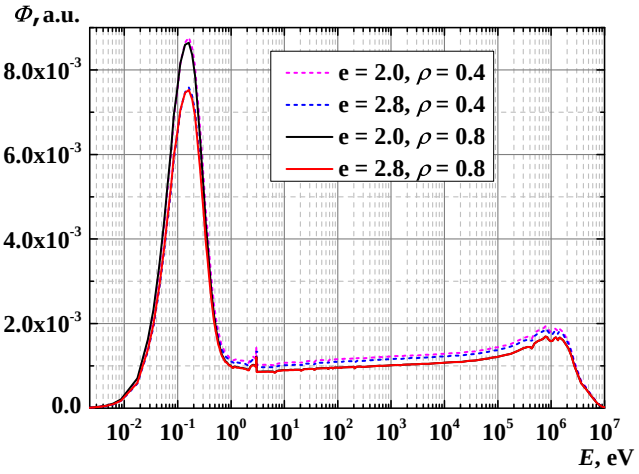

Figure 3.28: Neutron flux per unit lethargy spectra for 2.0% and 2.8% enrichment fuel in case of 0.4 g/cm^3 and 0.8 g/cm^3 water density inside the RBMK-1500 reactor fuel channel.

Studies were also performed regarding differences of the nuclide formation in inner and outer fuel rings of the same fuel channel [27]. Conclusions were drawn that the reason for concentration differences was the neutron flux variations and the heterogeneous neutron absorption. The harder neutron spectrum was observed in the inner fuel pellet ring of the assembly. Also more neutrons were absorbed in the lower part of the assembly due to the higher density of water there, i.e. fewer neutrons were available for fission reaction.

Table 3.2: Isotopic composition differences between 0.4 g/cm^3 and 0.8 g/cm^3 water density at 29 GWd/tU burn-up for different enrichment fuel.

Nuclide	$(N_{0.4}$-$N_{0.8})/N_{0.4}$	
	2.0% enr	**2.8% enr**
^{234}U	-0.1%	-1%
^{235}U	5%	11%
^{236}U	0.1%	-0.2%
^{238}Pu	14%	17%
^{239}Pu	1%	4%
^{240}Pu	3%	2%
^{241}Pu	6%	10%
^{242}Pu	2%	6%
^{237}Np	4%	7%
^{241}Am	5%	12%
^{243}Am	23%	22%

According to [22] ^{238}Pu, ^{241}Pu, ^{243}Am are the most sensitive to coolant density variations, the production of ^{241}Pu in the SNF can vary by up to 5% for different fuel assembly positions at different fuel burn-up. Variations in the thermal neutron spectrum affect the formation of ^{240}Pu and subsequently the formation of ^{241}Pu by the neutron capture reaction [27]. Results of this study show that ^{242}Cm and ^{244}Cm are also quite sensitive (difference of 25% at higher burn-up, Fig. 3.14 and 3.15), while the evaluation of ^{241}Pu shows the same sensitivity.

The calculation of fuel depletion in RBMK-1500 shows that concentration curves corresponding to different enrichment and water density values, which vary from 0.4 g/cm^3 to 0.8 g/cm^3, form four sets for every enrichment value

(2.0%, 2.4%, 2.6%, 2.8%), while limiting cases, which frame possible nuclide concentrations in our analysis, are 2.0% enrichment, 0.4 g/cm^3 water density and 2.8% enrichment and 0.8 g/cm^3 water density. At highest burn-up (29 GWd/tU) the isotopic composition differences between 0.4 g/cm^3 and 0.8 g/cm^3 for actinides important to burn-up credit applications reach 23% for 2.0% enrichment fuel and 22% for 2.8% enrichment fuel (see Table 3.2).

3.4. Conclusions

Calculations of fuel depletion in the RBMK-1500 type reactor using the infinite reactor lattice were performed and one group cross-section libraries were created for SNF composition calculations for 2.0–2.8% enrichment fuel without and with erbium burnable absorber. Concentrations of actinides important to the burn-up credit evaluation and Cm isotopes were obtained using implemented one group cross-section libraries and were compared to available experimental data and newest modeling results. The comparison shows an acceptable agreement between the values obtained using new one group cross-section libraries and experimental data as well as point depletion calculations, except for ^{238}Pu, caused by the initial composition of nuclear fuel, and ^{241}Am, which in our opinion was due to incorrect experimental values given as other studies show [23] results similar to our calculations. The comparison between available experimental data regarding fission products ^{142,143,144,145,146,148,150}Nd and ^{137}Cs was also performed. The fission product evaluation shows good agreement with experimental data, except for ^{142}Nd and ^{144}Nd isotopes.

Enrichment and the presence of burnable absorber play an important role in the SNF composition. At highest burn-up (29 GWd/tU) the isotopic composition differences between 2% enrichment fuel and 2.8% burn-up for actinides important to BUC applications vary from 11% to 52%.

The water density in the water channel during burn-up plays the crucial

role in the precise evaluation of nuclide concentrations. These differences are mainly determined by differences in the neutron spectrum caused by the water density and the fuel composition. At highest burn-up (29 GWd/tU) isotopic composition differences between 0.4 g/cm^3 and 0.8 g/cm^3 for actinides important to burn-up credit applications reach 14% for 2% enrichment fuel and 22% for 2.8% enrichment fuel. The obtained libraries could be applied to the evaluation of the RBMK-1500 spent nuclear fuel using the actinide-only approach in burn-up credit calculations, as well as for other purposes, e.g. for activity or toxicity evaluation of the spent nuclear fuel.

4. Criticality assessment of the cask

4.1. Burn-up credit in criticality analysis

Up to 200 of new CONSTOR®RBMK-1500/M2 type casks for storage and transportation are designed to be used for SNF storage in the dry type storage facility in the vicinity of the Ignalina NPP. Safety analysis and design justification were performed for the new interim dry type SNF storage facility [3, 4]. It claims that the SNF storage facility and its components are sufficiently safe. According to the Lithuanian national regulations the effective multiplication factor (k_{eff}) shall not exceed 0.95 during normal operation and postulated accident scenarios. However, only the conservative — fresh fuel — assumption regarding the SNF composition was used in this analysis. Burn-up credit approach calculations may be shortly described as taking into account the reduced SNF configuration reactivity due to depletion of fissile isotopes and the creation of neutron-absorbing isotopes when the fuel is irradiated in the reactor [8, 134]. Burn-up credit application is primarily related with the positive economical effect, e.g. possible increment of the number of SNF assemblies kept in a wet storage facility or increment of the number of SNF bundles allowed to store in the same SNF storage cask. Burn-up credit application is encouraged by the International Atomic Energy Agency (IAEA) and industry [9, 10].

RBMK-1500 type reactor SNF depletion calculations and SNF storage cask criticality calculations were performed and presented in 2001 and 2004 [28,135]. Burn-up credit application in criticality analysis in CASTOR® RBMK-1500 and CONSTOR®RBMK-1500 was presented in 2002 [9].

One of the possible ways of taking burn-up credit into account is the use of actinide-only burn-up credit. This approach is less conservative than the fresh fuel assumption but more conservative compared to burn-up credit calculations taking into account stable, long-lived fission products with relatively

large (n,γ) reaction cross-section together with actinides. The actinide-only approach reduces unnecessary conservatism and also gives acceptable safety margin in criticality calculations. Actinides used for actinide-only calculations may be different in different countries, but most of them are the same [11].

The changes of spent nuclear fuel composition due to burn-up were not taken into account analyzing CONSTOR®RBMK-1500 spent nuclear fuel cask criticality. Burn-up credit approach application and analysis would allow to optimize criticality analysis and as well to identify causes of changes in k_{eff}. For the first time, one neutron energy group cross-section libraries (see Chapter 3) were used to optimize criticality analysis of the spent nuclear fuel cask CONSTOR®RBMK-1500/M2 introducing different – actinide-only and full burn-up credit – approaches for RBMK reactor spent nuclear fuel. Also the average axial burn-up profile was introduced and studied to evaluate the end-effect on k_{eff} due to inhomogeneous burn-up of nuclear fuel assembly.

4.2. k_{eff} evaluation sequence

SCALE 6.1 code package was used for calculations [40]. STARBUCS analysis sequence for automating criticality safety calculations of spent fuel systems employing burn-up credit was used. It automatically performs all necessary calculations to determine spent fuel compositions, self-shielded cross sections and the k_{eff} of the spent fuel configuration [136].

A depletion calculation of a spent fuel bundle is performed using the ORIGEN-ARP sequence. In case of the axial burn-up simulation, calculations of each region nuclide concentrations and cross-sections were performed. ENDF/B-VII.0 238 energy group data library was used for calculations. ARP reads previously prepared one group RBMK fuel depletion libraries and interpolates a problem-dependent library for ORIGEN-S using defined parameters. This procedure simplifies and accelerates calculations. Library for RBMK-1000

fuel depletion modeling is also available with the SCALE 6.1 package, however there are no libraries for erbium fuel used in RBMK-1500 type reactors, therefore we generated our own library. The comparison of concentrations of actinides obtained from these libraries shows acceptable agreement with experimental values [137].

KENO-VI, a functional module in the SCALE system, is a Monte Carlo criticality program used to calculate the k_{eff} of three-dimensional (3-D) systems. Energy of average lethargy causing fission ($EALF$) is an additional parameter besides k_{eff} which is calculated by KENO-VI. $EALF$ is defined as the energy of the average fission group.

$$EALF = \frac{E_0}{e^{\bar{u}}} \tag{4.1}$$

$$\bar{u} = \frac{\sum_{z=1}^{Z} \sum_{g=1}^{G} \bar{u}_g \Phi_{g,z} \Sigma_{f,g,z}}{\sum_{z=1}^{Z} \sum_{g=1}^{G} \Phi_{g,z} \Sigma_{f,g,z}} \tag{4.2}$$

where E_0 is the maximum energy considered (10 MeV), $\bar{u}_g$ is the average lethargy of the energy group g, computed as $(u_g + u_{g+1})/2$, z is the index for material regions, $\Phi_{g,z}$ is the neutron flux of the energy group g in the region z, $\Sigma_{f,g,z}$ is the macroscopic cross-section of the energy group g for fission in the region z.

$EALF$ is a measure of "similarity" between physics of critical systems [20]. This integral spectrum parameter gives a fast but limited information about changes in the spectral distribution of fission (which answers to the question either thermal or epithermal neutrons are mostly involved in fission), when other parameters are modified. In case when a more detailed information of changes is needed, the spectrum of neutrons causing fission should be analyzed.

4.3. Model of the cask

The CONSTOR®RBMK-1500/M2 SNF cask consists of a cylindrical basket 32M containing 102 fuel bundles, a surrounding ring basket containing 80 fuel

bundles and other structural and shielding elements [4, 32, 33]. The detailed geometrical model of the CONSTOR®RBMK-1500/M2 SNF cask for Monte Carlo simulations of neutron transport was created using KENO-VI and is presented in Fig. 4.1.

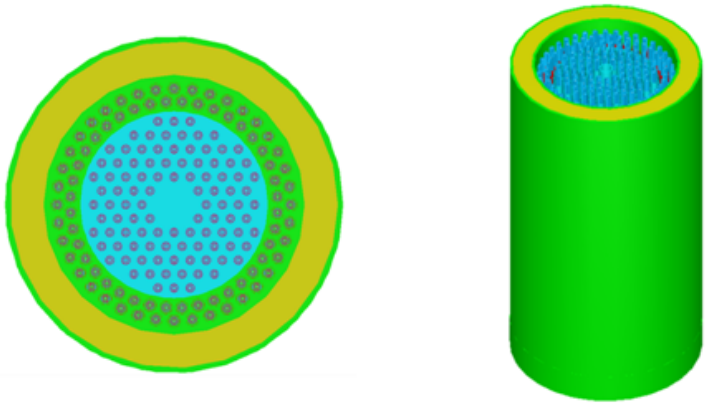

Figure 4.1: CONSTOR® RBMK-1500/M2 SNF cask geometrical model with design configuration of fuel bundle positions.

It is a stainless steel basket with a hollow 194 mm diameter central tube, 102 position tubes, a cylindrical shell and a closed bottom. The position tubes in 32M are arranged in a triangular pitch of 125 mm and have an outer diameter of 102 mm with 2 mm thick wall. The fuel bundle is assumed to be centered in its position tube. A ring basket is modeled as the 454 mm thick ring of the 1482 mm inner diameter made of aluminum alloy with 80 cylindrical holes with 2 mm thick stainless steel position tubes. All remaining cavities inside the cask were assumed to be filled with water.

The sidewall of the cask consists of two steel cylinders of a different size with the 40 mm wall thickness. The 340 mm thick annulus space between them is filled with heavy concrete CONSTORIT. The bottom of the cask is the CONSTORIT filled cylinder between two steel plates. The top of the cask body consists of a metallic head cylinder which is modeled as a 355 mm thick steel plate. Dimensions of the cask are: diameter — 2630 mm, height — 4850

m and mass of the loaded cask is up to 116 tons (see Fig. 4.1).

The CONSTOR®RBMK-1500/M2 cask is filled with RBMK-1500 fuel bundles in the model. A bundle consists of 18 fuel rods arranged in two concentrical rings with the central carrier rod at the centre [29]. The fuel rod is treated as a zirconium alloy tube homogeneously filled with uranium dioxide with or without burnable erbium absorber. The fuel pellet density was reduced to ensure that the amount of fuel material inside the tube corresponds to the design value. The central carrier rod was defined as a hollow tube made from zirconium alloy. Triangular pitch with half-pitch h=0.802 cm was chosen for CENTRM code calculations as a lattice cell parameter to assist self-shielding calculations [22, 133]. Several SNF loading schemes for the cask are foreseen in the cask design. However, only scenarios with the completely filled cask and with fuel of (one) specified enrichment were modeled. Fresh and different burn-up fuel with 2.0% ^{235}U enrichment and with 2.4%, 2.6% and 2.8% enrichment with erbium burnable absorber was modeled. In order to simulate normal operation (e.g. cask drying) and accident conditions (e.g. flooding), the water density in the cavities of the cask was changed. Fuel assemblies consisting of two fuel bundles are used in the RBMK reactor fuel channel. Fuel assembly is cut into two halves (bundles) before placing it into the spent nuclear fuel cask. Strict rules are set for fuel placing in the cask regarding its direction.

When actinide-only approach was used for fuel composition, only the most important actinides were included in k_{eff} calculations: ^{234}U, ^{235}U, ^{236}U, ^{238}U, ^{238}Pu, ^{239}Pu, ^{240}Pu, ^{241}Pu, ^{242}Pu, ^{237}Np, ^{241}Am, ^{242m}Am, ^{243}Am [11]. In the fission product case, besides these nuclides, these most important long-lived fission products with a relatively large (n,γ) reaction cross-section for burn-up credit additionally with erbium isotopes were included in the fuel composition: ^{95}Mo, ^{99}Tc, ^{101}Ru, ^{103}Rh, ^{109}Ag, ^{133}Cs, ^{143}Nd, ^{145}Nd, ^{147}Sm, ^{149}Sm, ^{150}Sm, ^{151}Sm, ^{152}Sm, ^{153}Eu, ^{155}Gd and ^{166}Er, ^{167}Er, ^{168}Er, ^{170}Er.

U, Pu, Am and Np isotopes are responsible for more than 80% of absorp-

tions in the RBMK SNF. Regarding stable fission products, their contribution is up to 2% for absorptions in low burn-up fuel. Other absorptions may be attributed to fission products which are not suitable for burn-up credit calculations due to their instability or volatility [11].

All k_{eff} values were calculated 5 years after the fuel bundle removal from the reactor, except those of k_{eff} evolution. Random k_{eff} errors associated with the Monte Carlo method do not exceed 0.001.

Table 4.1: RBMK upper fuel bundle relative power profile in the reactor [22].

Region	$\boldsymbol{H}$**, m**	$\boldsymbol{P}_{rel}$
1	3.75	1.116
2	4.25	1.155
3	4.75	1.150
4	5.25	1.128
5	5.75	1.036
6	6.25	0.858
7	6.75	0.631

Regarding the axial burn-up profile, a bundle model of the seven regions of the equal length and volume was used. The profile of the fuel bundle power was normalized, i.e. burn-up of each axial region was equally weighted, relative power coefficients used for axial regions were taken from [22] and are given in Table 4.1. The average profile was chosen. One should note that due to the power profile the burn-up in each bundle is unequal by height and lower burn-up is obtained at the top. We performed initial k_{eff} calculations of the SNF cask using burn-up profiles of upper and lower fuel bundles. Results of k_{eff} were obtained to be slightly higher for the upper fuel bundle profile. Therefore, calculations were continued using this profile. We assume that the higher reactivity of upper fuel bundles is determined by the lower water density

region (RBMK is a boiling water reactor) and subsequently relatively harder neutron spectra. This assumption gives us more reactive SNF for the same burn-up value and as a result more conservative estimation of k_{eff}. Axial distribution values of the water density varying from 0.8 to 0.2 g/cm^3 as well as temperatures of the fuel, cladding and moderator were taken from [130]. The impact of the axial burn-up evaluation on criticality results also known as "end-effect" [19, 138] of the RBMK fuel will be discussed in the light of presented calculation results in further sections. The horizontal burn-up profile was assumed to be uniform.

In the CONSTOR®RBMK-1500/M2 SNF cask model, we used a single fuel mixture (only a single fuel mixture defining the fresh fuel composition is allowed in STARBUCS [136] and a single burn-up value for calculations. This is only an approximate evaluation, however, the mean value of burn-up usually is used for such calculations [15, 56]. The burn-up range used for calculations was 0 (fresh fuel assumption) — 22.5 GWd/tU. The average discharged fuel burn-up for the RBMK reactor varies between 15.1 GWd/tU (for 2.0% enrichment fuel) and 30 GWd/tU (for 2.8% enrichment fuel) [30, 139].

Uniform water density distribution was used in the SNF cask for all cases, density values were changed between 0.1 and 1.0 g/cm^3. Regarding the fuel and SNF component temperature, we used a conservative uniform value of 100°C in order to minimize reduction of reactivity in fissile materials caused by Doppler effect. The cross-section data used in the problem are prepared by interpolating standard cross-section library data to the temperature needed in the problem. Regarding thermal scattering, data are available only for the limited number of materials (H_2O and UO_2 are included in the list), so incoherent inelastic scattering is evaluated for UO_2 and H_2O, for other materials elastic scattering is treated with the free-gas approximation in the KENO library. Temperature used for interpolation of these parameters was 100°C. Normally, burn-up credit calculations are performed at room temperature to increase the

conservatism, 100°C temperature was selected for our calculations in order to simulate accident conditions from the thermal hydraulics point of view. Design values set for cask components are: 400°C for fuel pellet, 279°C for fuel cladding in 32M basket, 91°C for the cask surface [4].

The SCALE calculation was run with 10000 neutrons, 100 generations and the CPU time was 22 min. per 3.4 GHz core. The mirror boundary conditions were applied for 2.64 x 2.64 x 4.52 m cask surrounding cuboid. Regarding possible introduction of bias due to not converged source distribution, a statement on the convergence of the $\tilde{\chi}^2$ test for normality at 95% level is given at the end of each calculation. It was carefully checked to ensure if this condition is satisfied in our calculations.

Uncertainties related with cross sections and other physical parameters are not subjects of this research.

4.4. Results of k_{eff} calculations

Further we present results from k_{eff} modeling of CONSTOR® RBMK-1500/M2 taking into account burn-up credit. The main parameters such as k_{eff}, $EALF$ as a function of water density for different fuel enrichment and burn-up for actinide-only case and most important fission products with actinides (hereafter "fission products") case were analyzed in order to investigate the trends of the parameters and to indicate the extreme points. The more detailed analysis including neutron absorption spectra and neutrons causing fission spectra was performed at these points. Also the influence of the axial burn-up profile on RBMK-1500 SNF burn-up credit was analyzed.

Impact of actinides and fission products on k_{eff} in the CONSTOR cask and *EALF* for 2% and 2.8% enrichment SNF

The average values of the neutron flux for fuel depletion of 2.0% and 2.8% enrichment fuel without burn-up profile in the reactor were 1.51×10^{14} n/cm^{2}s and 1.32×10^{14} n/cm^{2}s, respectively. At first different enrichment fuel with and without erbium burnable absorber was modeled taking into account actinide-only and full burn-up credit (including erbium) approaches. k_{eff} dependence on the water density inside SNF cask cavities for 0.45 to 22.5 GWd/tU burn-up fuel is given in Fig. 4.2 for different enrichment cases. The other enrichment cases were also checked for the same parameters, but here we present the marginal cases to see the main tendencies and the deviations. Maximum values are achieved at 0.35–0.4 g/cm^3, with maximum k_{eff}=0.924 for 2.8% fuel enrichment with actinides only.

Table 4.2: k_{eff} for 1 and 7 regions axial burn-up profile for 2.0% and 2.8% enrichment fuel taking into account actinide-only (Act) and fission products (Fp). Water density — 0.4 g/cm^3.

Enr	**Act, z=1**	**Act, z=7**	**Fp, z=1**	**Fp, z=7**
BU=0.45 GWd/tU				
2.0%	0.859	0.859	0.851	0.850
2.8%	0.924	0.923	0.829	0.829
BU=22.5 GWd/tU				
2.0%	0.623	0.655	0.578	0.615
2.8%	0.719	0.739	0.665	0.690

The characteristic dependence profile is observed for all fuel types for the new CONSTOR®RBMK-1500/M2 SNF cask, similar to the one which was

observed for the old type RBMK-1500 SNF cask [28]. One should note that without using BUC approach the k_{eff} reaches 0.937 value for 2.8% fuel enrichment with fresh fuel assumption and taking into account methodological uncertainty (0.012) barely satisfies the acceptance criteria of 0.95 for safe storage [4].

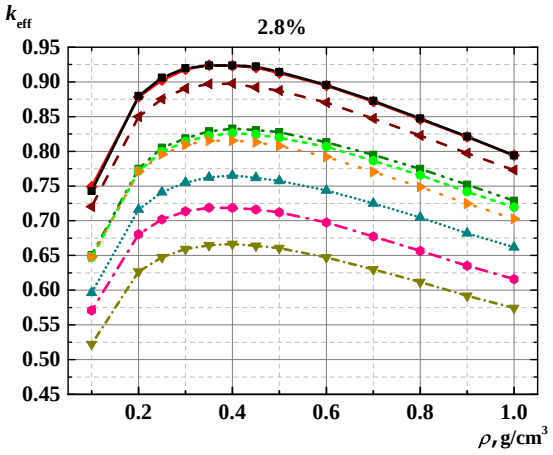

(a)

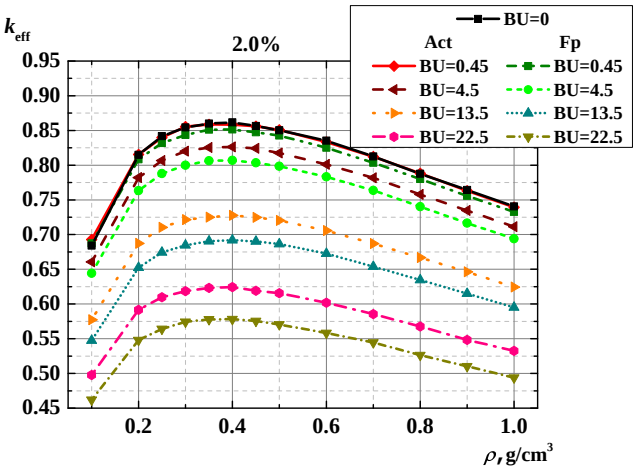

(b)

Figure 4.2: k_{eff} as a function of water density inside SNF cask cavities for different burn-up 2.8% and 2.0% enrichment fuel taking into account actinide-only (Act) and fission products including burnable absorber erbium (Fp).

The highest k_{eff} is obtained at the 0.38–0.4 g/cm^3 water density value for

both fuel enrichment cases. The increase of k_{eff} due to higher fuel enrichment is substantial ∼9% in case of 0.45 GWd/tU actinide-only case by comparing 2.0% and 2.8% enrichment cases (see Table 4.2). Actinide-only approach gives 6–13% higher k_{eff} value in comparison with fission-product approach for 2.8% enrichment fuel and 1-7% for 2.0% enrichment fuel for different burn-up cases (see Fig. 4.2). The highest difference between actinide-only and fission products cases k_{eff} is obtained in low burn-up 0.45 GWd/tU, 4.5 GWd/tU cases and a decrease by 0.1 and 0.08 is in k_{eff}, respectively, thus the fission product approach would allow even increment of the number of SNF assemblies kept in a wet storage facility in case of special need and after proper safety justification. The higher k_{eff} values of 2.8% fuel are determined by higher actinide concentration and slower burn-up due to the use of burnable absorber erbium, while accumulation of fission products determines its decrease. On the contrary, comparing the 2.0% fuel enrichment actinide-only and fission product cases, there is no large difference in k_{eff} (0.02 and 0.05) for low burn-up cases (0.45 GWd/tU and 4.5 GWd/tU). Taking into account reasonable fuel burn-up ∼22.5 GWd/tU for 2.8% fuel and ∼13.5 GWd/tU for 2.4% fuel enrichment, the k_{eff} values vary from 0.72 to 0.67 and from 0.73 to 0.69 in actinide-only and in fission products approaches respectively, and they are comparable.

In order to see the change in behavior of neutrons causing fission in the system we analyze the change of $EALF$ against the water density (see Fig. 4.3 for different fuel enrichment cases). Highest $EALF$ values (fission products, 22.5 GWd/tU burn-up at 0.1 g/cm^3) correspond to lowest values of k_{eff} in both cases, but in 2.0% case we have a broader distribution of energies when the same burn-up values are considered, which means a harder fission spectrum (0.6–7 eV energy range for 2.8% fuel case and 0.9–10.5 eV for 2.0% fuel case) and a more important role of fissile plutonium isotopes in case of a higher fuel burn-up.

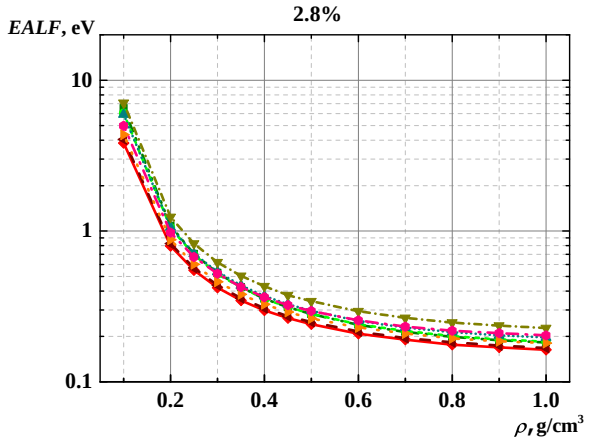

(a)

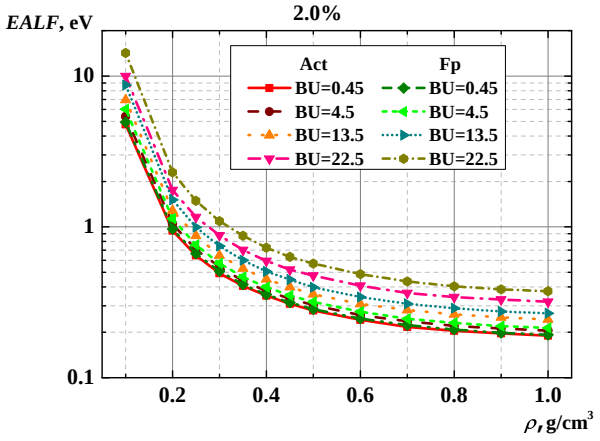

(b)

Figure 4.3: $EALF$ as a function of water density inside SNF cask cavities for different burn-up 2.8% and 2.0% enrichment fuel taking into account actinide-only (Act) and fission products including burnable absorber erbium (Fp).

Absorption rate spectra (Fig. 4.4) of low and high burn-up values (0.45 and 22.5 GWd/tU) give a more detailed information on differences between actinide-only and fission product burn-up credit approaches. For 2.8% enrichment the fuel absorption rate at ^{235}U absorption peak is higher when fission products are not included in k_{eff} calculations, but the difference between actinide-only and fission product burn-up credit decreases as erbium burns out in higher burn-up case. High burn-up creates a double absorption peak at

around 0.3 eV, which is attributed to ^{239}Pu and ^{241}Pu resonances. One must take into account that ^{241}Pu radioactive decay (and accumulation of non-fissile ^{241}Am) reduces resonant fission absorption in SNF during the expected storage time of the cask. An additional peak is observed at 1 eV which is due to ^{240}Pu resonance absorption.

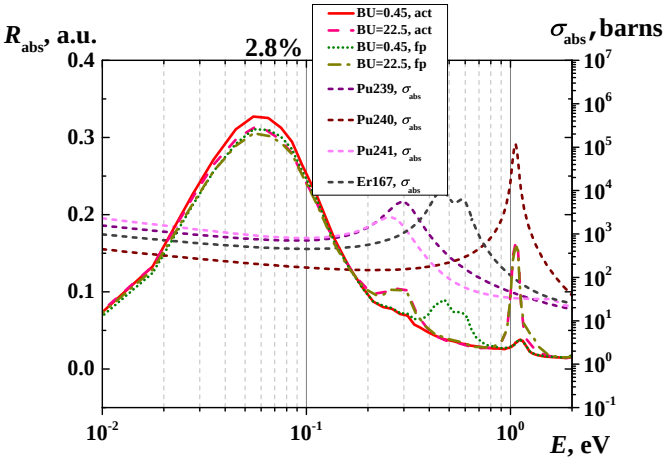

(a)

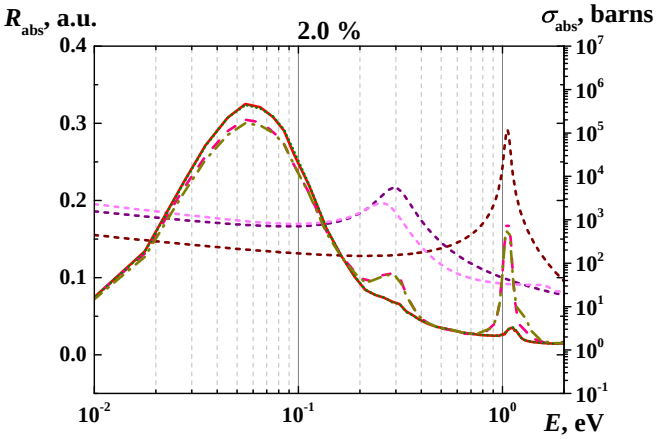

(b)

Figure 4.4: Neutron absorption rate ($R \propto \Phi \times \sigma_{abs}$) spectra inside SNF cask in case of 0.35 g/cm^3 water density for 2.8% and 2.0% enrichment fuel. Pu neutron absorption cross sections on the scale on the right for information.

Differences between low burn-up actinide-only and fission products absorp-

tion spectra could be seen at 0.4–0.6 eV, which are caused by ^{167}Er presence in fresh fuel [31, 140]. These peaks vanish with increasing burn-up, as erbium burns out. Therefore, a decrease of k_{eff} in high burn-up fission product burn-up credit approach is caused by the increasing concentration of fission products, but not due to residual erbium.

Absorption rate spectra analysis of 2.0% enrichment fuel shows coinciding spectra of low burn-up SNF for actinide-only and fission product cases and slightly higher absorption in ^{235}U for actinide-only case for high burn-up SNF. I.e. differences at high burn-up are determined by the increased concentration of neutron-absorbing fission products.

Influence of axial burn-up profile on RBMK-1500 SNF BUC

Inclusion of the axial burn-up profile allows investigation of the burn-up impact on k_{eff} as the evaluated distribution of different isotopes is closer to real conditions taking into account reduced SNF configuration reactivity due to depletion of fissile isotopes and the creation of neutron-absorbing isotopes.

The single axial region (z=1) and multiple axial regions ((z=7), see Table 4.1, for details) models with actinide-only BUC approach for 2.8% and 2.0% enrichment fuel were analysed, and a difference in terms of k_{eff} and $EALF$ (see Figs. 4.5, 4.6) were evaluated. k_{eff} dependence on the water density inside the SNF cask is given in Fig. 4.5. Higher water density has a positive impact on k_{eff} in case of the multiple regions model in higher burn-up cases. The multiple regions model gives up to 7% higher k_{eff} value in comparison with the single region model for 2.8% enrichment fuel and up to 10% for 2.0% enrichment fuel at 22.5 GWd/tU burn-up. This is the so called "end effect". Studies have shown that if a uniform axial distribution is assumed as conservative for low burn-ups, it becomes increasingly non-conservative as burn-up increases [141]. However, the magnitude of the reactivity increase associated with the axial

burn-up distribution in our case is larger than that which is typically observed for PWR fuel [18]. Similar to PWR fuel, the axial burn-up distribution results obtained by us show increasing reactivity with increasing burn-up taking into account actinides.

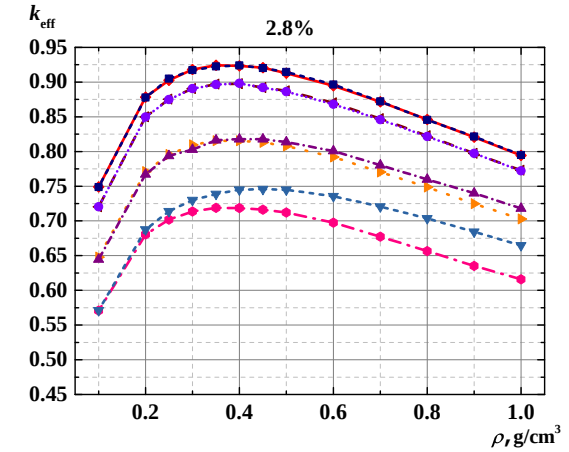

(a)

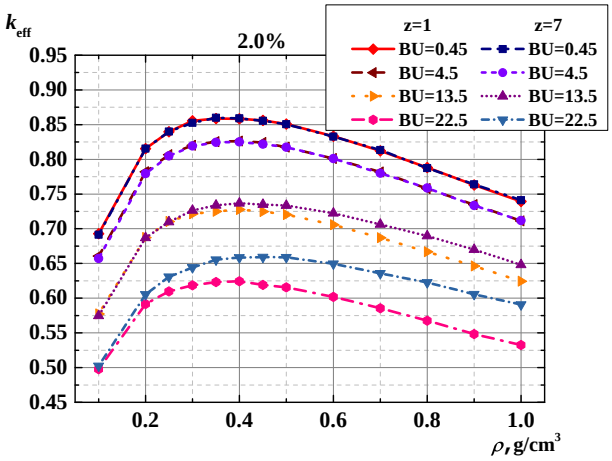

(b)

Figure 4.5: k_{eff} as a function of water density inside SNF cask cavities for different burn-up 2.8% and 2.0% enrichment fuel taking into account actinide-only axial (7 regions) burn-up profile.

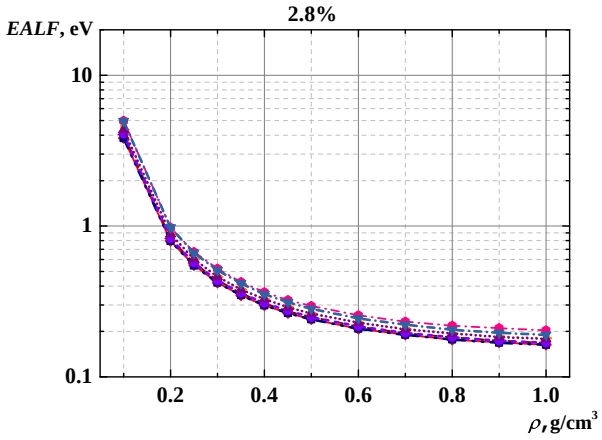

(a)

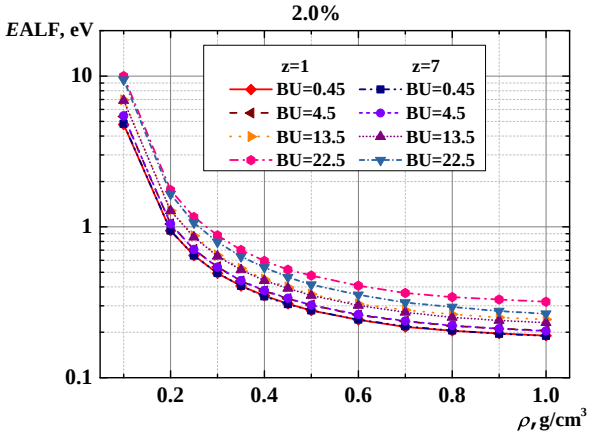

(b)

Figure 4.6: $EALF$ as a function of water density inside SNF cask cavities for different burn-up 2.8% and 2.0% enrichment fuel taking into account actinide-only axial (7 regions) burn-up profile.

$EALF$ as a function of the water density inside the SNF cask for different burn-up of 2.8% and 2.0% enrichment fuel taking into account actinide-only approach for the single (z=1) and multiple (z=7) regions burn-up profile is presented in Fig. 4.6. Comparing the $EALF$ dependence on the water density for the single (z=1) and multiple (z=7) regions burn-up profile we can observe that $EALF$ difference is about 5% for 2.8% enrichment fuel and about 20% for 2.0% enrichment fuel, i.e. $EALF$ values have a broader distribution in case

of higher burn-up and the water density comparing single (z=1) and multiple (z=7) regions model results for 2.0% enrichment fuel. Lower $EALF$ for the multiple regions model means that higher reactivity is determined by residual ^{235}U, but not the fissile plutonium isotopes. Increased fission of plutonium would increase the $EALF$ value.

Neutron absorption and neutron causing fission spectra inside the SNF cask in case of 0.35 g/cm^3 water density for 2.8% enrichment fuel taking into account actinide-only approach for single (z=1) and multiple (z=7) regions burn-up profile are presented in Fig. 4.7. Neutron absorption and neutron causing fission rate spectra of the same burn-up values coincide (see 4.7) for both analysed (z=1 and z=7) cases at 0.45 GWd/tU burn-up, and are slightly different at 22.5 GWd/tU burn-up. It can be seen that the peak attributed to uranium is lower for the single burn-up profile case and plutonium peaks are of the same height for high burn-up fuel. In case of neutrons causing fission rate spectrum of 2.0% enrichment fuel, the role of residual uranium is even more important (Fig. 4.8), but due to the lower amount of fissile material k_{eff} is significantly smaller (see Fig. 4.5a). As we see non-uniform uranium depletion is responsible for the "end effect" in RBMK-1500 SNF. Build-up of plutonium has no significant effect. Other independent studies regarding the concentration of nuclides in nuclear fuel show that increasing burn-up taking into account the burn-up profile increases the concentration of residual uranium, while differences in the concentration of plutonium isotopes are not significant [22].

k_{eff} dependence on burn-up shows a trend of reduction of reactivity with increasing burn-up (see Fig. 4.9a). Attention should be paid to fuel with erbium, which has stable k_{eff} value until erbium is burned out (5 GWd/tU) and then k_{eff} also starts to decrease gradually. A significant positive end effect, i.e. separation of lines, is visible from 15 GWd/tU burn-up for 2.8% enrichment fuel and from 9 GWd/tU for 2.0% enrichment fuel. Highest k_{eff} values are

achieved for 2.8% enrichment fuel using actinide-only approach. Taking into account the burn-up profile the increase in k_{eff} is by 0.02 for 2.8% enrichment fuel case at 22.5 GWd/tU burn-up. The maximal increase in k_{eff} by 0.065 is for 2.0% enrichment fuel case with fission products at 22.5 GWd/tU burn-up.

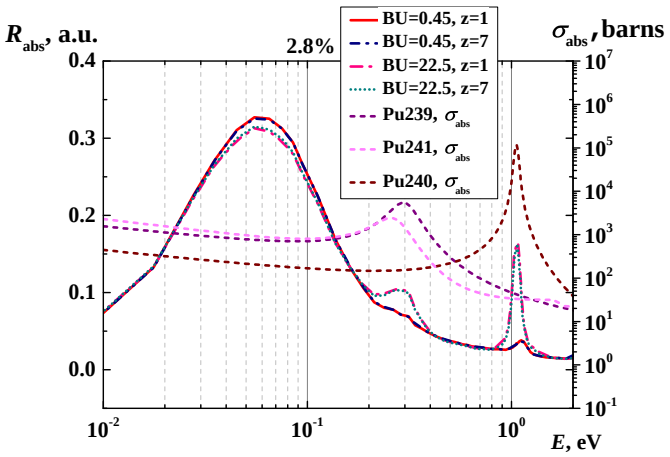

(a)

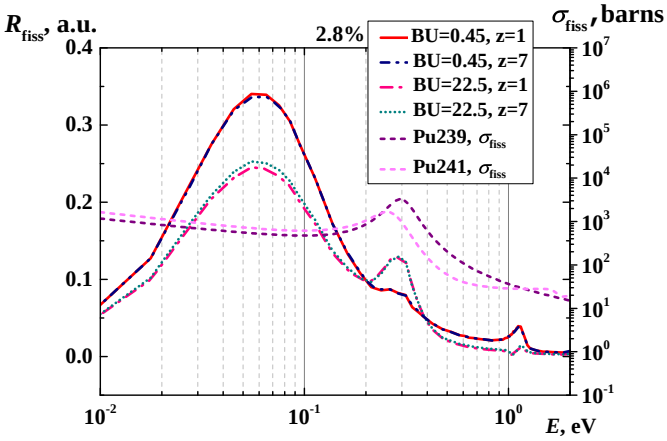

(b)

Figure 4.7: Neutron absorption ($R \propto \Phi \times \sigma_{abs}$) and neutrons causing fission rate ($R \propto \Phi \times \sigma_{fiss}$) spectra inside SNF cask in case of 0.35 g/cm^3 water density for 2.8% enrichment fuel taking into account actinide-only axial (7 regions) burn-up profile. Pu neutron absorption(a) and fission(b) cross sections on the right accordingly.

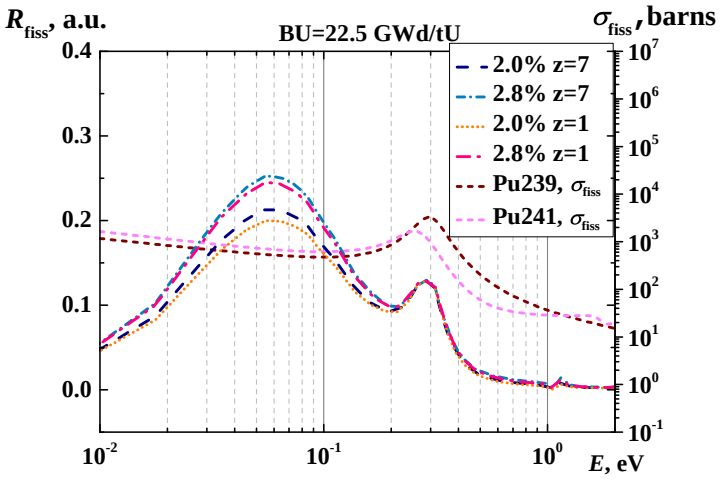

Figure 4.8: High burn-up SNF fission rate ($R \propto \Phi \times \sigma_{fiss}$) spectra inside SNF cask in the case of 0.35 g/cm^3 water density for 2.0% and 2.8% enrichment fuel taking into account actinide-only axial (7 regions) burn-up profile. Pu neutron fission cross-sections on the right.

The behaviour of k_{eff} is explained by $EALF$ (see Fig. 4.9b), which contrariwise increases with the burn-up. The highest values of $EALF$ are observed for 2.0% enrichment fuel with fission products and multiple (z=7) regions axial profile. 2.8% fuel shows a slower increase of $EALF$ during burn-up of fuel due to the higher initial fissile uranium content, and relatively less important role of ^{239}Pu compared with the 2.0% enrichment fuel case. Spectra of neutrons causing fission in Fig. 4.8 represent this situation, as it was commented previously.

The most reactive case (2.8% enrichment, multiple (z=7) regions, actinide-only case) was analyzed more exactly and the outline map of k_{eff} as a function of water density and burn-up is given in Fig. 4.10a. The most critical condition region was identified: 0–3 GWd/tU burn-up fuel and 0.3–0.5 g/cm^3 water density inside SNF. $EALF$ (see Fig. 4.10b) map shows that it is mostly determined by water density and burn-up has no significant influence on physical fission properties, except that burn-up determines the residual amount of fissile

material.

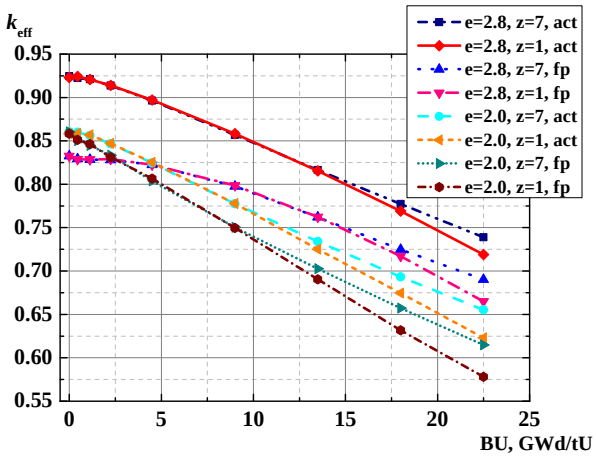

(a)

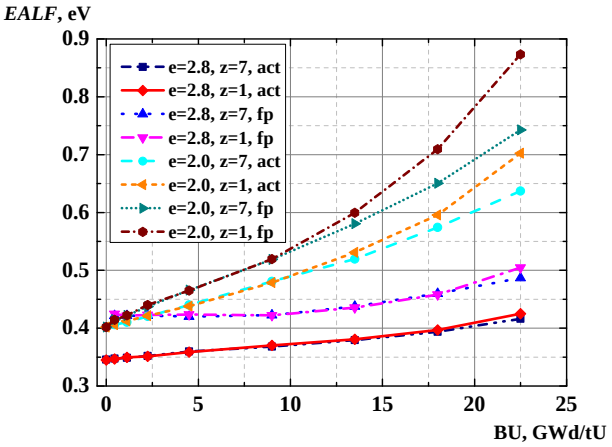

(b)

Figure 4.9: k_{eff}(a) and $EALF$(b) as a function of burn-up (BU) for 1 and 7 regions axial burn-up profile 2.0% and 2.8% enrichment fuel taking into account actinide-only and fission products.

Calculations for the most reactive case (actinide-only with axial profile, 2.8% enrichment fuel) were performed with 44-group library and Continuous energy library to assess k_{eff} variations due to the use of different libraries (see Fig 4.11). k_{eff} differences among calculation results are in the range of 1–2%. The result of 238-group calculations is most conservative.

Regarding k_{eff} evaluation at room temperature, calculations for the most

reactive case of actinide-only approach with multiple regions (z=7) axial profile were performed at room temperature of 20°C. Differences occur at water density of 0.1–0.5 g/cm^3. The results of lower temperature give more conservative values (up to Δk_{eff} =0.2) as it was expected (see Fig. 4.12).

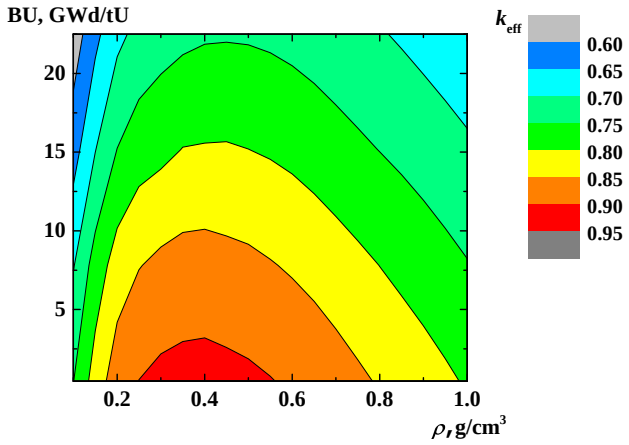

(a)

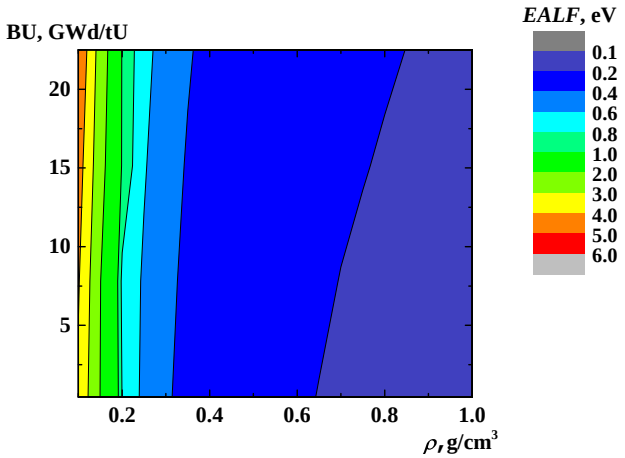

(b)

Figure 4.10: k_{eff}(a) and $EALF$(b) as a function of burn-up and water density for multiple (z=7) regions axial burn-up profile 2.8% enrichment fuel taking into account actinide-only.

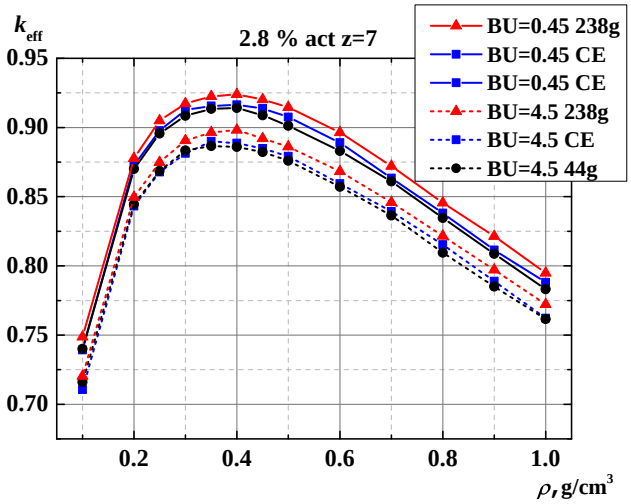

Figure 4.11: Comparison of k_{eff} in case of 238-group, 44-group and continuous energy libraries. k_{eff} as a function of water density inside SNF cask cavities for 0.45 and 4.5 GWd/tU burn-up for 2.8% enrichment fuel using actinide-only axial (7 regions) burn-up profile.

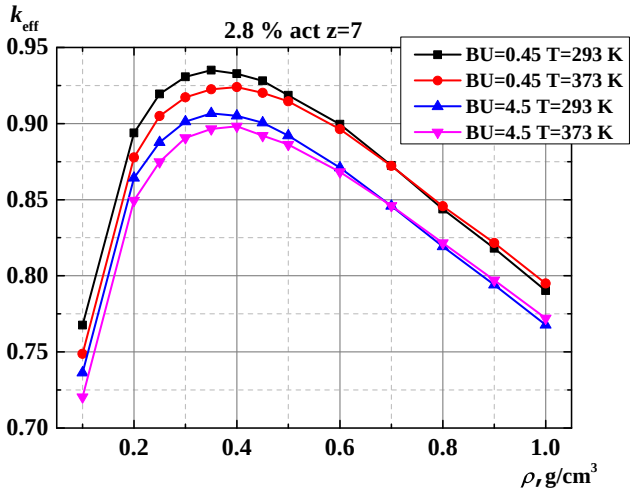

Figure 4.12: Comparison of k_{eff} in case of 373 K and 293 K temperatures. k_{eff} as a function of water density inside SNF cask cavities for 0.45 and 4.5 GWd/tU burn-up for 2.8% enrichment fuel using actinide-only axial (7 regions) burn-up profile.

k_{eff} evolution

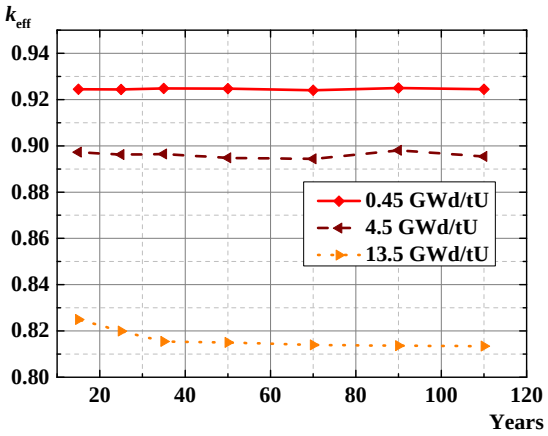

(a)

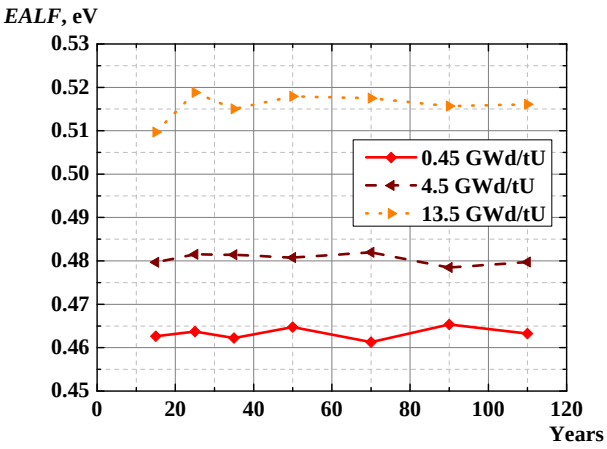

(b)

Figure 4.13: Evolution of effective multiplication factor (a) and evolution of energy of average lethargy causing fission (b) for different burn-up 2.8% enrichment fuel inside SNF cask.

Evolution of k_{eff} for 2.8% enrichment fuel for 100 years is evaluated and presented in Fig. 4.13a. k_{eff} evolution was modeled increasing SNF storage time, resulting in changes of fuel composition — concentration changes due to decay of isotopes. Then water density inside cask cavities corresponding

to most reactive conditions (0.35 g/cm^3) was taken and used for criticality evaluation. For low burn-up fuel k_{eff} does not change in this period of time. For higher burn-up fuel (13.5 GWd/tU) decrease of reactivity is observed for 30 years.

It may be associated with beta decay of ^{241}Pu and build-up of ^{241}Am as it may be seen in generic cask model of PWR reactor (Fig. 1.2). Significant amount of ^{241}Pu forms after sufficient period of irradiation of fuel in the reactor, therefore this effect is not noticeable for lower burn-up fuel. $EALF$ does not show significant changes during evaluated period (Fig. 4.13b).

4.5. Conclusions

Criticality calculations of spent nuclear fuel in the CONSTOR®RBMK-1500/M2 cask were performed using pre-generated ORIGEN-ARP spent nuclear fuel composition libraries for different fuel enrichment cases and including fuel with burnable poison erbium. Results of the impact of RBMK-1500 burn-up of different enrichment fuel on the effective neutron multiplication factor were obtained. SCALE 6.1 code package with STARBUCS BUC evaluation tool was used for modeling.

Conditions for the SNF storage in the CONSTOR®RBMK-1500/M2 cask were assumed to be unfavorable regarding filling with the highest enrichment SNF, water density, temperature and burn-up. Results with maximum k_{eff}= 0.924 for 2.8% ^{235}U fuel enrichment using the actinide-only approach were obtained at burn-up of 0.45 GWd/tU, i.e. k_{eff} did not exceed the value of 0.95 which is set in legal safety requirements of a number of countries worldwide, and taking into account the random k_{eff} errors associated with the Monte Carlo method 3σ (i.e., 0.003) it still satisfies the acceptance criteria.

Differences between k_{eff} results of low burn-up 2.8% enrichment fuel with erbium burnable absorber actinide-only and fission product approaches are

caused by the ^{167}Er presence in fresh fuel. A decrease of k_{eff} in high burn-up fission products burn-up credit approach is caused by the increasing concentration of fission products, but not due to erbium which burns out earlier.

Criticality evaluation of 2.0% ^{235}U enrichment fuel gives significantly lower k_{eff} values, up to 0.859, due to a smaller amount of fissile material. Differences between k_{eff} results of 2.0% enrichment fuel actinide-only and fission products approaches with increasing burn-up are caused by increasing the concentration of fission products.

The axial burn-up profile was evaluated for 2.8% ^{235}U enrichment fuel with erbium burnable absorber and 2.0% ^{235}U enrichment fuel. Actinide-only approach was used for the axial burn-up profile calculations. A significant positive end effect is noticed from 15 GWd/tU burn-up for 2.8% ^{235}U enrichment fuel and from 9 GWd/tU for 2.0% ^{235}U enrichment fuel. Non-uniform uranium depletion is responsible for the end effect in RBMK-1500 SNF whereas build-up of plutonium has no significant effect. The region of the most critical conditions is identified: 0–3 GWd/tU burn-up fuel and 0.3–0.5 g/cm^3 water density inside SNF. Burn-up has no significant influence on physical fission properties, but it determines the residual amount of fissile material and k_{eff}. The obtained results may be applied in practice for the evaluations of the RBMK type reactor SNF storage possibilities (for any type of containers) as well as may help to optimize the SNF storage volume inside the existing CONSTOR®RBMK-1500/M2 cask without compromising criticality safety.

Findings of this study regarding RBMK spent nuclear fuel composition influence on k_{eff} might be used analyzing disposal of spent nuclear fuel. Usually fuel is designed to be moved to other special casks for disposal, where fuel bundles should be packed as densely as possible. The principle of lowering the volume of radioactive waste would definitely require application of full burn-up credit while designing casks for disposal of RBMK spent nuclear fuel.

5. Actinides in irradiated graphite

5.1. Impurities in irradiated reactor graphite

Graphite is widely used in the nuclear industry since the first nuclear reactor has been started. It is used in a number of different current reactor designs (Magnox, AGR, HTR, RBMK, etc.) and is also designed to be used in generation IV reactors (VHTR, MSR). About 250,000 tons of spent graphite is already accumulated in still operating or being decommissioned nuclear reactors [142]. Graphite is mostly used as a moderator and a reflector of neutrons in the reactor core and during a long-lasting reactor operation period (20–30 years) it is activated by neutrons due to impurities in virgin graphite (usually <0.01% by weight fraction) and for some other reasons (for instance, nitrogen penetration due to operation of gaseous circuit) [90, 143–145]. Thinking about graphite reprocessing, which is attractive from the sustainability point of view, an essential topic is characterization of the most significant radioactive elements inside graphite. Radiological characterization of radionuclides is very important not only for solving the problem of efficient reprocessing but also for prediction of contamination in further applications.

Graphite is one of the key elements of the RBMK reactor technology — both units of Ignalina NPP contain about 3600 tons of graphite [143], thus strategy of radioactive waste management related to the irradiated graphite is one of the most critical issues. This strategy depends on characteristics of the irradiated graphite [29]. Graphite impurities are activated by (n, γ), (n, p), (n, α) reactions partially resulting in long-lived elements (e.g. ^{14}C, ^{36}Cl, transuranium elements). ^{14}C resulting from ^{13}C (n, γ) and ^{14}N by (n, p) reactions is one of limiting radionuclides for the RBMK-1500 reactor low and intermediate level radioactive waste and graphite itself [34, 146, 147]. Besides ^{14}C isotope, there is a wide variety of other elements contributing to the activity [90, 144].

Evaluation of concentrations of light and relatively short-lived elements was performed earlier in [148] and also was addressed in part in [149] but with different modeling schemes, i.e. a deterministic approach. Long-term power operation also results in buildup of long-lived isotopes of radioactive actinides, such as Pu, Am, Cm, etc. caused by activation of uranium and thorium impurities in the virgin nuclear graphite. Fission of actinides also contributes to concentrations of corresponding radioactive fission products. Analysis of concentration and evolution of actinides in the irradiated graphite and comparison with a set of legally established levels can show if specific activities of above mentioned elements exceed these limits.

We investigate buildup of long-lived actinides in the graphite from very small fraction of uranium impurities in the virgin nuclear graphite during operation of RBMK-1500 type reactor Unit 1 of the Ignalina NPP. The key issue of this problem is the knowledge of the reactor neutron spectrum, flux of neutrons, and impurities of the graphite (with the exception of accidental contamination). In spite of the fact that the reactor power history is known, separate parts of reactor graphite moderator undergo different conditions: neutron spectrum and flux changes with the radial and axial position in the reactor core causing inhomogeneous activation of graphite impurities.

Numerical modeling is an important tool for estimation of the neutron fluence in the graphite and the radioactive waste production in the nuclear reactors [27, 90, 150, 151]. Concentrations of minor graphite impurities were measured in the sample of graphite sleeve of the Ignalina NPP reactor using high resolution inductively coupled plasma mass spectrometry (ICP-MS) technique [152], while modeling was performed using two independent codes SCALE 6.1 with Origen [40], and MCNPX with Cinder [109,153,154]. In order to check the initial U impurity concentration and verify our calculation with both codes the calculation results of the graphite activation were compared with nuclear spectrometry measurements of the graphite sample taken from

the Ignalina NPP Unit 1 reactor core. According to the measurement results, the initial graphite impurity concentration was adjusted and the specific activities of actinides in the irradiated RBMK-1500 graphite constructions were obtained. The differences between two models, different graphite structure parts (sleeve and stack) as well as comparison with previous calculations [90] in terms of actinides inventory in the spent graphite will be discussed here. Also 3D model of RBMK reactor lattice will be developed for radiological characterization of graphite in the reactor plateau region.

5.2. Modeling of graphite impurities neutron activation

For estimation of neutron fluence and amount of radionuclides in the irradiated graphite from RBMK-1500 core two different codes, namely MCNPX (v2.7 which includes CINDER burnup capability) and SCALE 6.1 codes package, were used [109, 153, 154].

Monte Carlo N-Particle Code MCNPX is widely applied for the neutron transport calculation. In brief, particle transport using the Monte Carlo technique is based on the explicit tracking of particles following each particle from a source throughout its life to its death (by parasitic absorption or escape). Probability distributions are randomly sampled using transport data. In calculations these distributions are used to determine the type of interaction, energy of particles if it scatters the leakage of particles and the number of neutrons produced if the fission occurs. MCNPX is well suited to solve complicated three-dimensional, time-dependent problems. It was used in benchmark calculations of the RBMK-1500 reactor spent nuclear fuel isotopic composition [27], gas turbine–modular helium cooled reactor (GT-MHR) in the case of plutonium (uranium free) fuel cycle [150]. Also, it was used in obtaining nuclide inventory of radioactive waste for the RBMK-1500 reactor [146, 151]. In

our calculations MCNPX was used to obtain neutron flux in the RBMK-1500 graphite.

The burn-up capability of MCNPX is implemented including burn-up code CINDER, which uses 63 neutron energy groups and normalizes MCNPX tallies according to power (in 14 fuel assemblies in our case, see next section for details). ENDF/B-VII.0 nuclear data were used for neutron flux and cross sections calculation. Therefore, evaluation of fuel isotopic composition, activation and radioactive decay during irradiation was done with CINDER code incorporated in MCNPX. MCNPX (v2.6) has been benchmarked by calculating and measuring carbon activation in the RBMK graphite [148].

For inter-comparison purposes the SCALE 6.1 program package was used for radionuclide activation in graphite calculations. Standardized computer analyses for licensing evaluation (SCALE 6.1) code system has the capability to perform depletion/decay calculation, criticality assessment, shielding, and heat transfer analyses using well established functional modules tailored to the SCALE system. The numerical sensitivity study of irradiated nuclear fuel evolution in the RBMK reactor using SCALE 5 code package with deterministic approach T-DEPL sequence in [22] has shown that for the more precise results 3D approach and Monte Carlo method should be used for neutron flux calculation and subsequent generation of 238 group neutron capture cross-sections. Thus, in this particular case the graphite activation calculation was done with SCALE 6.1 TRITON control module using 3D Monte Carlo KENO-VI code to solve neutron transport equations and calculate neutron flux [40]. Deterministic ORIGEN code was applied for depletion and activation calculations. Fuel burn-up and uranium activation inside the graphite stack as well as in the graphite sleeve were modeled using separately depleted mixtures. Activation of low concentration uranium impurities was calculated using “deplete by flux” option which is available on SCALE 6.1, i.e. keeping constant neutron flux which is a correct approximation in the graphite moderator. ENDF/B-VII

238 energy group library was used for calculations.

The power history of the fuel assembly was chosen using officially available data [155] and is presented in Fig. 5.1. Ignalina NPP RBMK-1500 type Unit 1 reactor was operated for 21 years. The year-averaged power (taking into account outage time) was applied to the assemblies during irradiation time (see Fig. 5.1 for details). In this work, the UO_2 fuel enriched to 2.4% of ^{235}U and to 0.41% of burnable erbium poison has been modeled as it corresponds to the typical load of Unit 1 of the Ignalina NPP. The averaged burn-up of nuclear fuel in the RBMK-1500 reactor core was 12.43 GWd/tU. The graphite and cooling water temperatures were kept equal to 700 K and 550 K, respectively, which correspond to the real operating conditions of the RBMK-1500 reactor. The density of the cooling water in the model was equal to 0.5 g/cm^3 and of graphite — 1.675 g/cm^3. It has been accepted that the active height of the fuel assembly is 686 cm. The axial distribution of power in the RBMK-1500 reactor [156] has also been considered.

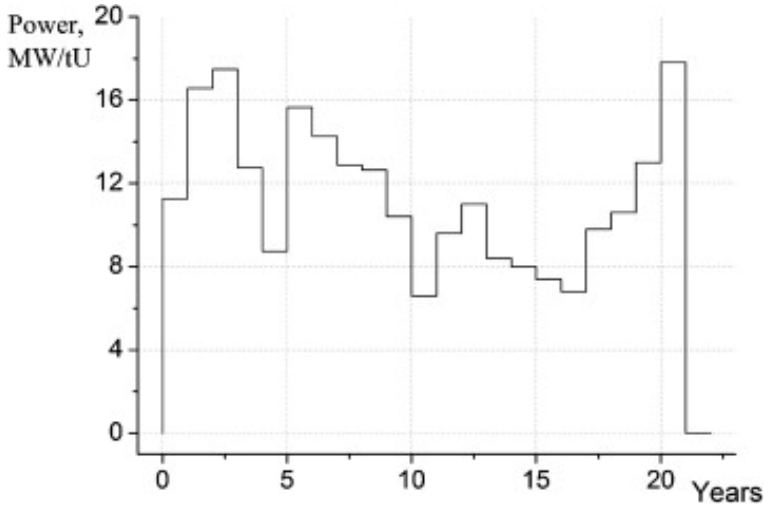

Figure 5.1: The power history of the RBMK-1500 reactor Unit 1 of the Ignalina NPP.

In the SCALE modeling case calculations consisted of two steps: the first step was depletion of fresh fuel to the average burn-up of 12 GWd/tU as well

as following activation of uranium and thorium impurities inside the graphite moderator. The second step was continuation of irradiation of actinides inside the graphite keeping the average fuel burn-up constant. This was done in order to simulate realistic conditions with the constant fuel burn-up and the evolution of impurities inside graphite throughout the reactor operation time. The average fuel burn-up during the second step of calculations was represented by a set of concentrations of 100 most important isotopes of fuel materials, activation and fission products. The neutron fluxes have been calculated in the fuel and graphite using time step duration of 365 days.

In the MCNPX case the graphite activation calculation was performed starting with the constant neutron flux determined by averaged 12 GWd/tU burn-up fuel in the RBMK-1500 reactor core and concentration of both uranium and thorium impurities was taken into account.

As an input data both the KENO-VI and MCNPX codes require a detailed geometry description, nuclear data, materials and impurities of materials. The RBMK-1500 graphite activation analysis due to impurities content in the graphite similarly but with different assumption (UO_2 fuel enrichment 2% of ^{235}U and averaged burnup of 10 GWd/tU) was performed in [90]. In order to compare two computer codes and to avoid time-consuming calculations because of a complicated all reactor core geometry structure (active core, side reflector, top and bottom reflectors, control rods, etc.), we admit a simplified 3D model of the RBMK-1500 reactor core fragment with 14 fuel assemblies and 2 control rods distributed according to the real RBMK-1500 reactor core geometry. This model represents the plateau region of active core and characterizes the realistic graphite activation. The details of the model are described in the next section and in the references therein.

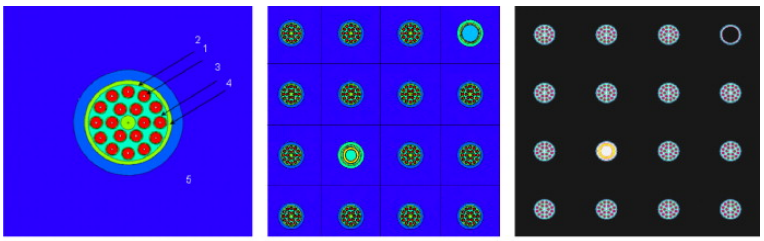

Figure 5.2: (a) One RBMK-1500 fuel assembly in the graphite matrix: 1 — UO_2 fuel with Zr + 1 wt.%Nb cladding, 2 — fuel channel tube from Zr + 2.5 wt.%Nb, 3 — coolant water, 4 -– graphite sleeve, 5 — graphite stack; 3D model of reactor fragment with 14 fuel assemblies and 2 control rods; (b) MCNPX case; (c) SCALE case.

The SCALE calculation was run with 10,000 neutrons, 37 generations and the computer time was 260 min, correspondingly for MCNPX — 800 neutrons, 50 generations and 5230 min of computer time. The main convergence criteria for MCNPX were the relative error of neutron flux energy distribution bins in the considered activation region (∼0.3% for thermal neutrons, ∼0.2% for total flux in the graphite stack and ∼0.3% for thermal neutrons, ∼0.3% for total flux in the sleeve) and the standard deviation of k_{eff} is 0.003. For SCALE calculations: ∼0.06% for thermal neutrons, 0.04% for total flux in the graphite stack and ∼0.1% for thermal neutrons, 0.06% for total flux in the sleeve, and the standard deviation of k_{eff} is 0.001.

The SCALE model was more simplified in terms of the geometry structure and it allows calculating actinide evolution in graphite with U concentration higher than 0.03 ppm, below which the calculation is impossible due to range limits. However, the higher actinides concentration values can be linearly approximated to lower ones taking into account the homogeneous impurity distribution and the fact that the self-shielding effect in the impurities is negligible.

The SCALE calculation will be a preferable choice compared to the much time consuming MCNPX calculation if discrepancies of the results appear to

be acceptable. Here we have concentrated on the comparison of nuclear spectrometry measurement and prediction of simulation using the above-mentioned codes with standard nuclear data libraries (ENDF/B-VII 238 energy group library for SCALE and ENDF/B-VII.1 point-wise data library for MCNPX, whose should be the same by default). The ability to reproduce the correct energy spectrum mostly depends on the geometry approximation and the treatment of resonance absorption of neutrons.

A small part of the specimen of a fresh RBMK-1500 graphite sleeve was separated and prepared for ICP-MS measurements, the preparation procedure and measurement details are comprehensively described in [143, 152]. The concentrations of 38 elements were measured and included in the MCNPX simulation, but for our interest in Table 5.2 only values of actinides impurity concentrations are presented. The measured values were compared with values obtained by the neutron activation analysis technique [90], where the 2.6 times higher values for Th and U were obtained. The minimal concentrations for U and Th are 0.002 ppm and 0.0001 ppm, the maximal concentration 0.2 ppm according to [149] and references therein. There are very few measurements of the actinides concentration in the reactor grade graphite. The minimum–maximum range in Table 5.2 demonstrates this fact and shows the demand of such kind of investigation, because if the maximal value (as a conservative approach) is applied then the activity of the graphite material will be changed drastically. Taking in to account the fact, that measurements have been performed in the different laboratories and using different methods, the obtained result that ratio U/Th is equal to 2 in both cases proves that both methods give correct relative results. The analysis of RBMK graphite impurity concentration determined by the ICP-MS method and comparison with results obtained in [90] was performed in [148]; the difference between results is of the same order of magnitude. However, both methods have weakness: ICP-MS precision is determined by the measured sample size, and neutron activation method can be

influenced by U resonance absorption because activation depends very much on the neutron spectrum. The new ICP-MS measured impurity values were used for further MCNPX and SCALE calculations characterizing the actinides content in the graphite waste.

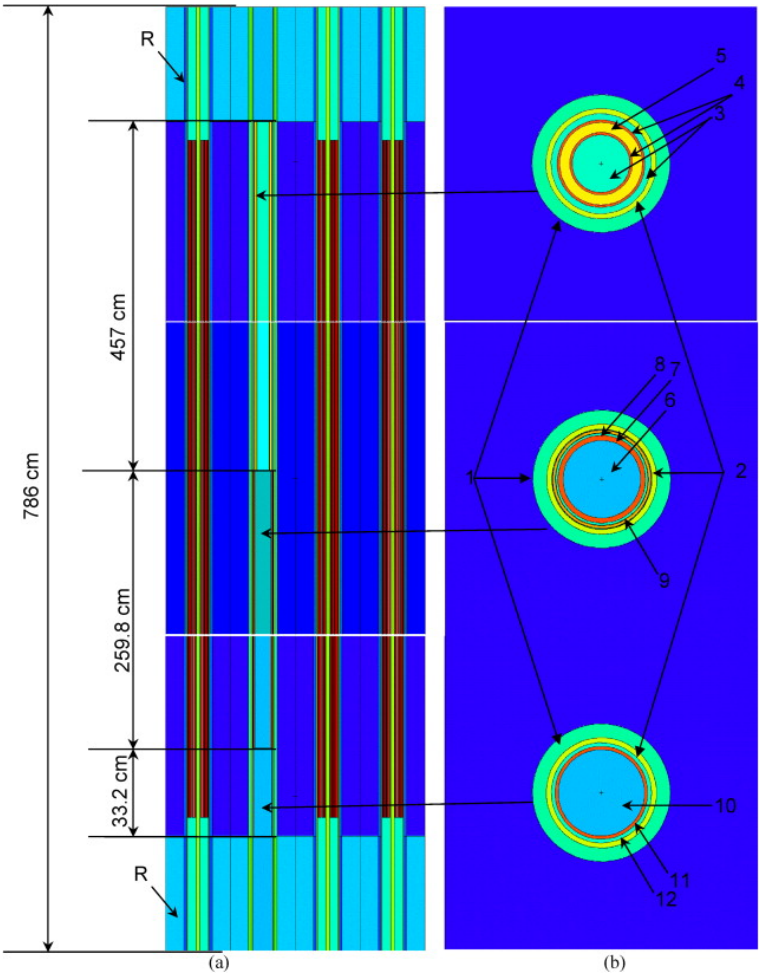

Figure 5.3: (a) Vertical section of core fragment with inserted CPS rod, here R stays for bottom and top reflectors, (b) horizontal cross sections of inserted CPS rod at different height. (1) Graphite stack and graphite sleeve, (2) CPS channel tube from Zr + 2.5wt.%Nb; top part consists of (3) coolant, (4) first and second concentric Al alloy tubes, (5) B_4C absorber; middle part consists of (6) graphite, (7) Al alloy cladding of displacer, (8) coolant, (9) Dy_2TiO_5 absorber with stainless steel cladding (0.4 mm of thickness); bottom part consist of (10) graphite; (11) Al alloy cladding of displacer, (12) coolant.

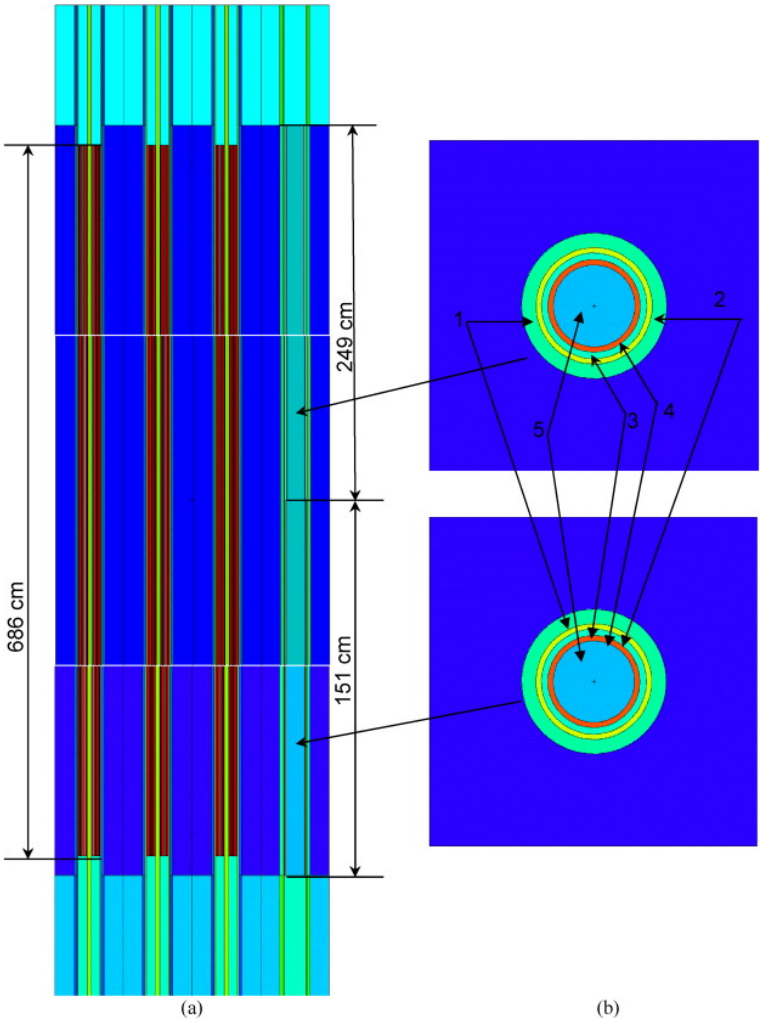

Figure 5.4: (a) Vertical section of core fragment with extracted CPS rod, (b) horizontal cross section of extracted CPS rod at different height. (1) Graphite stack and graphite sleeve, (2) CPS channel tube from Zr + 2.5wt.%Nb, (3) coolant, (4) Al alloy cladding, (5) B_4C absorber.

The sample was taken from the virgin RBMK reactor channel sleeve to represent the central part of the graphite sleeve (∼375 cm of the active length). A small part of the sample was separated and prepared for actinides activity determination by nuclear spectrometry techniques. The graphite sample was dissolved using mineral acids (H_2SO_4, $HClO_4$, HNO_3). The plutonium and americium isotopes were pre-concentrated by scavenging with $Fe(OH)_2$ and $Fe(OH)_3$. Actinides separation was performed using the UTEVA and TRU

Resins [157, 158]. Tracers were used to monitor chemical recoveries for reconstruction of the real results to improve the precision and accuracy. Plutonium and americium isotopes were deposited on the stainless steel disk. The activities of samples were measured using the OCTETE Plus-10600 spectrometer. The alpha peaks resolution was 24 keV (FWHM) at 4–6 MeV.

5.3. Results

The values of the neutron flux are higher in the SCALE 6.1 modeling case compared with MCNPX (see Table 5.1). For example, at the end of the second year of the RBMK-1500 reactor operation (taking into account that neutron flux depends on the power in the model) the neutron fluxes calculated by MCNPX and SCALE 6.1 are 1.24×10^{14} n/cm^{2}s and 1.32×10^{14} n/cm^{2}s in the graphite stack, and 1.19×10^{14} n/cm^{2}s and 1.29×10^{14} n/cm^{2}s in the graphite sleeve, 6% and 8% difference, respectively. The value of the averaged neutron flux in the bottom and top parts of the graphite reflector (50 cm below and above the core, respectively) was equal to 1.2×10^{13} n/cm^{2}s and 1.5×10^{13} n/cm^{2}s for MCNPX and SCALE 6.1, respectively — this makes a 20% increase of neutrons, which is due to a less detailed SCALE 6.1 model. As it was mentioned above, MCNPX model is more detailed geometry of the top and bottom reflectors is close to the real one (channels structure, filling, etc., see Fig. 5.3). In the case of SCALE 6.1 simple structure of top reflectors with openings filled by water is used. From this point of view, the MCNPX model is superior, but, as always, it should be benchmarked against the experimental measurements of the samples taken from this part of the graphite.

Table 5.1: Neutron fluxes in different parts of the reactor graphite calculated by MCNPX and SCALE 6.1, n/cm^{2}s.

Part	**MCNPX**	**SCALE 6.1**
Stack	1.24×10^{14}	1.32×10^{14}
Sleeve	1.19×10^{14}	1.29×10^{14}
Reflector	1.2×10^{13}	1.5×10^{13}

The neutron spectrum in the graphite does not change considerably during the irradiation time but depends on the graphite location in the reactor [143]. The thermal neutron spectrum in the graphite stack is higher by 8% compared with the graphite sleeve, the epithermal neutron spectrum is almost the same (the difference is less than 1%) and the fast neutron spectrum is by 9% higher in the graphite sleeve at the average fuel burn-up (see Fig. 5.5 for details) for both MCNPX and SCALE 6.1 modeling cases, although the energy spectrum calculated by MCNPX and SCALE 6.1 is slightly different: the thermal neutron spectrum is higher by 1% for the SCALE 6.1 and the fast neutron spectrum is higher by 2% for MCNPX. The variable neutron flux (i.e., variable macroscopic cross-sections) in the particular graphite structure (graphite stack, graphite sleeve) was taken into account for modeling of activation of actinides in the graphite.

Table 5.2: Actinides impurity concentrations in the graphite sleeve sample (ppm).

Isotope	**Present work**	**[90]**	**Min [149]**	**Max [149]**
Th	0.003 ± 0.001	0.0079±0.0004	0.0001	0.2
U	0.006±0.001	0.016±0.001	0.002	0.2

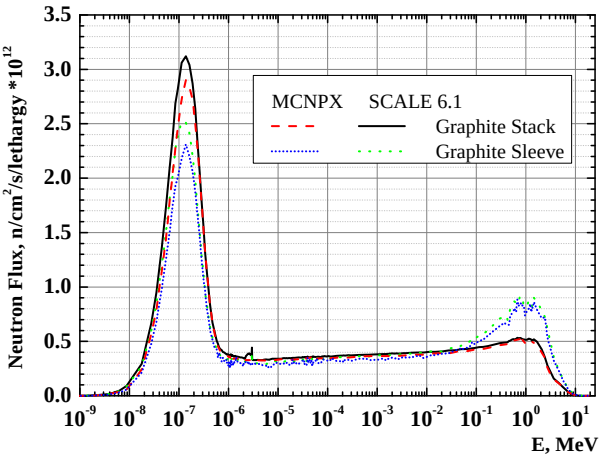

Figure 5.5: The neutron flux spectrum in graphite stack and graphite sleeve calculated by MCNPX and SCALE 6.1.

U and Th impurities in the virgin graphite are responsible for the presence of trans-uranium isotopes in the irradiated graphite. There are about 25 trans-uranium isotopes generated in the irradiated graphite construction with concentrations higher than 10^{-12}.

As it was already mentioned, measured by ICP-MS U and Th impurity concentrations (see Table 5.2) were used for the neutron activation calculation in the graphite using MCNPX (v2.6) and SCALE 6.1. It should be noted that for SCALE 6.1 case the initial U and Th concentration was increased and recalculated afterwards for comparison with MCNPX results. Additional SCALE 6.1 simulations with and without Th impurity pointed out that the increase of the total actinide activity due to Th impurity was less than 1%. The Th impurity activation is negligible compared with the U impurity activation due to both: the dominant thermal neutron flux (the (n, γ) reaction rate for ^{238}U is two times and for ^{235}U is six times higher comparing with ^{232}Th, which has neutron capture resonances in the epithermal energy range (1–10^{-3} eV) and that the activation of ^{232}Th does not lead to significant creation of plutonium and higher actinides.

Table 5.3: Actinide activity in the graphite sleeve sample.

Isotope	**Activity, Bq/kg**
^{241}Am	120 ± 50
^{242}Cm	90 ± 30
^{243}Cm + ^{243}Cm	11000 ± 2000
^{238}Pu	400 ± 70
^{239}Pu + ^{240}Pu	70 ± 20

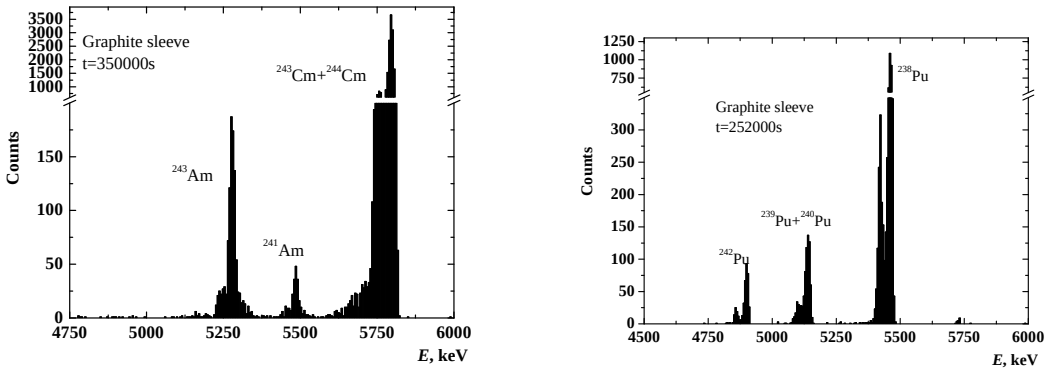

(a) (b)

Figure 5.6: (a) Americium and curium; (b) plutonium α spectra.

In order to check the initial U impurity concentration and verify our calculations with both codes the calculation results of the graphite activation after 19 years of irradiation in the RBMK-1500 reactor core were compared with nuclear spectrometry results, which are presented in Table 5.3 and Fig. 5.6. Further we present a comparison of modeling and experimental results of activation of the irradiated graphite sleeve for the same graphite structure part.

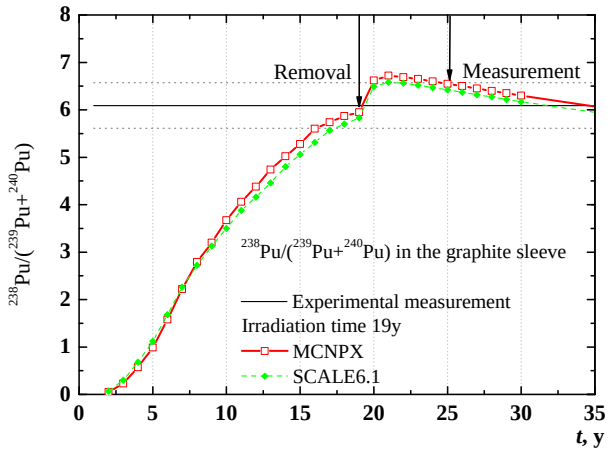

Figure 5.7: The change of modeled and measured ratio of ^{238}Pu/^{239}Pu + ^{240}Pu in time including 2σ confidence bands of experimental results.

As the measured absolute values of activities have large absolute uncertainties, it is difficult to compare them directly with calculation results. Thus, we have compared the ratios of α emitter isotopes, namely ^{238}Pu/(^{239}Pu + ^{240}Pu) and (^{243}Cm + ^{244}Cm)/^{241}Am. In Fig. 5.7 one can observe a change of the ratio of ^{238}Pu/(^{239}Pu + ^{240}Pu) in time for MCNPX and SCALE 6.1 modeling cases and the measured ^{238}Pu/(^{239}Pu + ^{240}Pu) ratio which is shown by black line (dotted lines stand for confident bands). The measured ratio of Pu isotopes agrees within the 2σ confidence level with calculation results at the measurement time in 2009. In the period of 1–5 years after sample removal the demonstrated ratio would exceed 2σ confidence bands limits. The increase of the ratio after 19 years of irradiation is observed due to α decay of ^{242}Cm after removal of the irradiated sleeve from the reactor core.

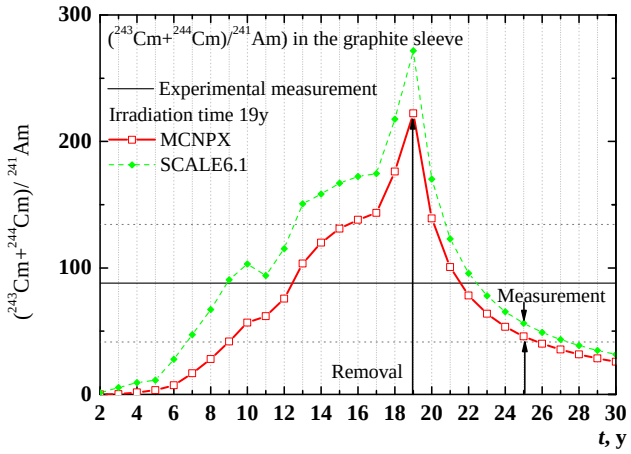

Figure 5.8: The change of the modeled and measured ratio of ^{243}Cm + ^{244}Cm/^{241}Am in time including 2σ confidence bands of experimental results.

The change of the modeled and measured ratio of ^{243}Cm + ^{244}Cm/^{241}Am in time is presented in Fig. 5.8. This ratio increases during the reactor operation and is very sensitive to the power history of the reactor, because ^{241}Am build-up is inversely proportional to the reactor power (^{241}Pu formation and decay, and ^{241}Am captures). This ratio also greatly depends on the time of the graphite sample removal and on the nominal power of a recent reactor operation or calculation step in our case. If the graphite sample had been taken after 20 or 21 years of INPP Unit 1 operation, the ^{243}Cm + ^{244}Cm/^{241}Am would be respectively two and three times higher compared with the present case of the sleeve removal after 19 years. After the termination of the irradiation, the ratio decreases because of Cm isotopes decay and buildup of ^{241}Am due to ^{241}Pu β-decay. According to the known date of the graphite sample removal (the year 2003) and the averaged reactor power in that year the modeled ratio falls in the 2σ confidence level of the experimental ratio value in the period from 20 to 26 years. This corresponds to the time of the sample measurement (in year 2009), but demonstrates that ^{243}Cm + ^{244}Cm/^{241}Am ratio is difficult to assess.

Comparative analysis has demonstrated that modeled and experimentally measured isotope ratios agree well within experimental uncertainties for both MCNPX and SCALE 6.1 modeling cases. In a further analysis step we compared absolute values of measured activities with modeled ones — the time-dependent ratios are presented in Fig. 5.9. At the point where measured graphite sleeve sample activities would be equal to the modeled ones the ratio should be equal to 1, except for ^{241}Am as it was discussed above. From the results presented in Fig. 5.9 we can see that this point is equal to approximately 7. Assuming that the actinide generation is directly proportional to the U impurity concentration in the virgin graphite sleeve we should reduce the initial U concentration to 8.6×10^{-4} ppm. This means that the RBMK-1500 graphite is a very pure material; it contains very low concentration of actinides. This experimentally tested initial U concentration was used for the actinide nuclide composition calculation in the graphite stack and graphite sleeve subsequently.

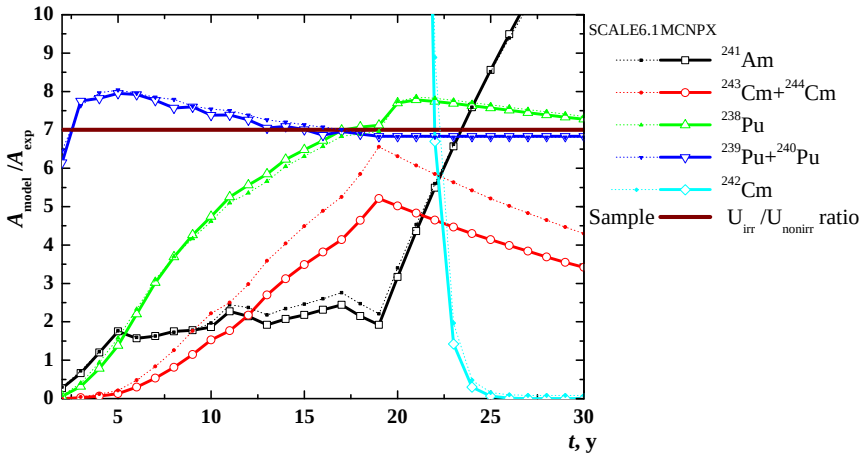

Figure 5.9: The time dependent ratios of absolute values of measured activities with modeled ones using SCALE 6.1 and MCNPX.

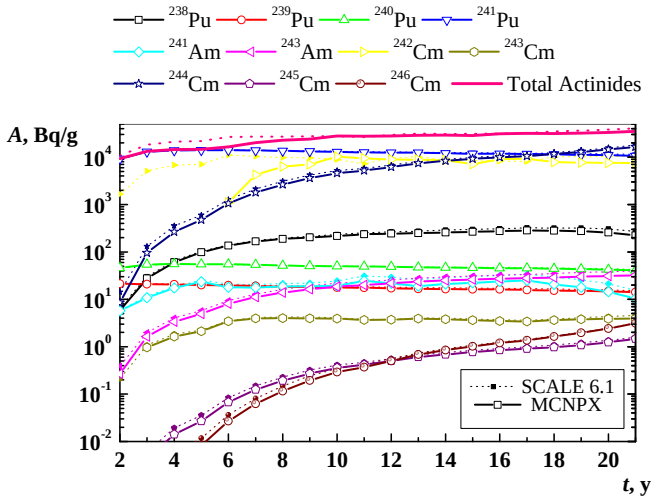

Figure 5.10: Specific activities of actinides in the graphite stack as a function of irradiation time modeled using MCNPX and SCALE 6.1.

The MCNPX and SCALE 6.1 calculations of generation of the most important actinides in the reactor graphite stack were evaluated with a modified U impurity concentration and the known reactor power history for the whole reactor operation time, namely 21 years. The results of the specific activities of actinides in the graphite stack as a function of irradiation time for MCNPX and SCALE 6.1 modeling cases are presented in Fig. 5.10. Comparison of the actinide generation in the reactor graphite in MCNPX and SCALE 6.1 model shows similarity for all most important actinides, but the higher specific activity values are generally obtained by SCALE 6.1, except for ^{244}Cm. The total activity in the graphite is determined by ^{241}Pu, ^{242}Cm, and ^{244}Cm and is of the order of 30 kBq/kg. The difference of radionuclide specific activities in the graphite stack between SCALE 6.1 and MCNPX modeling cases is presented in Fig. 5.11. It should be noted that the obtained actinides activities are less by 1–30% for different isotopes in the MCNPX case. The differences could be partly influenced by the calculation step and intermediate actinide cross section recalculation (predictor/corrector step) for intermediate actinide concentrations. The largest differences were obtained for ^{241}Am and ^{242}Cm

isotopes which are very sensitive to the neutron energy spectrum, the operational power and nuclear data library (concerning ^{242m}Am and ^{242}Am). The generation of ^{244}Cm (and subsequently ^{245}Cm and ^{246}Cm) is by 20% higher in MCNPX case due to the higher capture rate.

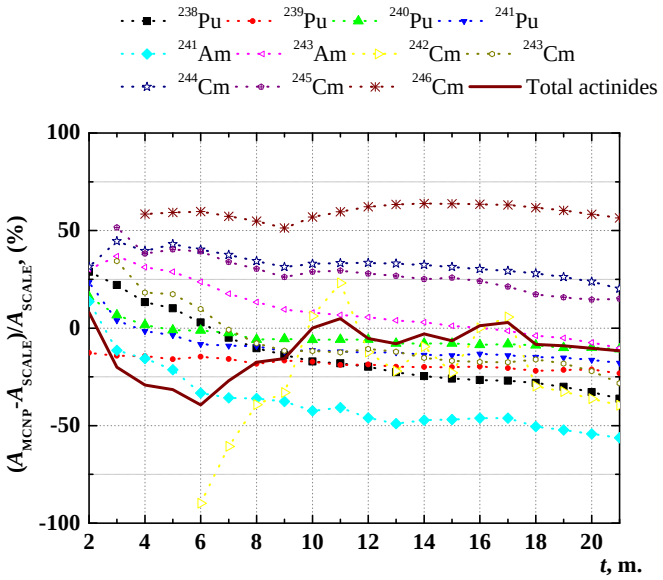

Figure 5.11: Relative difference of radionuclide specific activities due to activation of impurities in the graphite for SCALE 6.1 and MCNPX modeling cases.

The specific activities of actinides as a function of cooling time in the graphite stack and the graphite sleeve modeled by MCNPX and SCALE 6.1 are presented in Fig. 5.12. The total activity differs by 11% between modeling cases and by 3% between the graphite stack and the sleeve after the reactor shout down. ^{244}Cm and ^{241}Pu dominate during the first 200 years, afterwards ^{241}Am dominates until 1000 years. The main difference between two modeling cases was in the ^{242}Cm specific activity calculation due to the MCNPX neutron data library. The decay of ^{242}Cm was also recalculated manually, because MCNPX (coupled with CINDER) calculates the decay of ^{242}Cm incorrectly. CINDER uses CINDER data library which is based on ENDF/B-VII nuclear

data library, and there ^{242m}Am data exist, but, unfortunately, for ^{242}Cm decay evaluation it does not take metastable nuclide nuclear data into account due to, we suppose, incorrect communication with MCNPX working file. According to the obtained results of ^{242}Cm activity, we understood, that the input from ^{242}Am β-decay is included but contribution from ^{242m}Am IT is missing, so we recalculated manually the decay of ^{242}Cm. ^{244}Cm, ^{238}Pu, and ^{241}Am are the actinides the specific activity of which exceeds unconditional clearance levels [159] in the graphite stack and sleeve and which can cause a particular risk to waste management.

^{241}Pu and ^{240}Pu specific activity does not exceed the clearance levels, but in the stack specific activity of ^{240}Pu is almost at the limit boundary. The ^{244}Cm activity calculated by MCNPX and SCALE 6.1 is 1.5 and 1.3 times higher in the graphite stack than in the graphite sleeve, respectively. Comparing with [90] we obtain a much lower actinides concentration in the graphite sleeve due to 18.6 times lower experimentally proved initial U and Th impurity concentration, different impurities concentration for other nuclides such as B, Cl see [148] and slightly different irradiation conditions (∼6% higher thermal neutron spectrum due side reflectors included in the model). If the work [90] U and Th impurity concentration were proved experimentally and applied to this calculation, the radiotoxicity of actinides would be much worse in the long term: all important actinides, except ^{242}Cm, would exceed the clearance levels [159]. For example, the ^{241}Pu would exceed the clearance levels during the first 30 years, ^{244}Cm — during 200 years, and long-lived ^{239}Pu and ^{240}Pu during 50,000 years and 20,000 years, respectively (see Fig. 5.13 for detail).

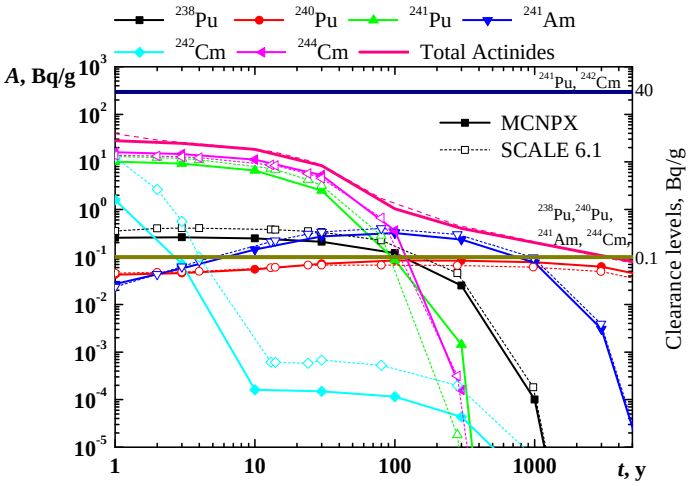

(a)

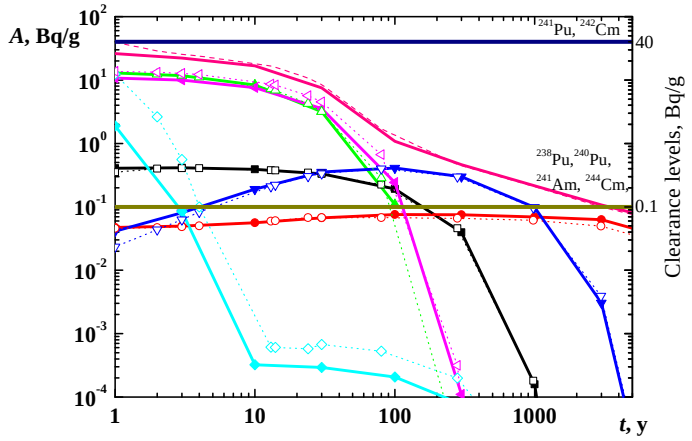

(b)

Figure 5.12: Specific activities of actinides, which exceed or approach their clearance levels, as a function of cooling time in the graphite stack (a) and graphite sleeve (b) modeled using MCNPX and SCALE 6.1. The clearance levels of the isotopes are shown on the right scale [159].

Both irradiated and virgin graphite samples are from the same source but not from the same batch — the graphite sleeve was made from the same grade of graphite at the same factory but at different time. As it was discussed above, the ICP-MS precision is determined by the measured sample size, ∼100 inde-

pendent measurements of different parts of the same grade of graphite should be made for complete characterization of graphite impurity concentration. This is not possible due to limited access to the nuclear objects. In this context, all experimental values obtained on the impurity concentration in the virgin graphite are of great value for the estimation of ranges of neutron activation of the graphite during reactor operation and decommissioning process.

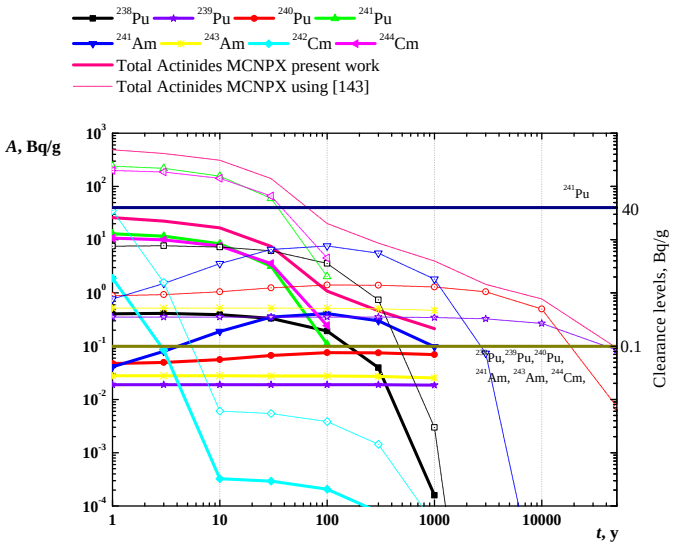

Figure 5.13: Specific activities of actinides, which exceed or approach their clearance levels, as a function of cooling time in the graphite sleeve modeled using MCNPX with different initial U concentration, namely 8.6×10^{-4} ppm and 0.016 ppm as in [90]. The clearance levels of the isotopes are shown on the right scale [159].

Relative differences of radionuclide specific activities due to activation of impurities in the graphite sleeve and the stack calculated using SCALE 6.1 and MCNPX are presented in Fig. 5.14. The differences are considerable (more than 10%) for the most of actinides, because they are sensitive to the neutron spectrum — small fluctuations in the thermal neutron flux cause large differences, up to 50%, of specific activities of some radionuclides. Taking into

account the same modeling conditions, the specific activities in SCALE 6.1 case are up to 15% less compared to MCNPX case, because of higher initial U concentration determined by calculation range limits, as it was reported in section 1.2.

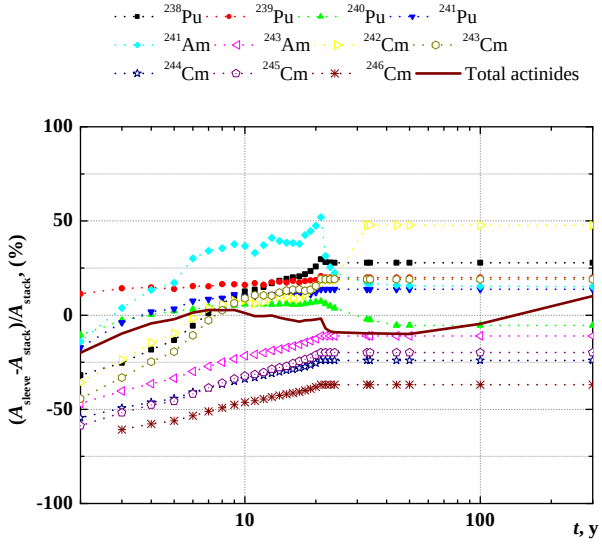

(a)

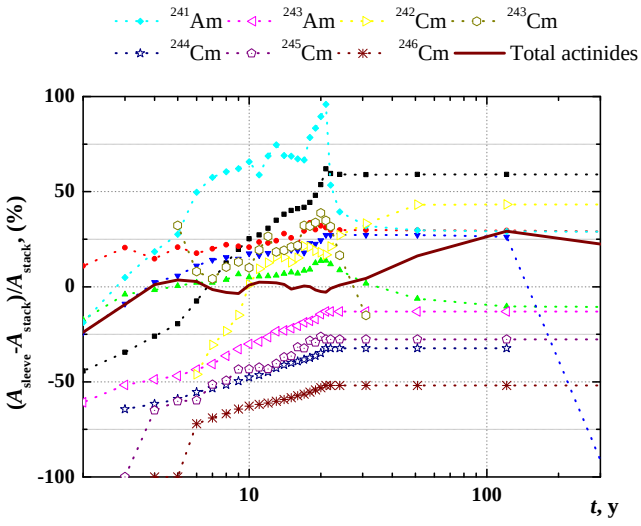

(b)

Figure 5.14: The relative difference of radionuclide specific activities due to impurities activation in the graphite sleeve and stack for SCALE (a) and MCNP (b) modeling cases.

The difference of specific activities in different constructions of graphite could affect the classification of the radionuclides whose amounts are in the clearance level range. For instance, ^{240}Pu activity in the sleeve is below the clearance level, but in the stack it is almost at the limit boundary.

5.4. Conclusions

The actinide composition in the irradiated graphite of the RBMK-1500 reactor has been modeled using MCNPX (v2.7 which includes CINDER burn-up capability) and SCALE 6.1 (with KENO VI) package. The same graphite actinide impurity concentration values obtained by ICP-MS were used in MCNPX and SCALE 6.1 models. The calculation results of the graphite activation were compared with nuclear spectrometry measurements of the graphite sample taken from the core of the Ignalina NPP Unit 1 reactor. The alpha spectrometry results of the ratios of α emitting isotopes, such as ^{238}Pu/(^{239}Pu + ^{240}Pu) and (^{243}Cm + ^{244}Cm)/^{241}Am, confirm the applicability of created models for prediction of graphite activation with actinides. It was figured out, that (^{243}Cm + ^{244}Cm)/^{241}Am ratio is sensitive on the time of the graphite sample removal and on the power level of a reactor operation in the last period and is difficult to assess. After comparison of the ratios of measured Pu, Am and Cm isotope activities in the irradiated graphite sample with activities calculated by SCALE 6.1 and MCNPX the initial U impurity concentration in the graphite was adjusted, i.e. was reduced to U concentration of 8.6×10^{-4} ppm. This signifies that the virgin RBMK-1500 graphite was a quite pure material; it contains very low concentration of actinides.

Experimentally tested initial U concentration was used for the actinide nuclide composition calculation in the graphite structures for the whole reactor operation time, namely 21 years. The satisfactory results were obtained with both models for all actinides, except ^{241}Am and ^{242}Cm, which are very sen-

sitive to the neutron energy spectra, the operational power and nuclear data library. For radiological graphite characterization in the reactor plateau region a less sophisticated SCALE 6.1 3D model can be used gaining considerably (20 times) in the computer time. To complete the radiological characterization of spent RBMK graphite additional experimental data are necessary for the top and bottom reflectors.

The difference of radionuclide specific activities due to impurity activation in the graphite sleeve and stack constructions is considerable (more than 10%) for the most of actinides; because actinides are sensitive to the neutron flux energy distribution which depends on the graphite location in the reactor. This can affect the estimation of the actinides which are at the limit boundary of the clearance levels. For instance, ^{240}Pu activity in the sleeve is below the clearance level, but in the stack it is almost at the limit boundary.

The obtained graphite actinide content has been compared with the previous calculation [90] made with different impurity concentrations obtained by neutron activation analysis and GDMS. In the present calculation significantly ($\sim$20 times) lower values of actinides specific activities in the graphite stack were obtained due to lower initial U and Th impurity concentration and slightly different irradiation conditions. ^{244}Cm is very important for dismantling management decision and a lower activity value is more favorable, but unfortunately ^{244}Cm, ^{238}Pu, and ^{241}Am still exceed unconditional clearance levels and can cause a particular risk to the waste disposal.

The measurement of the irradiated graphite activation of the certain sample with known position in the reactor core and known real neutron irradiation environment allows us to obtain the initial impurity concentration in this sample and to calibrate both an impurity concentration of the virgin graphite and modeling tools used for calculation (especially due to the fact that the results calculated with two different codes give good enough agreement for the nuclide evolution prediction). The obtained results are important for further

decommissioning process of the Ignalina NPP and other RBMK type reactors. Especially for ^{244}Cm estimation which is a critical parameter characterizing the total activity of actinides in the spent graphite for approximately 200 years. The calculated total specific activity of the actinides does not exceed values recommended by the IAEA for acceptance of waste packages with a wide margin of the order of magnitude.

Summary and conclusions

In this dissertation the influence of actinides and other strongly neutron-absorbing nuclides on nuclear safety characteristics of nuclear fuel and radiation safety characteristics of the actinides in the RBMK reactor moderator graphite have been studied.

The composition of the RBMK spent nuclear fuel with the erbium burnable absorber was evaluated using calculated one-group cross-section libraries. The effective neutron multiplication factor k_{eff} of the spent nuclear fuel cask was evaluated taking into account the spent nuclear fuel composition changes during burn-up as well as introducing the axial burn-up profile of the nuclear fuel assembly. The build-up of long-lived actinides in the RBMK reactor graphite from very small fraction of uranium impurities in the virgin nuclear graphite during operation of the reactor was calculated precisely by evaluating the reactor neutron spectrum characteristics through the novel use of the average burn-up composition of the nuclear fuel.

To sum up, it can be concluded that:

1. Concentrations of actinides important to the criticality evaluation calculated using one-group cross-section libraries were compared with the available experimental data. The comparison shows an acceptable agreement between modeling and experimental data, except for ^{238}Pu and ^{241}Am.

2. The isotopic composition differences between 2% enrichment fuel and 2.8% enrichment fuel with the erbium burnable absorber in case of the actinides important to the criticality evaluation vary from 11% to 52% depending on the nuclide for the same burn-up value.

3. Differences of k_{eff} results of low burn-up 2.8% enrichment fuel between actinide-only and fission product with burnable absorbers approaches are caused by the ^{167}Er presence in fresh fuel. The decrease of k_{eff} in high

burn-up spent nuclear fuel was found to be caused by the increasing concentration of the fission products, but not due to the erbium burnable absorber which burns-out.

4. A significant positive end-effect on k_{eff} was noticed from 15 GWd/tU burn-up for 2.8% enrichment fuel and from 9 GWd/tU burn-up for 2.0% enrichment fuel. Non-uniform fissile ^{235}U depletion is responsible for the end-effect in the RBMK spent nuclear fuel whereas build-up of plutonium has no significant effect.

5. Comparison with the experimental data confirms the applicability of the created numerical model for prediction of the graphite uranium activation products. The satisfactory results were obtained for all actinides, except ^{241}Am and ^{242}Cm, which are very sensitive to the neutron energy spectra, the operational power and nuclear data library.

Bibliography

[1] *IAEA Safety Glossary, 2016 revision*, Technical report, International Atomic Energy Agency (2016).

[2] G. Petrangeli, Chapter 3 — Safety systems and their functions, in G. Petrangeli (ed.), *Nuclear Safety* (Butterworth-Heinemann, 2006), 17–33.

[3] *Interim Storage of RBMK Spent Nuclear Fuel from Ignalina NPP Units 1 and 2 (Environmental Impact Assessment Report)*, Technical report, Lithuanian Energy Institute, Consortium GNS–NUKEM (2007).

[4] *Preliminary Safety Analysis Report of Interim Storage Facility for RBMK Spent Nuclear Fuel Assemblies from Ignalina NPP Units 1 and 2 (B1)*, Technical report, Lithuanian Energy Institute, Consortium GNS (2007).

[5] B. Davison, J. Sykes, *Neutron transport theory* (Oxford University Press, 1958).

[6] E. E. Lewis, W. F. Miller Jr., *Computational methods of neutron transport* (John Wiley and Sons, 1984).

[7] P. Reuss, *Neutron Physics* (EDP Sciences, 2008).

[8] *Implementation of Burn-up Credit in Spent Fuel Management Systems, IAEA-TECDOC-1013, Proceedings of an Advisory Group meeting held in Vienna, 20–24 October 1997*, Technical report, International Atomic Energy Agency (1998).

[9] *Practices and Developments in Spent Fuel Burn-up Credit Applications, IAEA-TECDOC-1378, Proceedings of a Technical Committee meeting held in Madrid, 22–26 April 2002*, Technical report, International Atomic Energy Agency (2003).

[10] *Advances in Applications of Burn-up Credit to Enhance Spent Fuel Transportation, Storage, Reprocessing and Disposition, IAEA-TECDOC-1547, Proceedings of a Technical Meeting held in London, 29 August–2 September 2005*, Technical report, International Atomic Energy Agency (2007).

[11] *Spent Nuclear Fuel Assay Data for Isotopic Validation*, Technical report, OECD Nuclear Energy Agency (2011).

[12] VATESI, Nuclear Safety Requirements BSR-3.1.1-2010, General requirements for dry type storage facility of spent nuclear fuel, Official Gazette **91-4846** (2010).

[13] P. Cousinou, C. Lavarenne, D. Biron, M. Douchet, J. Grouiller, N. Thiollay, E. Guillou, Taking burn-up credit into account in criticality studies: the situation as it is now and the prospect for the future, Nuclear Engineering and Design **208**(2), 205–214 (2001).

[14] J. J. Herrero, A. Vasiliev, M. Pecchia, H. Ferroukhi, S. Caruso, Review calculations for the OECD/NEA burn-up credit criticality safety benchmark, Annals of Nuclear Energy **87**(2), 48–57 (2016).

[15] R. Mahmoud, M. Shaat, M. Nagy, S. Agamy, A. Abdelrahman, Burn-up credit in criticality safety of PWR spent fuel, Nuclear Engineering and Design **280**, 628–633 (2014).

[16] H. Yun, D.-Y. Kim, K. Park, S. Hong, A criticality analysis of the GBC-32 dry storage cask with Hanbit nuclear power plant Unit 3 fuel assemblies from the viewpoint of burn-up credit, Nuclear Engineering and Technology **48**(3), 624–634 (2016).

[17] M. Tardy, S. Kitsos, G. Grassi, A. Santamarina, L. San Felice, C. Riffard, First burn-up credit application including actinides and fission products

for transport and storage cask by using French experiments, Journal of Nuclear Science and Technology **52**(7-8), 1008–1017 (2015).

[18] J. C. Wagner, M. D. DeHart, B. Broadhead, *Investigation of Burn-up Credit Modeling Issues Associated With BWR Fuel*, Technical report, Oak Ridge National Laboratory (2000).

[19] J. C. Wagner, M. D. DeHart, *Review of Axial Burn-up Distribution Considerations for Burn-up Credit Calculations*, Technical report, Oak Ridge National Laboratory (2000).

[20] B. L. Broadhead, B. T. Rearden, C. M. Hopper, J. J. Wagschal, C. V. Parks, Sensitivity- and uncertainty-based criticality safety validation techniques, Nuclear Science and Engineering **146**, 340–366 (2004).

[21] D. Rochman, C. Sciolla, Nuclear data uncertainty propagation for a typical PWR fuel assembly with burn-up, Nuclear Engineering and Technology **46**(3), 353–362 (2014).

[22] R. Plukienė, A. Plukis, D. Germanas, V. Remeikis, Numerical sensitivity study of irradiated nuclear fuel evolution in the RBMK reactor, Lithuanian Journal of Physics **49**(4), 461–469 (2009).

[23] M. W. Francis, C. Weber, M. Pigni, I. Gauld, *Reactor Fuel Isotopics and Code Validation for Nuclear Applications*, Technical report, Oak Ridge National Laboratory (2014).

[24] L. Fiorito, D. Piedra, O. Cabellos, C. Diez, Inventory calculation and nuclear data uncertainty propagation on light water reactor fuel using ALEPH-2 and SCALE 6.2, Annals of Nuclear Energy **83**, 137–146 (2015).

[25] H. Jeong, H. Jeong, E. Kim, M. Han, W. Hwang, Assessment of fission product inventory considering axial burn-up of a fuel assembly, Annals of Nuclear Energy **90**, 240–246 (2016).

[26] K. Yancey, P. Tsvetkov, Quantification of U.S. spent fuel inventories in nuclear waste management, Annals of Nuclear Energy **72**, 277–285 (2014).

[27] R. Plukienė, A. Plukis, V. Remeikis, D. Ridikas, MCNP and ORIGEN codes validation by calculating RBMK spent nuclear fuel isotopic composition, Lithuanian Journal of Physics **45**(4), 281–287 (2005).

[28] A. Šmaižys, *Analysis of nuclear and radiation characteristics of RBMK-1500 spent nuclear fuel casks and storage facilities*, Ph.D. thesis, Lithuanian Energy Institute (2004).

[29] K. Almenas, A. Kaliatka, E. Ušpuras, *Ignalina RBMK-1500. A source book.*, Technical report, Lithuanian Energy Institute (1998).

[30] G. Krivoshein, A. Kulko, A. Markelov, Fuel with burnable absorber for RBMK-1500, Energy News - Energy Agency of Lithuania (1997).

[31] V. N. Shevaldin, G. P. Negrivoda, B. A. Vorontsov, A. V. Robomko, E. V. Burlakov, A. V. Krayushkin, A. M. Fedosov, Y. A. Tishkin, V. G. Novikov, A. K. Panyushkin, A. I. Kupalov-Yaropolk, V. A. Nikolaev, Y. K. Bibilashvili, V. S. Yamnikov, Experience with uranium-erbium fuel at the Ignalinsk atomic power plant, Atomic Energy **85**(2), 517–522 (1998).

[32] V. Šimonis, A. Šmaižys, P. Poškas, Thermal assessment of new Ignalina NPP casks for spent nuclear fuel storage, Energetics **57**(3), 163–171 (2011).

[33] V. Šimonis, V. Ragaišis, A. Šmaižys, Thermal assessment of new Ignalina NPP casks for spent nuclear fuel storage at some abnormal conditions, Mechanika **19**(2), 159–166 (2013).

[34] E. Narkūnas, A. Šmaižys, P. Poškas, Analysis of nitrogen impurity impact on ^{14}C generation in RBMK-1500 reactor graphite, in *EPRI International Decomissioning and Radioactive Waste management Workshop, 6-7 October 2009, Hamburg, Germany* (2009).

[35] D. LaBrier, M. Dunzik-Gougar, Characterization of ^{14}C in neutron irradiated NBG-25 nuclear graphite, Journal of Nuclear Materials **448**(1-3), 113–120 (2014).

[36] M. Le Guillou, N. Toulhoat, Y. Pipon, N. Moncoffre, H. Khodja, Deuterium migration in nuclear graphite: Consequences for the behavior of tritium in CO_2-cooled reactors and for the decontamination of irradiated graphite waste, Journal of Nuclear Materials **461**, 72–77 (2015).

[37] N. Toulhoat, N. Moncoffre, N. Bérerd, Y. Pipon, A. Blondel, N. Galy, S. P., J.-N. Rouzaud, D. Deldicque, Ion irradiation of ^{37}Cl implanted nuclear graphite: Effect of the energy deposition on the chlorine behavior and consequences for the mobility of ^{36}Cl in irradiated graphite, Journal of Nuclear Materials **464**, 405–410 (2015).

[38] E. Narkūnas, A. Šmaižys, P. Poškas, G. Bartkus, Modelling of the spatial distribution of the induced activities in the RBMK-1500 reactor graphite blocks and rings/sleeves, Progress in Nuclear Energy **91**, 265–276 (2016).

[39] G. Hehn, B. Na, E. Sartori, NEA organised validation of multi- dimensional transport codes and cross-section sets used presently in reactor shielding, Journal of Nuclear Science and Technology **37** (2000).

[40] S. M. Bowman, SCALE 6: Comprehensive nuclear safety analysis code system, Nuclear Technology **174**(2), 126–148 (2011).

[41] W. Oberkampf, T. Trucano, Verification and validation benchmarks. Benchmarking of CFD codes for application to nuclear reactor safety, Nuclear Engineering and Design **238**(3), 716–743 (2008).

[42] A. Šmaižys, P. Poškas, E. Narkūnas, G. Bartkus, Numerical modelling of radionuclide inventory for RBMK irradiated nuclear fuel, Nuclear Engineering and Design **277**, 28–35 (2014).

[43] Y. P. Kovbasenko, M. Yeremenko, Isotopic composition evaluation of spent RBMK reactor nuclear fuel for spent nuclear fuel safety analysis taking into account burn-up credit, Nuclear and radiation safety **2**(50), 35–42 (2011).

[44] F. Damian, E. Brun, ORPHEE research reactor: 3D core depletion calculation using Monte-Carlo code TRIPOLI-4®, Annals of Nuclear Energy **82**, 203–216, joint International Conference on Supercomputing in Nuclear Applications and Monte Carlo 2013, SNA + MC 2013. Pluri- and Trans-disciplinarity, Towards New Modeling and Numerical Simulation Paradigms (2015).

[45] R. Sheu, C. Chao, O. Feynberg, Y.-W. Liu, A fuel depletion analysis of the MSRE and three conceptual small molten-salt reactors for Mo-99 production, Annals of Nuclear Energy **71**, 111–117 (2014).

[46] J. Neuber, J. Conde Lopez, Lecture 3 power point slides, in *Workshop on Criticality Safety / Burnup Credit (BUC) in Spent Fuel Handling and Storage State Office for Nuclear Safety, Prague* (2007).

[47] D. Mennerdahl, Burn-up credit bibliography.OECD NEA (2005).

[48] *Implementation of Burn-up Credit in Spent Fuel Management Systems, IAEA-TECDOC-1241, Proceedings of a Technical Committee meeting held in Vienna, 10–14 July 2000*, Technical report, International Atomic Energy Agency (2000).

[49] C. Parks, M. DeHart, J. Wagner, *Review and Prioritization of Technical Issues Related to Burn-up Credit for LWR Fuel*, Technical report, Oak Ridge National Laboratory (2000).

[50] I. C. Gauld, *Strategies for Application of Isotopic Uncertainties in Burn-up Credit*, Technical report, Oak Ridge National Laboratory (2002).

[51] G. Radulescu, D. Mueller, J. Wagner, *Sensitivity and Uncertainty Analysis of Commercial Reactor Criticals for Burn-up Credit*, Technical report, Oak Ridge National Laboratory (2007).

[52] *Limited Burn-up Credit in Criticality Safety Analysis: A Comparison of ISG-8 and Current International Practice*, Technical report, U.S. Nuclear Regulatory Commission (2001).

[53] *Burn-up Credit PIRT Report*, Technical report, U.S. Nuclear Regulatory Commission (2002).

[54] *Technical Basis for Peak Reactivity Burn-up Credit for BWR Spent Nuclear Fuel in Storage and Transportation Systems*, Technical report, U.S. Nuclear Regulatory Commission (2015).

[55] *Burn-up Credit in the Criticality Safety Analyses of PWR Spent Fuel in Transportation and Storage Casks*, Technical report, US Nuclear Regulatory Commission (2012).

[56] C. Velasquez, R. Sousa, A. Fortini, C. Pereira, A. Costa, C. da Silva, M. Veloso, A. de Oliveira, F. de Carvalho, Spent fuel criticality and compositions evaluation for long-term disposal in a generic cask, Nuclear Engineering and Design **275**, 168–178 (2014).

[57] O. Leray, D. Rochman, P. Grimm, H. Ferroukhi, A. Vasiliev, M. Hursin, G. Perret, A. Pautz, Nuclear data uncertainty propagation on spent fuel nuclide compositions, Annals of Nuclear Energy **94**, 603–611 (2016).

[58] R. Bratton, M. Avramova, K. Ivanov, OECD/NEA benchmark for uncertainty analysis in modeling UAM for LWRs — summary and discussion

of neutronics cases. Phase I, Nuclear Engineering and Technology **46**(3), 313–342 (2014).

[59] *Overview of Approaches Used to Determine Calculational Bias in Criticality Safety Assessment. State-of-the-Art Report (Part 1)*, Technical report, OECD Nuclear Energy Agency (2013).

[60] I. Günther-Leopold, N. Kivel, J. Kobler Waldis, B. Wernli, Characterization of nuclear fuels by ICP mass-spectrometric techniques, Analytical and Bioanalytical Chemistry **390**(2), 503–510 (2008).

[61] M. Betti, G. Tamborini, L. Koch, Use of secondary ion mass spectrometry in nuclear forensic analysis for the characterization of plutonium and highly enriched uranium particles, Analytical Chemistry **71**, 2616–2622 (1999).

[62] S. Portier, S. Brémier, C. Walker, Secondary ion mass spectrometry of irradiated nuclear fuel and cladding: An overview, International Journal of Mass Spectrometry **263**(2-3), 113–126 (2007).

[63] S. N. Ahmed, *Physics and Engineering of Radiation Detection* (Elsevier, 2007).

[64] S. Hsue, T. Crane, W. Talbert, J. Lee, *Non-destructive Assay Methods for Irradiated Nuclear Fuels*, Technical report, Los Alamos national laboratory (1978).

[65] A. Lebrun, G. Bignan, H. Recroix, M. Huver, E. Mesures, Characterization of spent fuel assemblies for storage facilities using non destructive assay, in *International Symposium on Storage of Spent Fuel from Power Reactors* (1999).

[66] S. Croft, et al., A technical review of non-destructive assay research for the characterization of spent nuclear fuel assemblies being conducted under the US DOE NGSI–11544, in *WM2011 Conference* (2011).

[67] C. Willman, *Applications of Gamma Ray Spectroscopy of Spent Nuclear Fuel for Safeguards and Encapsulation*, Ph.D. thesis, Uppsala University (2006).

[68] A. M. Bolind, M. Seya, *The State-of-the-art of the Non-destructive Assay of Spent Nuclear Fuel Assemblies — A Critical Review of the Spent Fuel NDA Project of the U.S. Department of Energy's Next Generation Safeguards Initiative*, Technical report, Japan Atomic Energy Agency (2015).

[69] I. Matsson, B. Grapengiesser, Developments in gamma scanning irradiated nuclear fuel, Applied Radiation and Isotopes **48**(10-12), 1289–1298 (1997).

[70] B. Biard, Quantitative analysis of the fission product distribution in a damaged fuel assembly using gamma-spectrometry and computed tomography for the Phébus FPT3 test, Nuclear Engineering and Design **262**, 469–483 (2013).

[71] G. Jonkmans, V. Anghel, C. Jewett, M. Thompson, Nuclear waste imaging and spent fuel verification by muon tomography, Annals of Nuclear Energy **53**, 267–273 (2013).

[72] M. Murphy, F. Jatuff, P. Grimm, R. Seiler, R. Brogli, G. Meier, H. Berger, C. R., Reactivity and neutron emission measurements of highly burnt PWR fuel rod samples, Annals of Nuclear Energy **33**(9), 760–765 (2006).

[73] N. Shinohara, Y. Nakahara, N. Kohno, K. Tsujimoto, Recent activity on the post-irradiation analyses of nuclear fuels and actinide samples

at JAERI, in *ICNC2003: Proceedings of the seventh international conference on nuclear criticality safety. Challenges in the pursuit of global nuclear criticality safety* (2003).

[74] K. Inoue, K. Taniguchi, T. Kobayashi, Mass spectrometric determination of burn-up, Journal of Nuclear Science and Technology **4**(3), 131–135 (1967).

[75] M. Kurosawa, Y. Naito, H. Sakamoto, T. Kaneko, *The Isotopic composition database system on spent fuels in light water rreactor (SFCOMPO)*, Technical report, Japan Atomic Energy Research Institute (1997).

[76] OECD/NEA Data bank computer program services website, *http://www.oecd-nea.org/dbprog/*.

[77] N. Gulliford, D. Hanlon, Measurement of reactivity loss with burn-up in PWR, BWR and MOX fuel made in the CERES collaborative programme, in *Proceedings of International Conference on the Physics of Reactors, PHYSOR96.* (1996), 151–160.

[78] D. Bernard, A. Santamarina, A. Sargeni, M. Antony, J. Hudelot, Experimental validation of the LWR reactivity loss with burn-up: Analysis of spent fuel oscillation experiments, in *PHYSOR-2006 Reactor Physics Topical Meeting* (2006).

[79] B. Roque, M. P., P. Bioux, H. Toubon, L. Daudin, The French post irradiation examination database for the validation of the depletion calculation tools, in *Proceedings of the 7th International Conference on Nuclear Criticality Safety ICNC2003* (2003).

[80] *ARIANE International Programme Final Report*, Technical report, Oak Ridge National Laboratory (2003).

[81] S. Caruso, *Characterisation of high-burnup LWR fuel rods through gamma tomography*, Ph.D. thesis, Ecole Polytechnique Federale de Lausanne (2007).

[82] T. Yamamoto, K. Kawashima, Y. Ando, K. Sakurada, Y. Hayashi, S. Aoki, K. Azekura, Analysis of core physics experiments on fresh and irradiated BR3 MOX fuel in REBUS program, Journal of Nuclear Science and Technology **46**(5), 484–509 (2009).

[83] H. Zwicky, J. Low, M. Granfors, C. Alejano, J. Conde, C. Casado, J. Sabater, M. Lloret, M. Quecedo, J. Gago, Nuclide analysis in high burn-up fuel samples irradiated in Vandellós 2, Journal of Nuclear Materials **402**(1), 60–73 (2010).

[84] G. Ilas, I. Gauld, *Analysis of Experimental Data for High-Burnup PWR Spent Fuel Isotopic Validation — Vandellós II Reactor*, Technical report, Oak Ridge National Laboratory (2011).

[85] T. Yamamoto, Y. Kanayama, Lattice physics analysis of burn-ups and isotope inventories of U, Pu, and Nd of irradiated BWR 9x9-9 UO_2 fuel assemblies, Journal of Nuclear Science and Technology **45**(6), 547–566 (2008).

[86] W. Martin, C. de Oliveira, A. Hecht, Reactor fuel depletion benchmark of TINDER, Annals of Nuclear Energy **73**, 547–551 (2014).

[87] Y.-K. Ha, J. Kim, Y. Jeon, S. Han, H. Seo, K. Song, Local burn-up characteristics of PWR spent nuclear fuels discharged from Yeonggwang-2 nuclear power plant, Nuclear engineering and technology **42**(1), 79–88 (2010).

[88] A. G. Korenkov, T. Makarova, A. Stepanov, E. Pevtsova, B. Belyaev, A. Voronkov, Destructive analysis determination of neutron emission from spent RBMK fuel, Atomic Energy **93**(4) (2002).

[89] T. P. Makarova, B. A. Bibichev, V. D. Domkin, Destructive analysis of the nuclide composition of spent fuel of WWER-440, WWER-1000, and RBMK-1000 reactors, Radiochemistry **50**(4), 414–426 (2008).

[90] D. Ancius, D. Ridikas, V. Remeikis, V. Plukis, R. Plukienė, M. Cometto, Evaluation of the activity of irradiated graphite in the Ignalina nuclear power plant RBMK-1500 reactor, NUKLEONIKA **50**(3), 113–120 (2005).

[91] R. Sanchez, M. N.J., A review of neutron transport approximations, Nuclear Science and Engineering **80**, 481–535 (1982).

[92] C. Dembia, G. Recktenwald, M. Deinert, Bondarenko method for obtaining group cross-sections in a multi-region collision probability model, Progress in Nuclear Energy **67**, 124–131 (2013).

[93] A. Hébert, A review of legacy and advanced self-shielding models for lattice calculations, Nuclear Science and Engineering **155**(2), 310–320 (2007).

[94] J. Fletcher, The solution of the time-independent multi-group neutron transport equation using spherical harmonics, Annals of Nuclear Energy **4**(9), 401–405 (1977).

[95] M. DeHart, *A discrete ordinates approximation to the neutron transport equation applied to generalized geometries*, Ph.D. thesis, Texas A&M University (1992).

[96] R. Garcia, An analytical discrete-ordinates solution for an improved one-dimensional model of three-dimensional transport in ducts, Annals of Nuclear Energy **86**, 55–64 (2015).

[97] A. Owens, J. Welch, J. Kópházi, M. Eaton, Discontinuous isogeometric analysis methods for the first-order form of the neutron transport

equation with discrete ordinate (SN) angular discretisation, Journal of Computational Physics **315**, 501–535 (2016).

[98] N. Metropolis, S. Ulam, The Monte Carlo method, Journal of the American Statistical Association **44**(247), 335–341 (1949).

[99] I. Lux, L. Koblinger, *Monte Carlo particle transport methods: neutron and photon calculations* (CRC Press, 1991).

[100] E. Wolters, *Hybrid Monte Carlo — Deterministic Neutron Transport Methods Using Nonlinear Functionals*, Ph.D. thesis, University of Michigan (2011).

[101] A. Haghighat, J. Wagner, Monte Carlo variance reduction with deterministic importance functions, Progress in Nuclear Energy **42**(1), 25–53 (2003).

[102] J. Willert, C. Kelley, D. Knoll, H. Park, Hybrid deterministic/Monte Carlo neutronics, SIAM Journal on Scientific Computing **35**(5), 62–83 (2013).

[103] H. Bateman, Solution of a system of differential equations occurring in the theory of radioactive transformations, Proceedings of the Cambridge Philosophical Society **15**, 423–427 (1910).

[104] M. DeHart, *NEWT: a new transport algorithm for two-dimensional discrete ordinates analysis in non-orthogonal geometries*, ORNL/TM-2005/39 edition (2009).

[105] T. Downar, D. Lee, Y. Xu, T. Kozlowski, *PARCS v2.6: U.S. NRC Core Neutronics Simulator* (2004).

[106] H. Golfier, R. Lenain, C. Calvin, J. Lautard, A. Baudron, P. Fougeras, P. Magat, E. Martinolli, Y. Dutheillet, APOLLO3: a common project

of CEA, AREVA and EDF for the development of a new deterministic multi-purpose code for core physics analysis, in *International Conference on Mathematics, Computational Methods and Reactor Physics* (2009).

[107] J. Rhodes, K. Smith, D. Lee, CASMO-5 Development and applications, in *PHYSOR-2006, ANS Topical Meeting on Reactor Physics* (2006).

[108] C. Diop, O. Petit, E. Dumonteil, F. Hugot, Y. Lee, A. Mazzolo, J. Trama, TRIPOLI-4: A 3D continuous-energy Monte Carlo transport code, in *PHYTRA1: First International Conference on Physics and Technology of Reactors and Applications* (2007).

[109] T. Goorley, et al., Features of MCNP6, in *Joint International Conference on Supercomputing in Nuclear Applications and Monte Carlo* (2013).

[110] S. Goluoglu, S. Bowman, D. M.E., KENO Monte Carlo code capabilities, Transactions of the American Nuclear Society **97**, 592–594 (2007).

[111] J. Leppanen, *Serpent Progress Report 2012*, Technical report, VTT (2014).

[112] T. Sato, K. Niita, N. Matsuda, S. Hashimoto, Y. Iwamoto, S. Noda, T. Ogawa, H. Iwase, H. Nakashima, T. Fukahori, K. Okumura, T. Kai, S. Chiba, T. Furuta, L. Sihver, Particle and heavy ion transport code system, PHITS, version 2.52, Journal of Nuclear Science and Technology **50**(9), 913–923 (2013).

[113] C. Parks, Overview of ORIGEN2 and ORIGEN-S: capabilities and limitations, in *International High-Level Radioactive Waste Management Conference* (1992).

[114] G. Ilas, B. Murphy, I. Gauld, Overview of ORIGEN-ARP and its application to VVER and RBMK, Transactions of the American Nuclear Society **97**, 601–603 (2007).

[115] H. Trellue, D. Poston, *User's Manual Version 2.0 for Monteburns 1.0, LAUR-99-4999* (1999).

[116] Y. Xu, T. Kim, D. T.J., *DEPLETOR: A Depletion Code for PARCS, Purdue University* (2000).

[117] W. W. Wilson, S. Cowell, T. England, A. Hayes, M. P., *A manual for CINDER90 version 07.4 codes and data* (2008).

[118] J. Sublet, J. Eastwood, J. Guy Morgan, *The FISPACT-II User Manual*, UK Atomic Energy Authority, Culham Science Centre (2014).

[119] The criticality safety benchmark evaluation project website, *http://icsbep.inel.gov/index.shtml*.

[120] T. Takeda, H. Ikeda, 3-D neutron transport benchmarks, Journal of Nuclear Science and Technology **28**(7), 656–669 (1991).

[121] Z. Zhong, T. Downar, Benchmarking the U.S. neutronics codes NEWT and PARCS with the VENUS-2 critical experiments, in *Nuclear Mathematical and Computational Sciences: A Century in Review, A Century Anew* (2003).

[122] M. Chadwick, et al., ENDF/B-VII.1 Nuclear data for science and technology: Cross sections, covariances, fission product yields and decay data, Nuclear Data Sheets **112**(12), 2887–2996 (2011).

[123] K. Shibata, JENDL-4.0: A new library for nuclear science and engineering, Journal of Nuclear Science and Technology **48**(1) (2011).

[124] JEFF-3.2 evaluated data library, *https://www.oecd-nea.org/dbforms/data/eva/evatapes/jeff32/*.

[125] W. Marshall, B. Rearden, *Criticality Safety Validation of SCALE 6.1*, Technical report, Oak Ridge National Laboratory (2011).

[126] O. Hermann, S. Bowman, M. Brady, C. Parks, *Validation of the SCALE System for PWR Spent Fuel Isotopic Composition Analyses*, Technical report, Oak Ridge National Laboratory (1995).

[127] A. M. Bolind, The use of the BIC set in the characterization of used nuclear fuel assemblies by non-destructive assay, Annals of Nuclear Energy **66**, 31–50 (2014).

[128] B. Murphy, *ORIGEN-ARP Cross-Section Libraries for Magnox, Advanced Gas-Cooled, and VVER Reactor Designs*, Technical report, Oak Ridge National Laboratory (2004).

[129] G. Ilas, I. Gauld, V. Jodoin, LWR cross section libraries for ORIGEN-ARP in SCALE 5.1, in *Transactions of the American Nuclear Society* (2006), volume 95, 706–708.

[130] B. D. Murphy, *ORIGEN-ARP Cross-Section Libraries for the RBMK-1000 System*, Technical report, Oak Ridge National Laboratory (2006).

[131] J. Kim, Y. Jeon, S. Park, S. Han, J. Kim, Burn-up determination of high burn-up and dry processed fuels based on isotope dilution mass spectrometric measurements, Journal of Nuclear Science and Technology **44**(7), 1015–1023 (2007).

[132] I. Gauld, P. Chare, R. Clarke, Development of ORIGEN-ARP methods and data for LEU and MOX safeguards applications, in *Institute of Nuclear Materials Management Annual Meeting* (2003), volume 44.

[133] V. Remeikis, A. Jurkevicius, Evolution of the neutron sensor characteristics in the RBMK-1500 reactor neutron flux, Nuclear Engineering and Design **231**(3), 271–282 (2004).

[134] *An Approach for Validating Actinide and Fission Product Burn-up Credit Criticality Safety Analyses Predictions, Nureg/Cr-7109*, Technical report, USA Nuclear Regulatory Commission (2012).

[135] A. Šmaižys, P. Poškas, Criticallity evaluation of spent nuclear fuel casks CASTOR RBMK-1500 and CONSTOR RBMK-150, Energetics **4**, 3–9 (2001).

[136] I. Gauld, S. Bowman, *STARBUCS: A Prototypic SCALE Control Module for Automated Criticality Safety Analyses Using Burn-up Credit*, Technical report, Oak Ridge National Laboratory (2001).

[137] V. Barkauskas, A. Plukis, Preparation of effective cross-section libraries for calculation of spent nuclear fuel inventory of RBMK type reactors, in *CYSENI conference proceedings* (2013).

[138] C. Park, H. Park, H. Shon, S. Hong, Y. Lee, End effect analysis with various axial burn-up distributions in high density spent fuel storage racks, Annals of Nuclear Energy **81**, 174–178 (2015).

[139] V. G. Aden, A. A. Petrov, A. I. Kupalov-Yaropolk, E. K. Kovalenko, D. V. Severinov, V. M. Panin, A. M. Fedosov, A. V. Krayushkin, E. V. Burlakov, Increasing the fuel utilization efficiency of RBMK-1000 reactors, Atomic Energy **103**(1), 547–552 (2007).

[140] T. Parish, V. V. Khromov, C. I. (eds.), *Safety Issues Associated with Plutonium Involvement in the Nuclear Fuel Cycle. Proceedings of the NATO Advanced Research Workshop on Safety Issues Associated with Plutonium Involvement in the Nuclear Fuel Cycle Moscow, Russia* (1997) (1997).

[141] H. Okuno, Y. Naito, Y. Ando, *OECD/NEA Burn-up Credit Criticality Benchmarks Phase IIIA: Criticality Calculations of BWR Spent Fuel*

Assemblies in Storage and Transport, Technical report, Japan Atomic Energy Research Institute (2000).

[142] J. Fachinger, W. von Lensa, T. Podruhzina, Decontamination of nuclear graphite, Nuclear Engineering and Design **238**(11), 3086–3091, hTR-2006: 3rd International Topical Meeting on High Temperature Reactor Technology (2008).

[143] V. Remeikis, A. Plukis, R. Plukienė, A. Garbaras, R. Barisevičiūtė, A. Gudelis, R. Gvozdaitė, G. Duškesas, L. Juodis, Method based on isotope ratio mass spectrometry for evaluation of carbon activation in the reactor graphite, Nuclear Engineering and Design **240**(10), 2697–2703 (2010).

[144] A. V. Bushuev, V. N. Zubarev, I. M. Proshin, Impurity composition and content in graphite from commercial reactors, Atomic Energy **92**(4), 331–335 (2002).

[145] B. K. Bylkin, G. B. Davydova, A. V. Krayushkin, V. A. Shaposhnikov, Computational estimates of the radiation characteristics of irradiated graphite after final shutdown of a nuclear power plant with an RBMK reactor, Atomic Energy **96**(6), 411–416 (2004).

[146] V. Remeikis, A. Plukis, L. Juodis, A. Gudelis, D. Lukauskas, R. Druteikienė, G. Lujanienė, B. Lukšienė, R. Plukienė, G. Duškesas, Study of the nuclide inventory of operational radioactive waste for the RBMK-1500 reactor, Nuclear Engineering and Design **239**(4), 813–818 (2009).

[147] E. Maceika, V. Remeikis, D. Ancius, D. Ridikas, Evaluation of the radiological consequences of ^{14}C due to contaminated Ignalina NPP graphite incineration, Lithuanian Journal of Physics **45**(5), 383–391 (2005).

[148] R. Plukienė, A. Plukis, A. Puzas, V. Remeikis, G. Duškesas, D. Germanas, Modelling of impurity activation in the RBMK reactor graphite using MCNPX, Progress in Nuclear Science and Technology **2**, 421–426 (2011).

[149] A. Šmaižys, E. Narkūnas, P. Poškas, Modelling of activation processes for GR-280 graphite at Ignalina NPP, Radiation Protection Dosimetry **116**, 270–275 (2005).

[150] R. Plukienė, D. Ridikas, Modelling of HTRs with Monte Carlo: from a homogeneous to an exact heterogeneous core with microparticles, Annals of Nuclear Energy **30**(15), 1573–1585 (2003).

[151] D. Lukauskas, R. Plukienė, A. Plukis, A. Gudelis, G. Duškesas, L. Juodis, R. Druteikienė, G. Lujanienė, B. Lukšienė, V. Remeikis, Method of determining the nuclide inventory for low-activity waste of the RBMK-1500 reactor, Lithuanian Journal of Physics **46**(4), 497–503 (2006).

[152] A. Puzas, V. Remeikis, v. Ežerinskis, P. Serapinas, A. Plukis, G. Duškesas, Mass spectrometric determination of impurities in reactor core graphite for radioactive waste composition modelling, Lithuanian Journal of Physics **50**(4), 445–449 (2010).

[153] D. Pelowitz, *MCNPX User's Manual, Version 2.7.0, Report LA-CP-11-00438*, Technical report, Los Alamos National Laboratory (2011).

[154] W. Wilson, T. England, K. van Riper, *Status of CINDER'90 Codes and Data*, Technical report, Los Alamos National Laboratory (1999).

[155] Power Reactor Information System (PRIS), *www.iaea.org/PRIS/*.

[156] *Unit 2 Safety Analysis Report, 2002. PTOab2-0345-5112V1*, Technical report, Ignalina NPP (2002).

[157] Q. Chen, A. Aarkrog, S. P. Nielsen, H. Dahlgaard, B. Lind, A. K. Kolstad, Y. Yu, *Procedures for determination of* $^{239,240}Pu$, ^{241}Am, ^{237}Np, $^{234,232}U$, $^{228,230,232}Th$, ^{99}Tc *and* ^{210}Pb-^{210}Po *in environmental materials.*, Technical report, Riso National Laboratory, Roskilde, Denmark. (2001).

[158] E. P. Horwitz, R. Chiarizia, M. Dietz, H. Diamond, D. Nelson, Separation and preconcentration of actinides from acidic media by extraction chromatography, Analytica Chimica Acta **281**(2), 361–372 (1993).

[159] VATESI, Nuclear Safety Requirements BSR-1.9.2, Derivation and use of clearance levels of radionuclides for materials and waste generated during activities in nuclear energy, Official Gazette **118-5608** (2011).